

# High Resolution Fourier Transform Infrared Spectroscopy

S. Albert, K. Keppler Albert, M. Quack

ETH Zürich, Laboratory of Physical Chemistry, Wolfgang-Pauli-Str. 10,  
CH-8093 Zürich, Switzerland, Email: [Martin@Quack.ch](mailto:Martin@Quack.ch)

reprinted from

## “Handbook of High-Resolution Spectroscopy”,

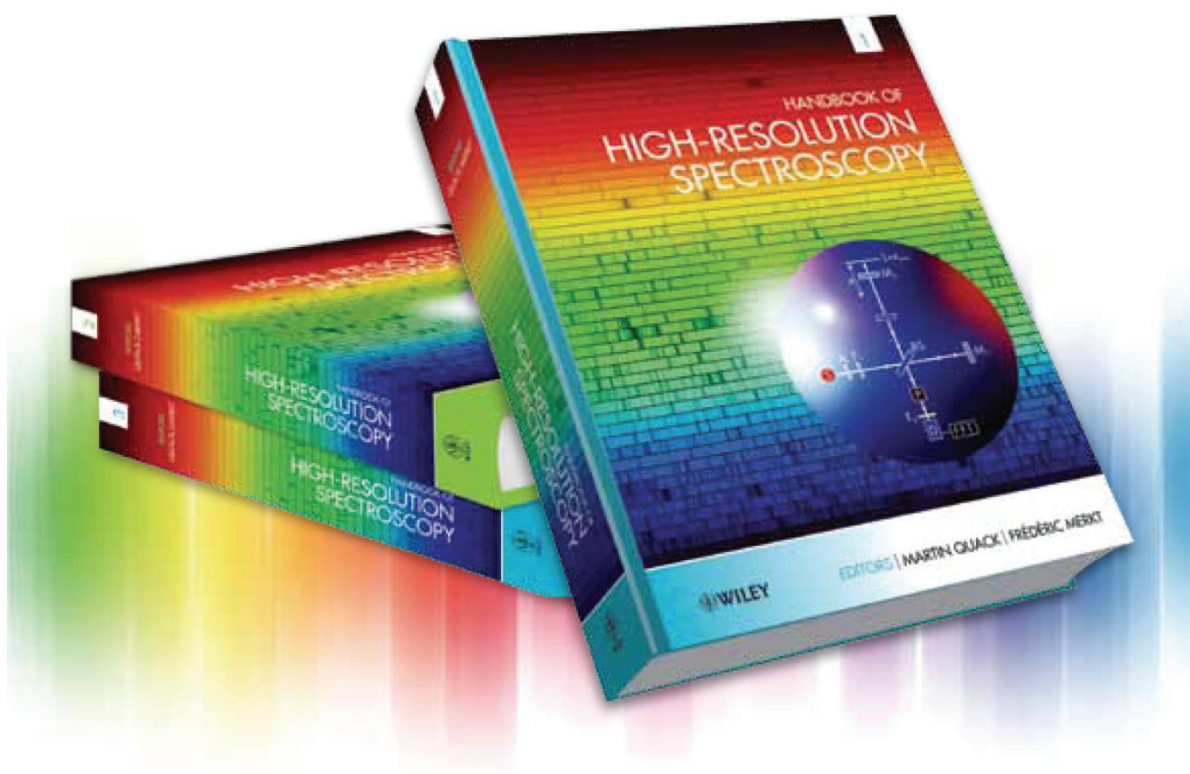
Vol. 2, chapter 26, pages 965–1019

M. Quack, and F. Merkt, Eds. Wiley Chichester, 2011,

ISBN-13: 978-0-470-06653-9.

Online ISBN: 9780470749593,

DOI: 10.1002/9780470749593



with compliments from Professor Martin Quack, ETH Zürich

## Abstract

Recent developments and applications of high-resolution Fourier transform spectroscopy are reviewed. A short historical summary of the development of high-resolution interferometric Fourier transform infrared (FTIR) spectrometers is given and the possibilities of the currently most highly resolving FTIR spectrometers, including a current prototype built for the Zürich group at the Swiss Light Source SLS as a synchrotron light source, are discussed. A short description of the principles of FTIR spectroscopy is given and the resolution of current spectrometers is illustrated by FTIR spectra of CO, CO<sub>2</sub>, OCS, N<sub>2</sub>O, CS<sub>2</sub>, and CH<sub>4</sub> and its isotopomers. The computational tools necessary to analyze FTIR spectra are described briefly. As examples of rovibrational analysis of more complex spectra, selected molecules CHCl<sub>2</sub>F, CDBrClF, pyridine (C<sub>5</sub>H<sub>5</sub>N) and pyrimidine (C<sub>4</sub>H<sub>4</sub>N<sub>2</sub>), and naphthalene (C<sub>10</sub>H<sub>8</sub>) are discussed. The spectrum of CHCl<sub>2</sub>F, a fluorochlorocarbon, is of interest for a better understanding of the chemistry of the Earth's atmosphere. It also possesses an isotopically chiral isotopomer CH<sup>35</sup>Cl<sup>37</sup>ClF analyzed in natural abundance. CDBrClF is a chiral molecule and therefore the analysis of its rovibrational spectra provides the basis for carrying out further experiments toward the detection of molecular parity violation. The analyses of the pyridine, pyrimidine, and naphthalene FTIR spectra illustrate the potential of the new generation of FTIR spectrometers in the study of spectra and rovibrational dynamics of aromatic systems and molecules of potential biological interest. In particular, naphthalene is a prototype molecule useful in gaining an understanding of the unidentified infrared bands (UIBs) detected in several interstellar objects.

**Keywords:** high-resolution spectroscopy; resonance; FTIR spectroscopy; chiral molecules; aromatic molecules; infrared spectroscopy; isotopes; isotopomers; symmetry; asymmetric tops; synchrotron light sources; CDFClBr; CHFClBr; CHFCl<sub>2</sub>; fluorohydrocarbons, methane, CH<sub>2</sub>D<sub>2</sub>; CHD<sub>3</sub>; CH<sub>3</sub>D; CH<sub>4</sub>; naphthalene; pyridine; pyrimidine; benzene; carbondioxide; CO<sub>2</sub>; CO; OCS; N<sub>2</sub>O; CS<sub>2</sub>

# High-resolution Fourier Transform Infrared Spectroscopy

Sieghard Albert, Karen Keppler Albert and Martin Quack

Laboratorium für Physikalische Chemie, ETH Zürich, Zürich, Switzerland

## 1 INTRODUCTION

### 1.1 General Aspects

Traditional high-resolution spectroscopy in the ordinary “optical” domain of the spectrum, defined here as ranging from the far infrared (FIR) (wavenumber  $\tilde{\nu} = 10 \text{ cm}^{-1}$ , frequency  $\nu = 0.3 \text{ THz}$ , or wavelength  $\lambda = 1 \text{ mm}$ ) to the vacuum UV ( $\tilde{\nu} = 100\,000 \text{ cm}^{-1}$ ,  $\nu = 3000 \text{ THz}$ ,  $\lambda = 100 \text{ nm}$ ), has used dispersive elements such as prisms or gratings to obtain wavelength-selected spectra (Herzberg 1945, 1966, 1991) with either photographic, or later, electronic recording for two centuries, following the work of Fraunhofer, Bunsen, and Kirchhoff, and many others in the nineteenth century (*see* Merkt and Quack 2011: **Molecular Quantum Mechanics and Molecular Spectra, Molecular Symmetry, and Interaction of Matter with Radiation**, for some of the history). Herzberg’s classic books covering the spectroscopic literature until about 1965 provide ample examples of spectra obtained in this way. Developments in spectroscopy during the decades following 1965 have importantly used two new experimental principles:

1. lasers as monochromatic tunable light sources extending the frequency domain of the tunable Hertzian oscillator from the radio frequency range into the IR, visible, and UV. The developments in laser spectroscopy are discussed in several other articles in this handbook (*see also* Sigrist 2011: **High-resolution Infrared Laser Spectroscopy and Gas Sensing Applications**, Snels *et al.* 2011: **High-resolution FTIR and Diode**

**Laser Spectroscopy of Supersonic Jets**, Jäger and Xu 2011: **Fourier Transform Microwave Spectroscopy of Doped Helium Clusters**, Havenith and Birner 2011: **High-resolution IR-laser Jet Spectroscopy of Formic Acid Dimer**, Hippler *et al.* 2011: **Mass and Isotope-selective Infrared Spectroscopy**, Amano 2011: **High-resolution Microwave and Infrared Spectroscopy of Molecular Cations**, Guennoun and Maier 2011, Pratt 2011: **Electronic Spectroscopy in the Gas Phase**, Schmitt and Meerts 2011: **Rotationally Resolved Electronic Spectroscopy and Automatic Assignment Techniques using Evolutionary Algorithms**, Weber 2011: **High-resolution Raman Spectroscopy of Gases**, Wester 2011: **Spectroscopy and Reaction Dynamics of Anions**, Merkt *et al.* 2011: **High-resolution Photoelectron Spectroscopy**, Eikema and Ubachs 2011: **Precision Laser Spectroscopy in the Extreme Ultraviolet**, Demtröder 2011: **Doppler-free Laser Spectroscopy**, Häber and Kleinermanns 2011: **Multiphoton Resonance Spectroscopy of Biological Molecules** and Stanca-Kaposta and Simons 2011: **High-resolution Infrared–Ultraviolet (IR–UV) Double-resonance Spectroscopy of Biological Molecules**, this handbook).

2. interferometric Fourier transform infrared (FTIR) spectroscopy making the principle of the Michelson interferometer useful for broad coverage spectroscopy discussed in this article.

While the optical principles of the Michelson interferometer have been known for more than a century (Michelson 1881) and have been used for specialized purposes, the application for high-resolution spectroscopy covering broad spectral ranges required the development of fast computers

to carry out the necessary mathematical operations of the Fourier transformation of the measured “interferogram” which is a signal as a function of the mirror displacement in the interferometer, to obtain the desired spectral signal as a function of frequency (Section 2). Indeed, until about 1970–1980 this computational task was still a bottleneck in using FTIR spectroscopy at very high resolution. The development of FTIR spectroscopy is thus clearly connected to parallel development in numerical computation using fast computers and the corresponding algorithms. Today, the Fourier transformation is no longer the limiting factor and the previously revolutionary FTIR spectroscopy has become the reference technique to which other methods should be compared. The term FTIR suggests restriction to the IR range, where indeed the most important applications can be found, ranging from the FIR ( $\tilde{\nu} = 10\text{--}200\text{ cm}^{-1}$ ,  $\nu = 0.3\text{--}6\text{ THz}$ ), to the mid-IR ( $\tilde{\nu} = 200\text{--}4000\text{ cm}^{-1}$ ,  $\nu = 6\text{--}120\text{ THz}$ ) and the near infrared (NIR) ( $\tilde{\nu} = 4000\text{--}12\,000\text{ cm}^{-1}$ ,  $\nu = 120\text{--}360\text{ THz}$ ). The use of FTIR spectroscopy can be extended into the visible and UV ranges ( $\tilde{\nu} = 12\,000\text{--}100\,000\text{ cm}^{-1}$ ). This demonstrates the enormous spectral coverage, scanning power, and scanning range extending over about four orders of magnitude in photon energy, which is not achievable by any laser with the exception of the free electron laser, which is still far from a routine laboratory equipment. Although the term is frequently overused, one may well state that Fourier transform spectroscopy has introduced a revolution in high-resolution IR spectroscopy over the last 30 years comparable in power to, but along different lines than laser spectroscopy.

The principle of measuring a signal including all frequencies of a “white light” source as a function of an experimental parameter (here the position of an interferometer mirror) and then obtaining the spectral signal by Fourier transformation of the measured signal can be related to time domain Fourier transform spectroscopy in the radio frequency and microwave regions. As is well known, radio frequency nuclear magnetic resonance (NMR) spectroscopy has been revolutionized in a comparable historical period over the last decades by introducing FT-NMR spectroscopy (Ernst *et al.* 1987) and the principle has been extended to the microwave ranges for ESR spectroscopy (Schweiger and Jeschke 2001) and rotational molecular spectroscopy (*see also*, Bauder 2011: **Fundamentals of Rotational Spectroscopy** and Shipman and Pate 2011: **New Techniques in Microwave Spectroscopy**, this handbook). In the optical spectrum (IR to UV), time domain Fourier transforms have also been used, but play a less dominant role (*see also*, Frey *et al.* 2011: **High-resolution Rotational Raman Coherence Spectroscopy with Femtosecond Pulses**, and Hamm 2011: **2D-Infrared Spectroscopy**, this handbook).

This article provides an overview of the current status and some recent results in FTIR spectroscopy, with an emphasis on the work done by our group. We draw from a recent brief review (Albert and Quack 2007a), which we follow in some aspects quite closely but which has been updated and extended for the present purpose. We also refer to other articles in this handbook, which report on results from FTIR spectroscopy (*see also* Snels *et al.* 2011: **High-resolution FTIR and Diode Laser Spectroscopy of Supersonic Jets**, Flaud and Orphal 2011: **Spectroscopy of the Earth’s Atmosphere** and Herman 2011: **High-resolution Infrared Spectroscopy of Acetylene: Theoretical Background and Research Trends**, this handbook).

## 1.2 Brief Historical Review

Interferometric FTIR spectroscopy has a long history, going back to the development of the Michelson interferometer for use in spectroscopy (Michelson 1881, 1927), the work of Rubens and Wood on FIR interferograms (Rubens and Wood 1911), and the work of Rubens and von Baeyer (Rubens and Baeyer 1911). The early history connected with the names of Jacquinot (Jacquinot 1954), Fellgett (Fellgett 1958), and Connes (Connes 1961) among others is well described in Chamberlain’s classic book (Chamberlain 1979) (*see also* the books by Bell (Bell 1972), Davis *et al.* (Davis *et al.* 2001), and Kauppinen and Partanen (Kauppinen and Partanen 2001)). While some homemade high-resolution FTIR spectrometers existed before 1980 (Guelachvili 1978, Kauppinen 1979, Henry *et al.* 1983, Brault 1985), it is probably fair to say that the real breakthrough occurred with the advent of commercially available high-resolution instruments. From then on, advances could concentrate on new scientific questions and developments of the necessary spectroscopic and theoretical techniques, rather than instrument development. Prior to 1980, the resolution of most FTIR spectrometers was limited to about  $0.04\text{ cm}^{-1}$ , hardly superior to the traditional grating instruments.

A first breakthrough arrived with the Bomem instruments with maximum optical path difference  $d_{\text{MOPD}} = 250\text{ cm}^{-1}$ , corresponding to an unapodized resolution defined as  $\Delta\tilde{\nu} = 0.61 d_{\text{MOPD}}^{-1} = 0.0024\text{ cm}^{-1}$ . The stated resolution refers here to the instrumental bandwidth ( $\Delta\tilde{\nu}$ , Full Width at Half Maximum, FWHM). For a detailed discussion of the implications and consequences of apodization, we refer to Section 2 and Chamberlain (1979), Bell (1972), Davis *et al.* (2001), Kauppinen and Partanen (2001). There was an improvement by more than a factor of 10 in resolution at that time, made possible by the invention of dynamic alignment (Kendall *et al.* 1982, Buijs 1979). The

**Table 1** Current nine-chamber systems ( $MOPD = 9.8\text{ m}$ ) of the Bruker IFS 125 HR as well as extended high-resolution system prototype (last entry).

ETH Zürich, Laboratory for Physical Chemistry (Albert <i>et al.</i> 2003b, Albert and Quack 2007a)	Zürich	Switzerland
University of Saskatchewan, Canadian Light Source Inc. (McKellar 2010, McKellar <i>et al.</i> 2007)	Saskatoon	Canada
Australian Synchrotron (Chimdi <i>et al.</i> 2008)	Clayton, Melbourne	Australia
Institute of Atmospheric Optic, Russian Academy of Sciences (Ulenikov <i>et al.</i> 2010a)	Tomsk	Russia
Institute of Spectroscopy - RA, Center for Fourier Spectroscopy, Chemical Department (Chukalina <i>et al.</i> 2010)	Troitsk	Russia
National University of Defense Technology	Changsa, Hunan Province	China
Advanced Light Source Division, Lawrence Berkeley National Laboratory (Carr <i>et al.</i> 2008)	Berkeley, California	USA
Synchrotron Soleil, CEA L'Orme des Merisiers Gif-sur-Yvette (Roy <i>et al.</i> 2006)	Paris	France
Swiss Light Source, ETH Zürich and Paul-Scherrer Institute, 11 chamber interferometer (Albert <i>et al.</i> 2010)	Villigen	Switzerland

availability of these instruments led to early developments in Doppler-limited high-resolution FTIR-supersonic jet techniques (Dübal *et al.* 1984, Amrein *et al.* 1987a,b, 1988a,b) (see review (Quack 1990) and Snels *et al.* 2011: **High-resolution FTIR and Diode Laser Spectroscopy of Supersonic Jets**, for further references). It also contributed importantly to the high-resolution spectroscopic approach to short-time (as-fs-ps) intramolecular quantum dynamics and kinetics (Marquardt and Quack 2001, Quack 1990, 2001, 2003, 2004, Albert *et al.* 2011: **Fundamentals of Rotation–Vibration Spectra**, this handbook).

Another important step was the development of the Bruker IFS 120 HR instrument with an unapodized resolution of  $\Delta\tilde{\nu} = 0.0012\text{ cm}^{-1}$  ( $d_{MOPD} = 5\text{ m}$ , five-chamber system) (Birk *et al.* 1989). It is a modular system consisting of chambers of 55 cm length. Numerous spectrometers of the IFS 120 HR series based on the 1987 Giessen prototype are currently working worldwide (Keens 2004, McNaughton 2002, Nelander 1993). The resolution of these instruments made it possible to analyze the rovibrational spectra of linear and quasi-linear molecules up to the mid-IR region at room temperature. We would like to mention here the analysis of the classical quasi-linear molecule HCNO and its isotopomers (Wagner *et al.* 1991, Quapp *et al.* 1993, Albert *et al.* 1996, 1997a,b, 1998a, 2001b, Schulze *et al.* 2000). It turned out that the rovibrational spectra of HCNO and its isotopomers are strongly perturbed in the overtone region (Albert *et al.* 1996). In spite of recent calculations (Mladenovic *et al.* 2009), up to now there is still no complete theoretical description of these phenomena, especially in the overtone region, which would account for the rotational structure of the fulminic acid spectra and, thus, no full understanding of the dynamics of the quasi-linear molecule HCNO. A new theoretical approach for an understanding of these quasi-linear phenomena was

recently shown using quantum monodromy (Winnewisser *et al.* 2005).

Further advances have been achieved with the Bruker Zurich prototype 2001 spectrometer (IFS 125 HR ZP 2001 prototype), a nine-chamber system, which is capable of an unapodized resolution of  $0.00062\text{ cm}^{-1}$  ( $d_{MOPD} = 9.8\text{ m}$ ) with a specified resolving power of  $2 \times 10^6$  at  $2000\text{ cm}^{-1}$  (Albert and Quack 2002, 2007a, Albert *et al.* 2003b). The Bruker IFS 125 HR spectrometer is based on this prototype and was developed subsequently. Spectrometers of this series are now connected to several synchrotron sources worldwide (McKellar 2010, McKellar *et al.* 2007, Roy *et al.* 2006, Chimdi *et al.* 2008, Carr *et al.* 2008). Table 1 lists the current working nine-chamber systems of the IFS 125 HR series. Very recently, a new prototype of the Bruker IFS 125 HR series, the Bruker ETH-SLS 2009 spectrometer prototype (11-chamber system), was developed for our group by Bruker optics. This new spectrometer is connected to the Swiss Synchrotron, the Swiss Light Source (SLS), and it has an improved unapodized resolution of  $0.00053\text{ cm}^{-1}$  ( $d_{MOPD} = 11.7\text{ m}$ ). The spectra of the heavier molecules discussed here, taken at room temperature, can often be resolved using a resolution of better than  $0.001\text{ cm}^{-1}$ , avoiding then the need for complicated jet-cooling experiments.

### 1.3 Overview of the Article

First, we discuss briefly the experimental foundations of FTIR spectroscopy, in particular, the influence of aperture and self-apodization with regard to resolution. Spectra of CO, OCS, benzene ( $^{13}\text{C}_6\text{H}_6$ ),  $\text{NO}_2$ , and  $\text{CH}_4$  with its isotopomers covering the spectral range  $50\text{--}3100\text{ cm}^{-1}$  are presented and the line shape and width are discussed in relation to the  $d_{MOPD}$ , aperture, and molecular parameters.

Following this survey of experimental aspects, we review here the spectra of several molecules of current interest as examples and demonstrate current possibilities of the technique.  $\text{CHCl}_2\text{F}$  (Albert *et al.* 2004a) including cold cell spectra (Albert *et al.* 2007) is an example of a hydrochlorofluorocarbon of importance as a pollutant in the Earth's atmosphere, a molecule which can be isotopically chiral if one considers the  $^{37}\text{Cl}/^{35}\text{Cl}$  isotopomer. CDBrClF (Albert and Quack 2007b) is an example of an ordinary chiral molecule, and the heterocyclic compounds pyrimidine (Albert and Quack 2007b), pyridine, and naphthalene (Albert *et al.* 2010) are examples of aromatic systems.

The IR spectra of hydrochlorofluorocarbon molecules such as  $\text{CHCl}_2\text{F}$  and their rovibrational analysis are of crucial importance for understanding the absorption behavior of trace gases in the Earth's atmosphere, in particular, with respect to ozone depletion (Rinsland *et al.* 1989, Snels and Quack 1991) (and references cited therein). Recently, new satellite missions such as the Mipas experiment (Nett *et al.* 2001, Flaud and Oelhaf 2004) on Envisat and the ACE experiment (Nassar *et al.* 2005) have been underway to obtain more detailed information and more highly resolved spectra of fluorochlorohydrocarbons and other greenhouse gases. In addition, spectral analysis is an excellent approach for understanding the IR laser chemistry of these compounds (Lupo and Quack 1987, Quack 1989a, 1995) (and references therein). Analyses were possible in the past for many of these molecules only by using advanced FTIR and laser spectroscopic techniques in combination with supersonic jet cooling (Quack 1990, Snels and Quack 1991, Bauder *et al.* 1997, Snels *et al.* 2011: **High-resolution FTIR and Diode Laser Spectroscopy of Supersonic Jets**, this handbook) (and references therein). Now it is possible to record the spectra of fluorochlorohydrocarbons at low temperatures (120–170 K) in combination with high-resolution FTIR spectroscopy.

The chiral isotopomer  $\text{CH}^{35}\text{Cl}^{37}\text{ClF}$  is of potential importance for general aspects of isotopic chirality and parity violation (Quack 1989b, 2002, Berger *et al.* 2005, Albert and Quack 2007a). In particular, the rovibrational analysis of the  $2\nu_3$  mode of  $\text{CH}^{35}\text{Cl}^{37}\text{ClF}$  can make it possible to carry out quasiresonant two-photon transitions with a  $\text{CO}_2$  laser based on the assignments of the  $2\nu_3$  band (Albert *et al.* 2007).

CDBrClF, the deuterated isotopomer of CHBrClF, is a prototype chiral molecule like CHBrFI (Albert *et al.* 2008b) with asymmetric substitution at the "tetrahedral" carbon (van't Hoff 1899) with  $C_1$  point group symmetry. A detailed understanding of its properties, its spectra, and its dynamics is of fundamental interest. CHBrClF has been analyzed in detail with respect to its spectra and its intramolecular vibrational redistribution (IVR) dynamics (Beil *et al.* 1994b, 1996, 1997) as well as parity violation

(Bauder *et al.* 1997, Daussy *et al.* 1999, Quack and Stohner 2000, Laerdahl *et al.* 2000). CDBrClF offers the opportunity to investigate the effect of deuterium substitution on the spectrum. The vibrational spectrum of CDBrClF has been analyzed from the FIR to the NIR region (Beil *et al.* 2000). In addition, CDBrClF has been investigated together with CHBrClF in the fundamental region at lower resolution (Diem and Burow 1976, 1977, Diem *et al.* 1978). Studies of its vibrational circular dichroism (Marcott *et al.* 1977) and its Raman optical activity (Prasad and Burow 1979) have been reported. This molecule has also been investigated to study the effects of coupled anharmonic vibrations on molecular parity violation (Quack and Stohner 2003).

The rovibrational analysis of the CDBrClF spectra is challenging because of the congested spectra resulting from the low symmetry of the molecule and the presence of four different isotopomers and two quadrupolar nuclei in the same molecule. Very few rovibrational spectral analyses of chiral or isotopically chiral molecules have been reported to date, for CHBrClF (Bauder *et al.* 1997), fluorooxirane  $c\text{-C}_2\text{FH}_3\text{O}$  (Hollenstein *et al.* 1997), substituted thiiran-1-oxides (Gross *et al.* 1998), CDBrClF (Albert and Quack 2001, Albert *et al.* 2001a, 2003b),  $\text{CH}^{35}\text{Cl}^{37}\text{ClF}$  (Snels and Quack 1991, Albert *et al.* 2004a, Albert and Quack 2007b) and  $\text{C}_2\text{H}_3\text{DO}$  (Albert *et al.* 2003a), CHClFI (Soulard *et al.* 2006) (in an approach following closely the original work on CHBrClF (Bauder *et al.* 1997, Beil *et al.* 1994a)) and very recently CHBrIF (Albert *et al.* 2008b,c), aziridine-2-carbonitrile ( $\text{C}_3\text{H}_4\text{N}_2$ ), (Albert *et al.* 2008a), and oxirane carbonitrile ( $\text{C}_3\text{H}_3\text{NO}$ ), (Albert *et al.* 2009a), *see also* Quack 2011: **Fundamental Symmetries and Symmetry Violations from High-resolution Spectroscopy**, this handbook.

Few aromatic systems have been the subject of high-resolution FTIR spectroscopic studies to date. We mention here the benzene molecule (Hollenstein *et al.* 1990, Domenech *et al.* 1991, Pliva *et al.* 1996) and its isotopomers (Snels *et al.* 1997, 2002, Hippler and Quack 2005) and heterocyclic systems (Hegelund *et al.* 2005a,b, Palmer *et al.* 1998). In addition, high-resolution diode laser spectroscopy was carried out on fluoro- (Basterretxea and Escribano 2004) and chlorobenzene (Uskola *et al.* 2000) and there have been studies by isotope-selective spectroscopy (Hippler *et al.* 2003, 2011: **Mass and Isotope-selective Infrared Spectroscopy**, this handbook). We have recently studied chloro- and fluorobenzene systematically using high-resolution FTIR spectroscopy (Albert *et al.* 2006a, Albert and Quack 2006). These rovibrational analyses have also recently been extended to the more complicated aromatic systems 1,4 para-difluoro benzene, phenol (Albert and Quack 2008), and aniline, with large amplitude modes such as torsional and inversion modes.

The history of the low- and intermediate-resolution IR spectroscopy of pyridine,  $C_5H_5N$  (Turkevich and Stevenson 1943, Kline and Turkevich 1944, Stidham and DiLella 1979, 1980, DiLella 1980, Wong and Colson 1983, 1984, Walters *et al.* 1986, Klots 1998, Partal Urena *et al.* 2003), a heterocyclic molecule containing nitrogen, and the calculation of the vibrational modes are rich indeed and for a detailed survey the reader is referred to Partal Urena *et al.* (2003), Rauhut *et al.* (1999), Barone (2004) and references therein. There exists one rovibrational analysis of the partially resolved  $\nu_{11}$  band of pyridine (Thiel *et al.* 1991). A new and complete analysis of this band also including an analysis of the  $\nu_4$  and  $\nu_{12}$  bands is given by Albert *et al.* (2005). Here, we present only a part of the  $\nu_{11}$  band to demonstrate the visible influence of spin statistical weights. In particular, the complete analysis of the  $\nu_{11}$  and  $\nu_4$  bands provides a starting point for a successful interstellar search for pyridine in the IR region because these bands lie in the same absorption window as the recently detected  $\nu_4$  band of benzene (Cernicharo *et al.* 2001). Submillimeter measurements up to 400 GHz (Ye *et al.* 2005) were used to obtain extended rotational constants of the ground state and first spectroscopic constants of five excited states.

The history of the analysis of the low-resolution IR spectrum of pyrimidine ( $C_4H_4N_2$ ), a heterocyclic molecule containing two nitrogen atoms, started with a report in the book by Barnes (Bowling Barnes *et al.* 1944) and the papers of Brownlie (Brownlie 1950), Short and Thompson (Short and Thompson 1952), Lord *et al.* (Lord *et al.* 1957), and Ito *et al.* (Ito *et al.* 1956). For a detailed survey of the low-resolution IR spectroscopy of pyrimidine and the calculation of the vibrational modes, the reader is referred to a review by Innes *et al.* (Innes *et al.* 1988) and to some recent work by Billes *et al.* (Billes *et al.* 1998), Breda *et al.* (Breda *et al.* 2006), Barone (Barone 2004), and Boese and Martin (Boese and Martin 2004) and references therein. Despite extensive work, the vibrational assignment of the normal modes of pyrimidine is still ambiguous.

The electronically excited states of pyrimidine and its photodissociation dynamics (Lin *et al.* 2006) are the subject of several papers. We mention here an analysis of highly resolved rovibrational lines in the  $^1B_1$  electronic excited state by Konings *et al.* (Konings *et al.* 1988), Philis (Philis 2005), and a recent analysis of singlet and triplet electronic excited states by Fischer *et al.* (Fischer *et al.* 2003), to which we refer for a more detailed survey of the status of the electronic spectrum of pyrimidine. The rotational spectrum of pyrimidine was analyzed up to the submillimeter region by Kisiel *et al.* (Kisiel *et al.* 1999). In addition, these authors assigned the rotational absorption lines of the three lowest excited vibrational states, the  $\nu_{16a}$ ,  $\nu_{16b}$ , and  $\nu_{6b}$  states. The high-resolution FTIR spectrum of pyrimidine has been completely analyzed in the region  $600\text{--}1000\text{ cm}^{-1}$

including the modes  $\nu_{6b}$ ,  $\nu_4$ , and  $\nu_{10b}$  (Albert and Quack 2007b). The rotational constants  $A$  and  $B$  of the ground state of pyrimidine have also been determined by time-resolved femtosecond Raman spectroscopy (Lavorel *et al.* 2004).

The heterocyclic molecule pyrimidine is a prototype system for biologically important molecules such as the RNA and DNA bases. Indeed, the pyrimidine bases are perhaps crucial in molecular evolution (Eschenmoser 1997, Mittapalli *et al.* 2007). An analysis of the rovibrational spectrum of pyrimidine may provide a starting point for a better understanding of the spectra of the DNA bases and their dynamics. Considering the astrochemical aspect, the analysis of the  $\nu_4$  band may be a starting point for a successful interstellar search for pyrimidine in the IR region because this band lies in the same absorption window as the recently detected  $\nu_4$  band of benzene (Cernicharo *et al.* 2001). Here, we describe the analysis of the  $\nu_4$  band of pyrimidine.

One of the great challenges of astronomical IR spectroscopy is the identification of the unidentified infrared bands (UIBs) found in several interstellar objects. Polycyclic aromatic hydrocarbons (PAHs) have been proposed to be the carrier of the UIBs (Tielens 2008). For this reason, we have investigated the rotationally resolved FTIR spectrum of the bicyclic molecule naphthalene (Albert *et al.* 2010) as a simple prototypical spectrum for a PAH IR spectrum. Naphthalene has already been analyzed at high resolution in the UV region (Majewski and Meerts 1984, Kabir *et al.* 2003) and in the IR region (Pirali *et al.* 2009, Hewett *et al.* 1994). We present an analysis of the out-of-plane mode  $\nu_{46}$  of naphthalene at  $12.78\text{ }\mu\text{m}$ , which includes more than 3000 absorption lines. On the basis of rotational constants, we have simulated the band at resolutions that are used for the interstellar detection of the UIBs. Clearly, this band is not responsible for the UIB at  $11.25\text{ }\mu\text{m}$ . However, the shape of the recorded naphthalene band,  $\nu_{46}$ , provides valuable insights into the shape of bands of out-of-plane modes of PAHs. There is a coincidence with the unidentified infrared band (UIB) at  $7.8\text{ }\mu\text{m}$  (Tielens 2008).

## 2 EXPERIMENTAL PRINCIPLES OF INTERFEROMETRIC FOURIER TRANSFORM INFRARED SPECTROSCOPY

### 2.1 Basic Experimental Setup

The heart of an FTIR spectrometer is the Michelson interferometer (Michelson 1881, Brault 1985, Genzel 1998) as shown in Figure 1. Light is emitted from a source  $S$ , which can be a mercury arc lamp, a globar, a tungsten

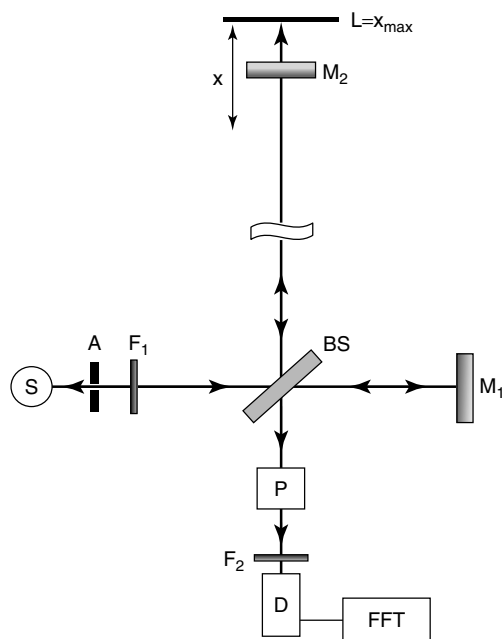


**Figure 1** A schematic drawing of the Michelson interferometer as the heart of an FTIR spectrometer (S: source, A: aperture,  $F_1$ : focal parabolic mirror, BS: beam splitter,  $M_1$ : fixed corner cube mirror,  $M_2$ : movable retro reflector mirror (scanner), P: probe,  $F_2$  focal parabolic mirror, D: detector, FFT: fast Fourier transformation,  $x$ : path length,  $L = x_{\max} = d_{\text{MOPD}}/2$  with  $d_{\text{MOPD}}$  = maximum optical path difference).

lamp, or a synchrotron radiation beam. The light is then focused on the aperture A, which has a diameter between 0.5 and 3 mm. The diverging light emitted from the aperture is made parallel using the parabolic mirror  $F_1$ , which has a focal length of 41.8 cm in the Bruker IFS 120/125 series. The parallel beam waist is of diameter 68 cm. The parallel beam is then split using a beam splitter BS consisting of mylar, Quartz, KBr or  $\text{CaF}_2$  typically. One half of the beam travels through the beam splitter to a fixed retroreflector  $M_1$  and is reflected. The other half of the beam is reflected at the beam splitter and travels to the movable retroreflector  $M_2$ , the scanner, and is also reflected. The reflected beams are then combined at the beam splitter again. The recombined beam illustrates constructive or destructive interference depending on the path difference between the fixed retroreflector  $M_1$  and the movable retroreflector  $M_2$ . The recombined beam then passes through the probe P and is focused again through the parabolic mirror  $F_2$  on the detector chip D. The interference pattern, as a function of the optical path difference of the two beams, is the interferogram. By the use of a Fourier transformation, performed with the fast Fourier transform (FFT) algorithm, the interferogram is transformed into the spectrum.

The use of retroreflectors requires a more detailed description (Murty 1960). At the retroreflectors  $M_1$  and  $M_2$ ,

the incoming and reflected beams are different; therefore, two beams result after the recombination at the beam splitter. The recombined beam from the two beams that were reflected at the beam splitter is called the *balanced output* and is used for the measurement; it passes through the probe onto the detector. The other recombined beam for which one beam is passed through the beam splitter and the other beam is twice reflected at the beam splitter is called the *unbalanced output* and is removed by high pass filters. In the case of plane parallel mirrors, the unbalanced output is routed straight back into the source.

The Zurich prototype 2001 spectrometer Bruker IFS 125 HR, a nine-chamber system, is a newly designed version based on the Bruker IFS 120 HR, a five- to seven-chamber system. Its maximum optical path difference ( $d_{\text{MOPD}}$ ) is 9.8 m. It is equipped with apertures as small as 0.5 mm, making it possible to record rovibrational spectra with a resolution up to  $0.00062 \text{ cm}^{-1}$  (unapodized). It has a theoretical resolving power of up to  $2 \times 10^6$  at  $2000 \text{ cm}^{-1}$ . The ETH-SLS prototype 2009 spectrometer Bruker IFS 125 HR is a new extended version of the IFS 125 series. It is an 11-chamber interferometer-arm system with a  $d_{\text{MOPD}}$  of 11.7 m, which corresponds to a theoretical maximum unapodized resolution of  $0.00053 \text{ cm}^{-1}$ .

## 2.2 Interferogram, Spectrum and Line Shape

In this section, we briefly review the basic equations of interferometric FTIR spectroscopy and refer to the books of Chamberlain (Chamberlain 1979) and Davis *et al.* (Davis *et al.* 2001) for a more detailed discussion. We then illustrate the quantitative aspects with examples of spectra obtained using the highest resolution FTIR spectrometers currently commercially available, the 2001 ETH Zürich prototype and the ETH-SLS 2009 prototype interferometers built by Bruker Optics.

The basic principle of interferometric spectroscopy using the Michelson interferometer in Figure 1 is readily understood, starting out from an ideal monochromatic light source S. It is seen that the two ideal monochromatic sine wave partial beams from the beam splitter BS are reflected at  $M_1$  and  $M_2$  and recombined at the beam splitter BS, interfering constructively or destructively depending on the variable position  $x$  of the movable mirror  $M_2$ . The signal  $I^{\text{interf}}(x)$  measured at the detector D (neglecting effects from other optical elements and the probe P) has the intensity function (with a source constant A):

$$I^{\text{interf}}(x) = A [1 + \cos(2\pi \tilde{\nu}_0 x)] \quad (1)$$

When one has instead a broad band “white light” source S with a wavenumber-dependent intensity distribution  $I(\tilde{\nu})$ ,

one obtains the interference signal (Chamberlain 1979):

$$I^{\text{interf}}(x) = \int_0^{\infty} I(\tilde{\nu}) d\tilde{\nu} + \int_0^{\infty} I(\tilde{\nu}) \cos(2\pi\tilde{\nu}x) d\tilde{\nu} \quad (2)$$

which is obtained by integrating over all wavenumbers  $\tilde{\nu}$ . Because we have for  $x = 0$

$$I^{\text{interf}}(x) = 2 \int_0^{\infty} I(\tilde{\nu}) d\tilde{\nu} \quad (3)$$

we obtain

$$I^{\text{interf}}(x) = \frac{1}{2} I^{\text{interf}}(0) + \int_0^{\infty} I(\tilde{\nu}) \cos(2\pi\tilde{\nu}x) d\tilde{\nu} \quad (4)$$

The variable part of  $I^{\text{interf}}(x) - 0.5I^{\text{interf}}(0) = F(x)$  is called the *interferogram*:

$$F(x) = \int_0^{\infty} I(\tilde{\nu}) \cos(2\pi\tilde{\nu}x) d\tilde{\nu} \quad (5)$$

$F(x)$  is the cosine Fourier integral of the wavenumber-dependent spectral density  $I(\tilde{\nu})$  and by inversion of the transform, one obtains

$$I(\tilde{\nu}) = C \int_0^{\infty} F(x) \cos(2\pi\tilde{\nu}x) dx \quad (6)$$

where  $C$  can be considered to be a normalization constant. This inverse transform allows us, therefore, to calculate the wavenumber-dependent intensity  $I(\tilde{\nu})$ . We write here the dimension of  $I(\tilde{\nu})$  as  $\text{dim}(\text{Wm}) = \text{dim}(\text{W}/\text{m}^{-1})$  because of Equation (4) and

$$\int_0^{\infty} I(\tilde{\nu}) d\tilde{\nu} = I_{\text{total}} \quad (7)$$

and  $\text{dim}(I_{\text{total}}) = \text{dim}(\text{W})$ . Further considerations become necessary when the measurement and the corresponding integration in Equation (6) are carried out over a finite interval to some maximum value  $x_{\text{max}}$  instead of  $x = \infty$ .

The finite maximum optical path difference ( $d_{\text{MOPD}}$ ) leads to a multiplication of the interferogram with a rectangular function  $\Pi$ , which results in the instrumental line function  $S_{\text{inc}}(\tilde{\nu})$  in the spectral domain by the use of the  $\text{sinc} = \sin(\pi x)/(\pi x)$  function shown in Figure 2 (Davis *et al.* 2001):

$$\begin{aligned} S_{\text{inc}}(\tilde{\nu}) &= 2d_{\text{MOPD}} \left( \frac{\sin(2\pi\tilde{\nu}d_{\text{MOPD}})}{(2\pi\tilde{\nu}d_{\text{MOPD}})} \right) \\ &= 2d_{\text{MOPD}} \text{sinc}(2\tilde{\nu}d_{\text{MOPD}}) \end{aligned} \quad (8)$$

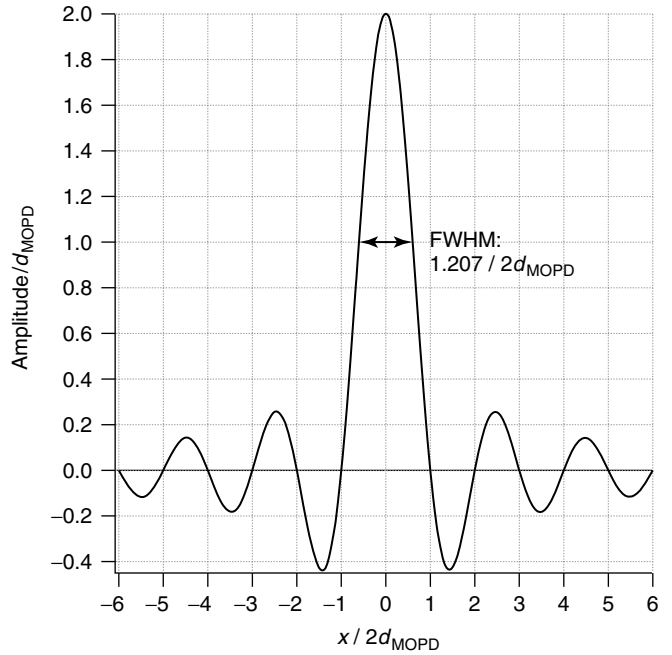


**Figure 2** The  $2d_{\text{MOPD}} \text{sinc}(2\tilde{\nu}d_{\text{MOPD}})$  function where  $\text{sinc}(2\tilde{\nu}d_{\text{MOPD}}) = \sin(2\pi\tilde{\nu}d_{\text{MOPD}})/(2\pi\tilde{\nu}d_{\text{MOPD}})$ .

The full width at half maximum  $\Delta\tilde{\nu}_{\text{FWHM}}$  of this instrumental line function is

$$\Delta\tilde{\nu}_{\text{FWHM}} = \left( \frac{1.207}{2d_{\text{MOPD}}} \right) \quad (9)$$

The  $\Delta\tilde{\nu}_{\text{FWHM}}$  of the *sinc* function is defined as the “unapodized” resolution of the interferometer. Using Equation (9) we obtain for the ETH Zurich FTIR 2001 prototype spectrometer a value of  $0.00062 \text{ cm}^{-1}$  for  $d_{\text{MOPD}} = 980 \text{ cm}$  and for the ETH-SLS 2009 prototype spectrometer a value of  $0.00053 \text{ cm}^{-1}$  for  $d_{\text{MOPD}} = 1170 \text{ cm}$ .

Because of the use of a finite aperture (Brault 1985, Connes 1970, Ridgway and Brault 1984), we have to consider two other important effects, an additional broadening of the absorption line and a shift of the line position (Davis *et al.* 2001). The finite aperture  $d$  produces circular fringes at the interferometer output at a certain finite path difference. This implies that the envelope of the interferogram is multiplied by a wavenumber-dependent *sinc* function. This effect is called *self-apodization*. To find an optimum aperture diameter  $d$ , we want a maximum fringe amplitude for the largest measurable wavenumber  $\tilde{\nu}_{\text{max}}$  at the longest optical path difference so that we have constructive interference. Considering the solid angle  $\Omega_{\text{max}}$  defined as

$$\Omega_{\text{max}} = \frac{(\pi/4) d^2}{f^2} = \frac{\pi}{d_{\text{MOPD}} \tilde{\nu}_{\text{max}}} \quad (10)$$

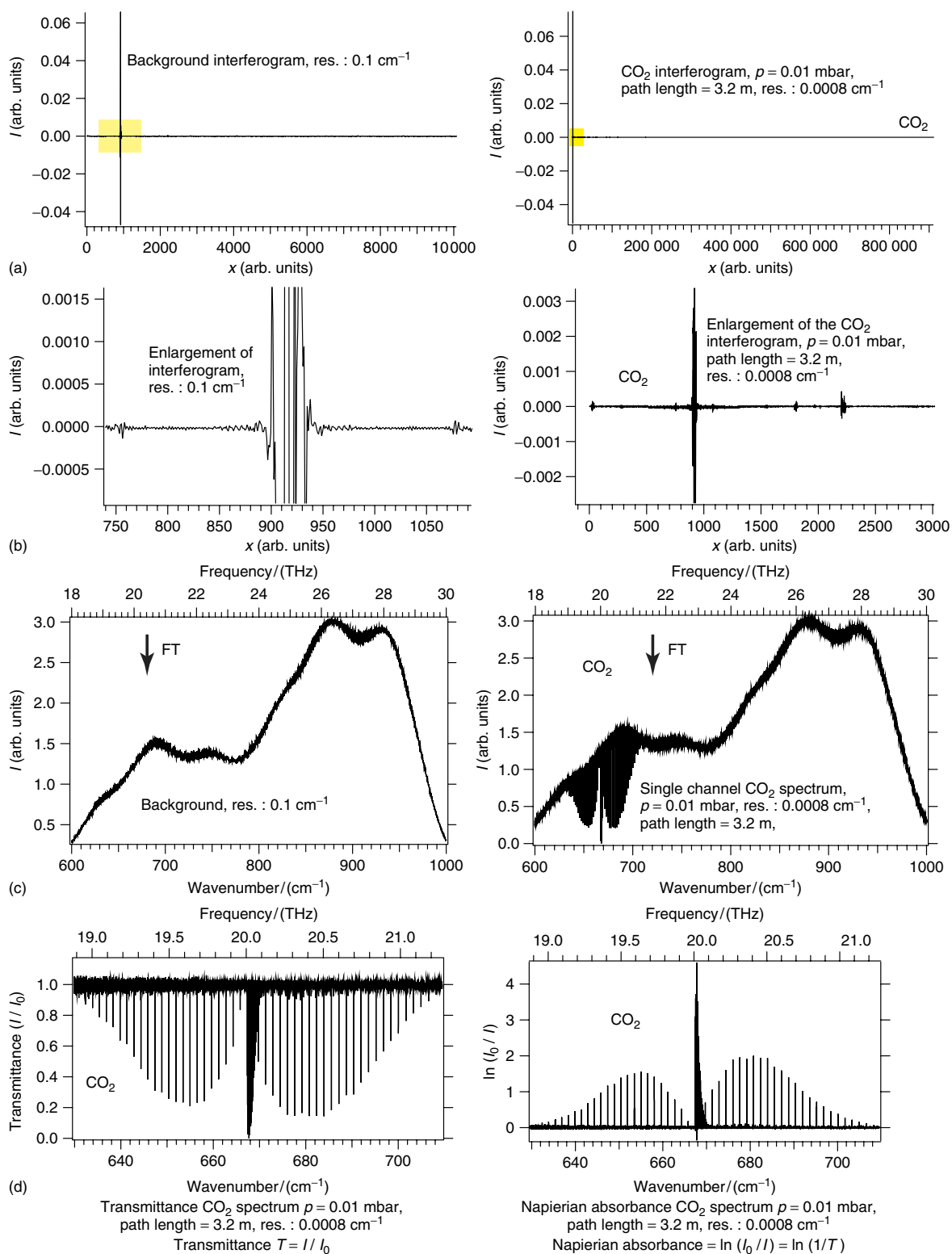


**Figure 3** Calculating transmittance and absorbance spectra. (a) The interferogram of an empty cell (left), which is an interferogram of the background, and an interferogram of the cell filled with  $0.01 \text{ mbar}$   $\text{CO}_2$  (right). (b) Enlargements of the interferograms in the centerburst region. (c) Single-channel spectra of the background (left) and of  $\text{CO}_2$  (right) calculated by Fourier transformation (FT) from the interferograms. The background spectrum is recorded at low resolution,  $0.1 \text{ cm}^{-1}$ , and the  $\text{CO}_2$  spectrum at high resolution,  $0.0008 \text{ cm}^{-1}$ . (d) Transmittance spectrum of  $\text{CO}_2$  (left) in the bending region ( $01^{1e,f}0-000$ ) calculated from the single-channel spectra of  $\text{CO}_2$  and the background, and the Napierian absorbance spectrum of  $\text{CO}_2$  (right).

we can choose the optimum diameter  $d$  of the aperture according to

$$d = \sqrt{\frac{4f^2}{d_{\text{MOPD}} \tilde{\nu}_{\text{max}}}} \quad (11)$$

For our setup, we have, for instance,  $f = 41.8$  cm as the focal length of the parabolic mirror of both Bruker spectrometers (Bruker 1989).

Practically speaking, this means that the real line-shape function, which would typically have a Gaussian–Doppler-limited profile with a peak position  $\tilde{\nu}_0$ , is convoluted with the instrumental line-shape function:

$$S_I(\tilde{\nu}) \simeq \left[ \Omega_{\text{max}} \frac{2\pi}{\tilde{\nu}_0 \Omega_{\text{max}}} \Pi \left( \frac{2\pi \tilde{\nu}}{\tilde{\nu}_0 \Omega_{\text{max}}} \right) \right] \otimes 2 d_{\text{MOPD}} \text{sinc}(2\tilde{\nu} d_{\text{MOPD}}) \quad (12)$$

due to the finite path difference ( $\text{sinc}(2\tilde{\nu} d_{\text{MOPD}})$ ), and with an external rectangular “boxcar” function  $\Pi$  with width  $(\tilde{\nu}_0 \Omega_{\text{max}})/(2\pi)$  due to the finite aperture (Davis *et al.* 2001). In even more general terms, the instrumental line-shape function  $S_I(\tilde{\nu})$  can be considered to be the experimental line shape measured for an extremely sharp line with  $\Delta\tilde{\nu}_{\text{true}} \ll \Delta\tilde{\nu}_I$ , which thus becomes an experimentally defined and measurable quantity.

In practice, one uses optical filters to restrict the broad band “white light” source to the spectral range of interest for a particular absorption band. This then defines the intensity  $I_0(\tilde{\nu})$ . Figure 3 shows the spectrum of the broad band source (c, left) and the corresponding interferogram (a, left) that corresponds to an empty probe volume  $P$ , and hence to the reference intensity  $I_0(\tilde{\nu})$ . In the example, we show the spectral range 600–1000  $\text{cm}^{-1}$  including a filter used to measure the  $\text{CO}_2$  spectrum in the region of the bending fundamental. By repeating the measurement with a sample of  $\text{CO}_2$  in the (Figure 3c, right) probe volume, we obtain an analogous function  $I(\tilde{\nu})$  (Figure 3c, right) and the relevant interferogram (Figure 3a,b, right). Finally, we can compute the transmittance spectrum from  $I_0(\tilde{\nu})$  and  $I(\tilde{\nu})$

$$T(\tilde{\nu}) = \frac{I(\tilde{\nu})}{I_0(\tilde{\nu})} \quad (13)$$

shown in Figure 3(d, left) and the Napierian absorbance spectrum ( $\ln = \log_e$ )

$$A_e(\tilde{\nu}) = \ln(T^{-1}(\tilde{\nu})) \quad (14)$$

shown also in Figure 3(d, right). Under certain conditions, the Napierian absorbance  $A_e(\tilde{\nu})$  can be related to the molecular absorption cross section  $\sigma(\tilde{\nu})$  by means of the Lambert–Beer law:

$$A_e(\tilde{\nu}) = \sigma(\tilde{\nu}) C l \quad (15)$$

where  $C$  is the molecular concentration as particle density and  $l$  the effective absorption path length. Frequently one also uses the decadic absorbance ( $\lg = \log_{10}$ )

$$A_{10}(\tilde{\nu}) = \lg(T^{-1}(\tilde{\nu})) \quad (16)$$

All these effects exclude surface and window contributions that one must take into account if appropriate. For definitions of further frequently used quantities related to such absorption measurements, we refer to Stohner and Quack 2011: **Conventions, Symbols, Quantities, Units and Constants for High-resolution Molecular Spectroscopy**, this handbook. Equation (15) is valid if  $\sigma(\tilde{\nu})$  is independent of  $C$  and  $C$  independent of  $l$ . If this is not the case, appropriately modified relations can be used.

Figure 4(a) left shows the survey of the absorbance spectrum of  $\text{CO}_2$  in the range of the bending fundamental, causing an important absorption in the Earth’s atmosphere, in part at the origin of the greenhouse effect. Figure 4(a) right shows the corresponding FTIR spectrum of air at 298 K and 1013 mbar. The pressure broadened  $\text{CO}_2$  lines are visible. In Figure 4b, a line in absorbance and transmittance is shown. The absorbance line shape is fit to a Gaussian line shape and the value of the Doppler width obtained through this fit (see below) is slightly larger than the calculated Doppler width.

The measured spectral signal is the convolution of the true spectrum  $I(\tilde{\nu})$  with an instrument function  $S_I(\tilde{\nu})$ :

$$I_{\text{eff}}(\tilde{\nu}) = I(\tilde{\nu}) \otimes S_I(\tilde{\nu}) \quad (17)$$

In considering the line-shape functions of sharp individual spectral lines, because of the finite length interferogram, the true sharp spectral line is convoluted with a *sinc* function in the case of an ideal “boxcar apodization”. This will lead to minimal effects if the width of the true absorption line is large compared to the width of the instrumental *sinc* function. If, however, the instrumental line width is large compared to the true line width, the oscillatory behavior of the *sinc* function will appear as side lobes to the measured line (“feet”) and one has to reduce this artifact by multiplying the interferogram with an “apodization function” (from the Greek *πous*, gen. *ποδος* and the negation “a-”, “removing” the feet that is at the origin of the expression). The general expression in Equation (6) is multiplied by a weighting function  $W(x)$  such that, with an appropriate normalization constant  $a$ ,

$$I_{\text{eff}}(\tilde{\nu}) = a \int_0^\infty F(x) W(x) \cos(2\pi \tilde{\nu} x) dx \quad (18)$$

In the simplest ideal case, the weighting function takes into account the length of the interferogram that removes the

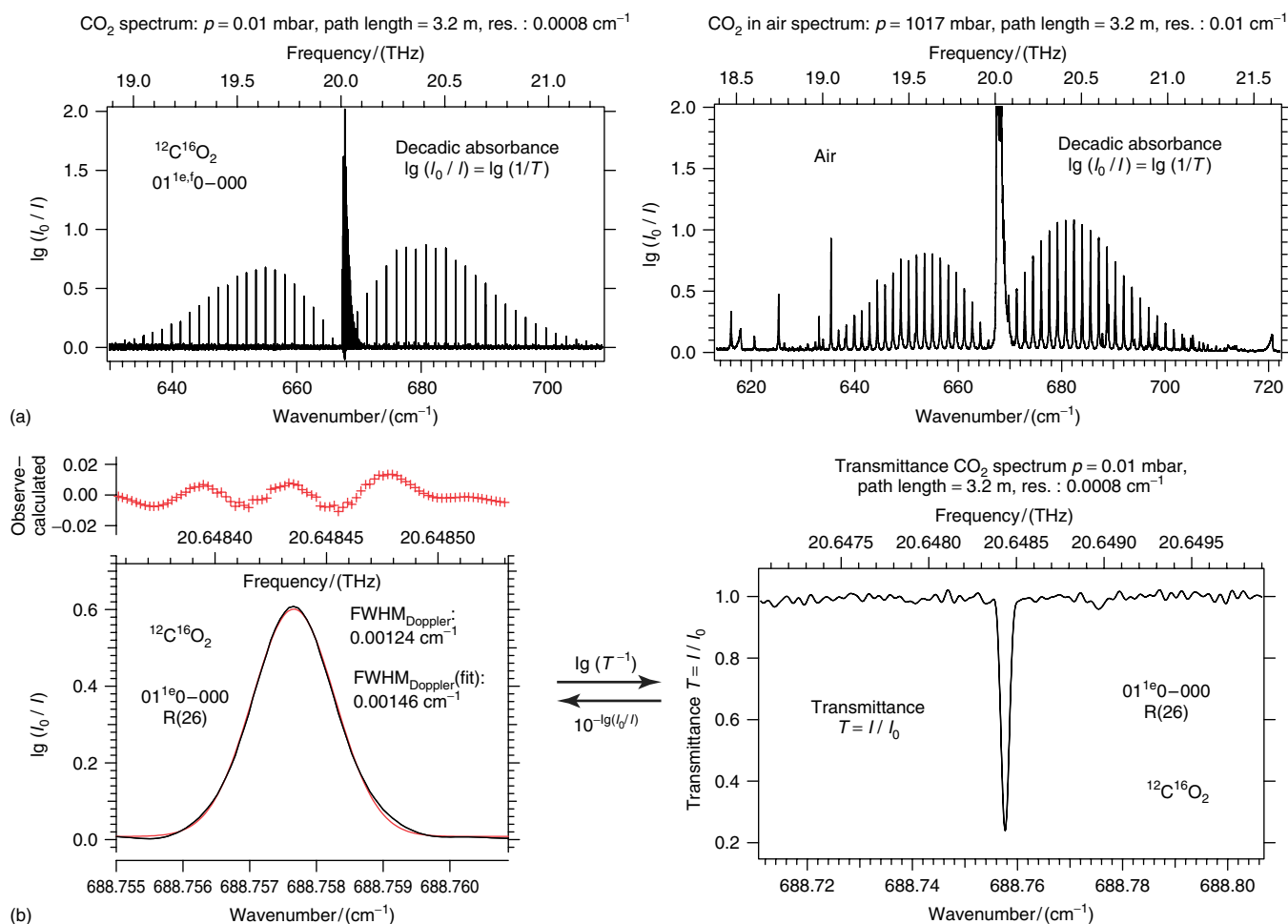


**Figure 4** (a) Decadic absorbance spectrum of CO<sub>2</sub> (left) and air (right) in the CO<sub>2</sub> bending region ( $01^{16}0-000$ ). The air spectrum is pressure broadened. (b) The R(26) absorption line of the CO<sub>2</sub>  $01^{16}0-000$  band (left). The line profile is fitted to a Gaussian line profile. The apparent Doppler width  $\Delta\tilde{\nu}_D = 0.00146\text{ cm}^{-1}$  is slightly larger than the calculated Doppler width due to the use of a larger aperture. The transmittance spectrum of this line is shown on the right.

signal for  $x > L$  where  $L = d_{\text{MOPD}}$ , and thus

$$W_b(x) = 1 - h(x - L) \quad (19)$$

where  $h(z)$  is the Heaviside unit step function with

$$h(z < 0) = 0 \quad (20)$$

$$h(z > 0) = 1 \quad (21)$$

It is the step function that leads to the oscillating *sinc* function. Using a function with a more gradual cutoff decreases the amplitude of the side lobes arising from the *sinc* function, while, at the same time, the width of the main peak increases, reducing the resolution. In principle, one can also define weighting functions that increase resolution at the cost of having larger oscillations. All these functions are called *apodization functions*, even though some of them do not remove the “feet”. The problem of

finding optimum apodization functions under appropriate constraints has a long history in signal processing (Dolph 1946, Vagin 1980) and Norton and Beer (Norton and Beer 1976, 1977) have provided a useful practical summary for FTIR spectroscopy. From the present point of view of very high-resolution interferometric spectroscopy, the spectra are measured in self-apodization and the physically truncated path difference  $d_{\text{MOPD}}$  is mathematically expressed as apodization with the boxcar truncation function  $W_b(x)$  in the mid-IR and NIR where the spectra are usually Doppler limited (i.e.,  $\Delta\tilde{\nu}_D > \Delta\tilde{\nu}_I$ ). In these regions, no other apodization functions are needed. The situation is different in the FIR when using samples at low temperature and with high molecular mass. Then the various side peaks can cause trouble in the analysis of the spectra and have to be removed by the use of an appropriate apodization function if self-apodization alone is not sufficient.

### 2.3 Observed Line Shape and Simulation of Spectra

In considering spectral line broadening and line shapes in IR spectra, one must consider the true physical line shape in addition to the instrumental line shape discussed above. The following contributions are dominant in IR spectra:

1. Gaussian line shape corresponding to the Doppler effect arising from the thermal Maxwell–Boltzmann distributions of molecular velocities. In terms of the resulting molecular absorption cross section  $\sigma(\nu)$  as a function of frequency  $\nu$ , this results in the following line shape:

$$\sigma_G(\nu) = \sigma_0 \exp\left[\frac{-c^2(\nu - \nu_0)^2}{v_w^2 \nu_0^2}\right] \quad (22)$$

Here  $\sigma_0$  is the maximum cross section,  $\nu_0$  the frequency at this maximum,  $c$  the speed of light in vacuo, and  $v_w$  the most probable velocity in the distribution:

$$v_w = \sqrt{\frac{2kT}{m}} \quad (23)$$

The full width at half maximum ( $\Delta\nu_D$ ) for the line shape is conveniently given by the dimensionless reduced form is

$$\frac{\Delta\nu_D}{\nu_0} = \frac{\Delta\tilde{\nu}_D}{\tilde{\nu}_0} = \sqrt{\frac{8kT \ln 2}{mc^2}} \simeq 7.162 \cdot 10^{-7} \sqrt{\frac{T(\text{K})}{m(\text{Da})}} \quad (24)$$

At low gas densities in the vapor or in molecular beams, this is usually the dominant contribution in high-resolution FTIR spectroscopy, and in mid-IR and NIR regions it is also the usual limiting factor in the effective resolution because Doppler-free techniques are not readily applied with FTIR spectroscopy (laser spectroscopy is more suitable for such approaches; see also Demtröder 2011: **Doppler-free Laser Spectroscopy**, this handbook). For a given molecule with mass  $m$  and spectral line position  $\nu_0$ , the Doppler broadening can be reduced by lowering the temperature. Recent very successful techniques are nonequilibrium cooling in supersonic jets (Quack 1990) or (Snels *et al.* 2011: **High-resolution FTIR and Diode Laser Spectroscopy of Supersonic Jets**, this handbook) spectroscopy in collisional cooling cells operated either under equilibrium or nonequilibrium conditions (Albert *et al.* 2007 and references therein).

2. The other important line shape in the IR corresponds to the Lorentzian (or Cauchy) distribution, again for the

molecular absorption cross section  $\sigma_L(\nu)$ :

$$\sigma_L(\nu) = \sigma_0 \frac{(\Delta\nu_L/2)^2}{(\nu - \nu_0)^2 + (\Delta\nu_L/2)^2} \quad (25)$$

$\sigma_0$  is again the maximum cross section in the line and  $\nu_0$  the corresponding frequency, while  $\Delta\nu_L$  is the full width at half maximum (FWHM) of the absorption line. The factors contributing to the Lorentzian line shape are exponential (first-order) decay processes, which contribute in an additive way to the line width. We discuss three of these:

$$\Delta\nu_L = \Delta\nu_n + \Delta\nu_i + \Delta\nu_c \quad (26)$$

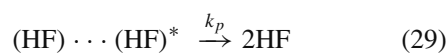
These contributions correspond to first-order rate constants for the corresponding rate process:

$$k_L = k_n + k_i + k_c \quad (27)$$

The “natural line width”  $\Delta\nu_n$  is related to the rate constant  $k_n$  for spontaneous emission:

$$k_n = 2\pi \Delta\nu_n = 2\pi c \Delta\tilde{\nu}_n = \frac{2\pi \Gamma_n}{h} \quad (28)$$

where  $\Gamma_n$  is the full width at half maximum of the Lorentzian line in the absorbance spectrum. In the IR  $k_n$  rarely exceeds  $10^3 \text{ s}^{-1}$  for rovibrational spectra, so the natural line width contribution from spontaneous emission can be usually neglected in FTIR spectroscopy except when observing electronic transitions in the IR or visible part of the spectrum. The second factor  $k_i$  can arise, for instance, if one has a predissociating molecular complex, where vibrational excitation in the IR can lead to dissociation of a weak bond such as in the hydrogen-bonded dimer (HF)<sub>2</sub> (Puttkamer and Quack 1989, Hippler *et al.* 2007):



$$k_i = k_p = 2\pi \Delta\nu_i \quad (30)$$

Other intramolecular processes that can lead to broadening are internal conversion after electronic excitation or intramolecular vibrational redistribution (IVR) in highly excited or very large polyatomic molecules at high vibrational densities of states (Puttkamer *et al.* 1983). At low densities of states, for small stable molecules at modest excitation, these processes are absent in terms of an exponential relaxation to a continuum and thus do not contribute to the Lorentzian line widths. Indeed, the dominant Lorentzian contribution  $\Delta\nu_c$  in the IR usually arises from bimolecular collisions. If the collisions of molecules  $A$  occur with inert

gaseous “solvent” molecules or atoms  $M$  as collision partners  $\Delta\nu_c$  is related to a pseudo first-order rate constant  $k_c$  for collisions:

$$k_c = 2\pi \Delta\nu_c = 2\pi c \Delta\tilde{\nu}_c \quad (31)$$

where  $k_c$  is given by

$$k_c = \sqrt{\frac{8kT}{\pi\mu}} \langle\sigma_{AM}\rangle [M] \quad (32)$$

where  $\mu$  is the reduced mass for the collision

$$\mu = \frac{m_A \cdot m_M}{m_A + m_M} \quad (33)$$

where  $k$  is the Boltzmann constant,  $[M]$  the particle density (concentration) of the collision partner  $M$  assumed to be in excess (for example,  $M = \text{He}$  or  $\text{N}_2$  in a collisional cooling cell) and  $\langle\sigma_{AM}\rangle$  is the thermally averaged collision cross section. Its exact calculation is highly nontrivial and typical values can range over several orders of magnitude depending on the collision partners. However, a first estimate for inert collision partners results in a pressure proportional line width  $\Delta\tilde{\nu}_c = 0.1 \text{ cm}^{-1} p / \text{bar}$ . Thus, at pressures below 1 mbar, collisional broadening can normally be neglected except sometimes for larger molecules such as pyridine and naphthalene and dipolar molecules. Measurements at low density also avoid the problem of the collisional line shift (i.e.,  $\nu_0([M]) \neq \nu_0([M] \rightarrow 0)$ ).

The convolution of Lorentzian and Gaussian (Doppler) broadening results in the Voigt line shape:

$$P(x, y) = \frac{c}{\nu_0 \nu_w} \frac{1}{\sqrt{\pi}} K(x, y) \quad (34)$$

with

$$x = \frac{2(\nu - \nu_0)\sqrt{\ln 2}}{\Delta\nu_D} \quad (35)$$

and

$$y = \frac{\Delta\nu_L/2}{\Delta\nu_D} \sqrt{4 \ln 2} \quad (36)$$

The Voigt function  $K(x, y)$  is given by the integral

$$K(x, y) = \frac{y}{\pi} \int \frac{\exp(-r^2)}{y^2 - (x-r)^2} dr \quad (37)$$

which is usually evaluated numerically. The use of the variables  $x$  and  $y$  can be considered as a scaling of the

frequency axis with the Doppler widths. One can easily verify that for vanishing Lorentzian width  $\Delta\nu_L \rightarrow 0$  (i.e.,  $x \rightarrow 0$  for given  $\Delta\nu_D$ ), one obtains a function  $P(x, 0)$  that is the Gaussian line shape and for vanishing Doppler width ( $\Delta\nu_G \rightarrow 0, x \rightarrow \infty$  and  $y \rightarrow \infty$  one has  $P(x \rightarrow \infty, y \rightarrow \infty)$  for given  $\Delta\nu_L$ ) as the Lorentzian function. However, the physical line shape cannot always be represented as a convolution of Doppler and Lorentzian line shapes because the kinetic phenomena are not independent. Particularly in the case of self-collisions, further phenomena arise that can even lead to collisional narrowing with increasing pressure over some ranges (Dicke effect, Dicke 1953). The generally very complex situation of non-Voigt line shapes under collisional conditions, including line mixing and line shifting, is discussed in the book by Hartmann *et al.* 2008 (see also Albert *et al.* 2011: **Fundamentals of Rotation–Vibration Spectra**, this handbook). One also must note that lineshapes due to intramolecular processes with  $\Delta\nu_i$  need not be Lorentzian, in general, and Doppler line shapes need not to be Gaussian in nonthermal situations, for example, in supersonic jets.

In simulating FTIR spectra with the physical line shapes discussed above and the instrumental line shapes derived in the previous section, one has to recognize that the former apply to the molecular absorption cross section and thus (under certain conditions) are proportional to the absorbance,  $\ln(I_0/I)$  or  $\lg(I_0/I)$  (Equations 15 and 16), whereas the latter apply to the signal intensity  $I(\tilde{\nu})$  or to  $T(\tilde{\nu})$  (Equation 13), which is proportional to  $I(\tilde{\nu})$  if  $I_0(\tilde{\nu})$  is smooth, effectively constant over the range of a line shape. However,  $T(\tilde{\nu})$  and  $\sigma(\tilde{\nu})$  have a nonlinear relationship in general. A proper simulation of spectral line shapes is thus best carried out as a “forward simulation” by simulating the spectral line shapes using the appropriate line-shape function for every spectral line and composing a complete “true” absorbance spectrum from all relevant lines for the given experimental conditions. From this, one calculates the transmission spectrum  $T(\nu)$  (with obviously neither Gaussian nor Lorentzian line shape because of the exponential relationship). This transmission spectrum is then convoluted with the instrumental line-shape function  $S_I$ . Even more generally, one must convolute  $I_0(\tilde{\nu})$  and  $I(\tilde{\nu})$  separately with the instrument function and then calculate  $T(\nu)$ . However, in general, this procedure is not necessary for a smooth  $I_0(\tilde{\nu})$ , which is effectively constant over the range of the line shape. For a final comparison of simulated spectra, one may recompute an effective absorbance from the simulated transmission by means of Equation (14) and compare this to the experimental absorbance. In the limit of small absorptions, one can “linearize” the Lambert–Beer relation by means of the Taylor expansion of the exponential function:

$$T(\nu) = \frac{I(\nu)}{I_0(\nu)} = \exp(-\sigma(\nu) C l) \quad (38)$$

using for small values of  $\alpha = (I_0(\nu) - I(\nu))/I_0(\nu) = \Delta I(\nu)/I_0(\nu)$  the approximation

$$T(\nu) = \frac{I_0(\nu) - \Delta I(\nu)}{I_0(\nu)} = 1 - \alpha \simeq 1 - \sigma(\nu) C l \quad (39)$$

or representing the spectrum as absorbance  $\alpha$

$$\alpha \simeq \sigma(\nu) C l = A_e \quad (40)$$

This simplifies the simulations, but depending on accuracy requirements, it is at best acceptable when the absorbance  $\alpha$  is at most 1–10%.

We may finally quote some simple rules in relating various combined line widths that result from the convolution integrals for certain functions (see Lewerenz 1987 and Suhm 1990, where various approximate line shapes resulting from different apodizations have been discussed). For the convolution of two Gaussian widths  $\Delta\nu_{G1}$  and  $\Delta\nu_{G2}$ , one has exactly for the combined width  $\Delta\nu_{G12}$

$$\Delta\nu_{G12} = \sqrt{\Delta\nu_{G1}^2 + \Delta\nu_{G2}^2} \quad (41)$$

if one convolutes the Gaussian  $\Delta\nu_G$  with a “boxcar” apodized *sinc* function  $\Delta\nu_S$ , the combined line width is always less than what would result from Equation (41) (typically up to 15% less). A good approximation is obtained from the formula:

$$\Delta\nu_{GS} \simeq \left[ \Delta\nu_G^{12} - \left(\frac{\Delta\nu_G}{2}\right)^{12} + \left(\frac{\Delta\nu_S + \sqrt{\Delta\nu_G^2 + \Delta\nu_S^2}}{2}\right)^{12} \right]^{1/12} \quad (42)$$

Interestingly, one has from this approximately for the combined width

$$\Delta\nu_{GS} \simeq \Delta\nu_G \text{ when } \Delta\nu_S \leq \frac{\Delta\nu_G}{2} \quad (43)$$

This provides a good rule for the choice of the optical path difference in an experiment to obtain essentially Doppler-limited spectra.

For the convolution of two Lorentzians with widths  $\Delta\nu_{L1}$  and  $\Delta\nu_{L2}$ , one has exactly

$$\Delta\nu_{L12} = \Delta\nu_{L1} + \Delta\nu_{L2} \quad (44)$$

for the combined width. If one convolutes a Lorentzian with  $\Delta\nu_L$  with a boxcar apodized *sinc* function with  $\Delta\nu_S$ , one

finds positive and negative deviations from the Gaussian combination rule (Equation 41) with an approximate relation:

$$\Delta\nu_{LS} = \left[ \Delta\nu_L^6 - \left(\frac{\Delta\nu_L}{3}\right)^6 + \left(\Delta\nu_S + \frac{\Delta\nu_L}{3}\right)^6 \right]^{1/6} \quad (45)$$

Again, one has an approximation to this given by

$$\Delta\nu_{LS} \simeq \Delta\nu_L \text{ when } \Delta\nu_S \leq \frac{\Delta\nu_L}{3} \quad (46)$$

which is useful for the choice of the optical path difference in the case of pressure-broadened spectra. It is perhaps surprising, but in any case very useful to remember that by choosing the unapodized instrumental width to be smaller than about a third of the expected true line widths one can, in general, obtain a very good estimate of the true line widths directly from the measured spectra. However, for a careful examination, the effect of self-apodization must be considered. On the other hand, if one wishes to determine the instrumental line widths experimentally from a measured spectrum with known underlying true line shape, the true line widths should be at most about up to twice the instrumental width; otherwise, the enterprise is essentially hopeless. It is, of course, better to choose an example with true line widths being substantially less than the instrumental line widths. All of the measurements discussed here were carried out at very low pressures so that pressure-broadening effects could be neglected. To obtain a symmetric line shape, a complex Fourier transformation and a phase correction are also required. For the phase correction, we use the Mertz method extensively discussed in Mertz (1965), Brault (1985, 1987).

### 3 SOME ILLUSTRATIONS OF HIGH-RESOLUTION FTIR SPECTROSCOPIC RESULTS ON RELATIVELY SIMPLE TEST SPECTRA

#### 3.1 CO FTIR Spectra under Instrumental Line-shape Limitations

Figure 5 shows a CO spectrum in the range 36–100  $\text{cm}^{-1}$ . CO and water lines are visible. The lower trace of Figure 5 displays an extended part of the spectrum with three  $^{12}\text{C}^{16}\text{O}$  lines. Figure 6 shows CO absorption lines around 60  $\text{cm}^{-1}$  recorded with the Bruker ZP 2001 (Figure 6a) and ETH-SLS 2009 (Figure 6b). The calculated Doppler line width,  $\Delta\tilde{\nu}_D = 0.00014 \text{ cm}^{-1}$ , can be neglected in a first approximation and the measured line width is mainly determined by the instrumental line width.  $\Delta\tilde{\nu} = 0.00083 \text{ cm}^{-1}$

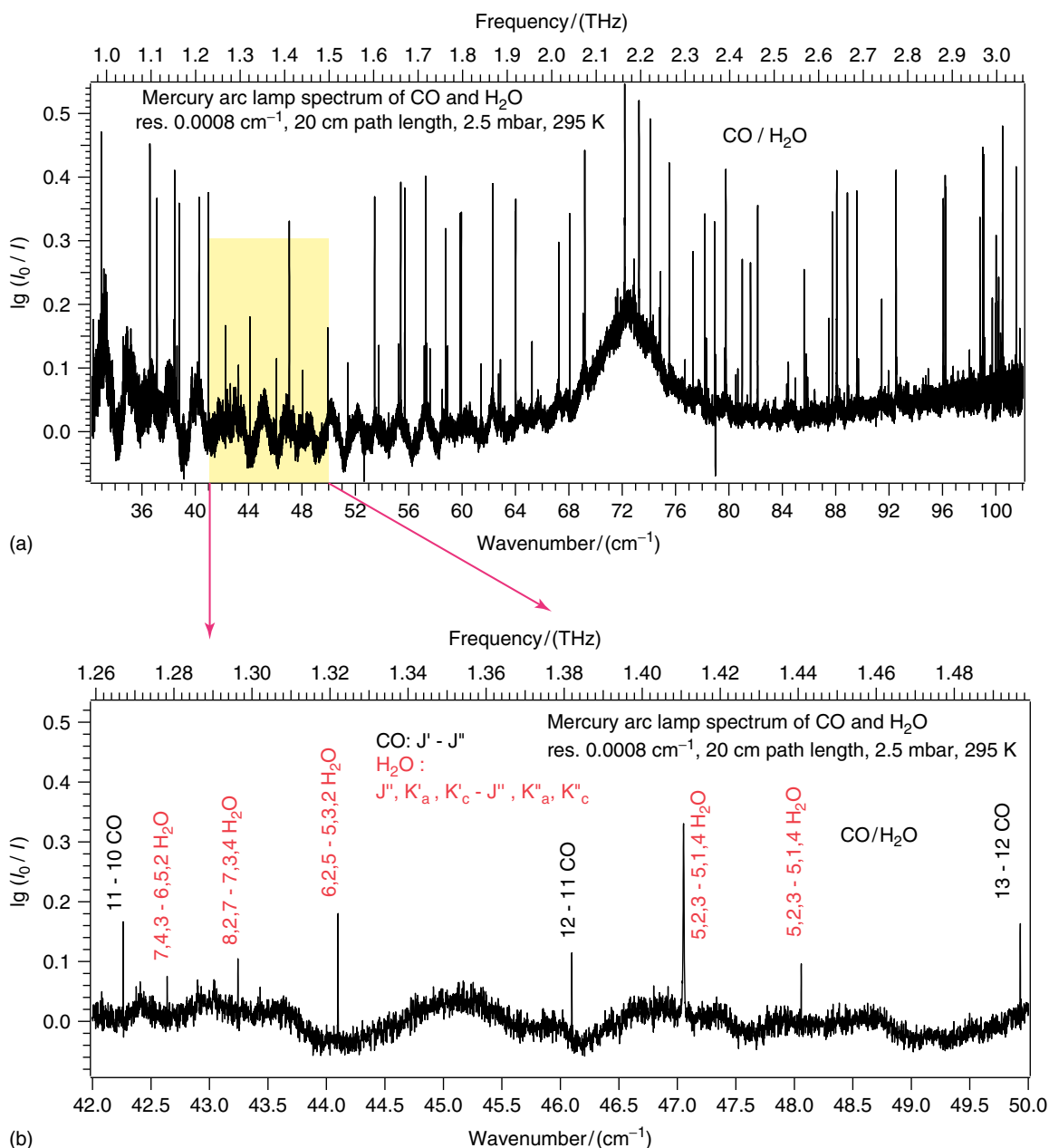


**Figure 5** (a) FIR CO spectrum in the range 36–100  $\text{cm}^{-1}$  recorded with the Bruker ETH-SLS 2009 prototype (resolution:  $\leq 0.0008 \text{ cm}^{-1}$ , 20 cm path length,  $T = 295 \text{ K}$ ). (b) displays an expansion of the spectrum in the range 42–50  $\text{cm}^{-1}$ . Rotational water absorption lines are visible in addition to the CO lines in both spectra.

is experimentally determined for the measurement with the Bruker ZP2001. Compared to the  $\Delta\tilde{\nu}_S = 0.00062 \text{ cm}^{-1}$  and  $\Delta\tilde{\nu}_D$ , the CO line is broadened by a factor of 1.31 through the effect of the finite aperture ( $d = 1 \text{ mm}$ ). The CO line,  $\Delta\tilde{\nu} = 0.00068 \text{ cm}^{-1}$ , recorded with the ETH-SLS 2009 spectrometer, is broadened through the finite aperture by a factor of 1.20 ( $\Delta\tilde{\nu}_S = 0.00053 \text{ cm}^{-1}$ ). Because of larger optical path difference, the noise is higher for the CO spectrum recorded with the ETH-SLS 2009 spectrometer than for that measured with the Zurich (2001)

spectrometer as illustrated on the left in Figure 6. Both measurements used the thermal mercury arc emission source. The synchrotron source was not used here.

One of the great challenges of high-resolution FTIR spectroscopy is to measure unperturbed true absorption line profiles. In our case, we obtain basically Gaussian profiles only if the instrumental line width is smaller than one-third of the Gaussian–Doppler line width. We can neglect the Lorentzian and Voigt line profiles due to the low pressure of the measurements.

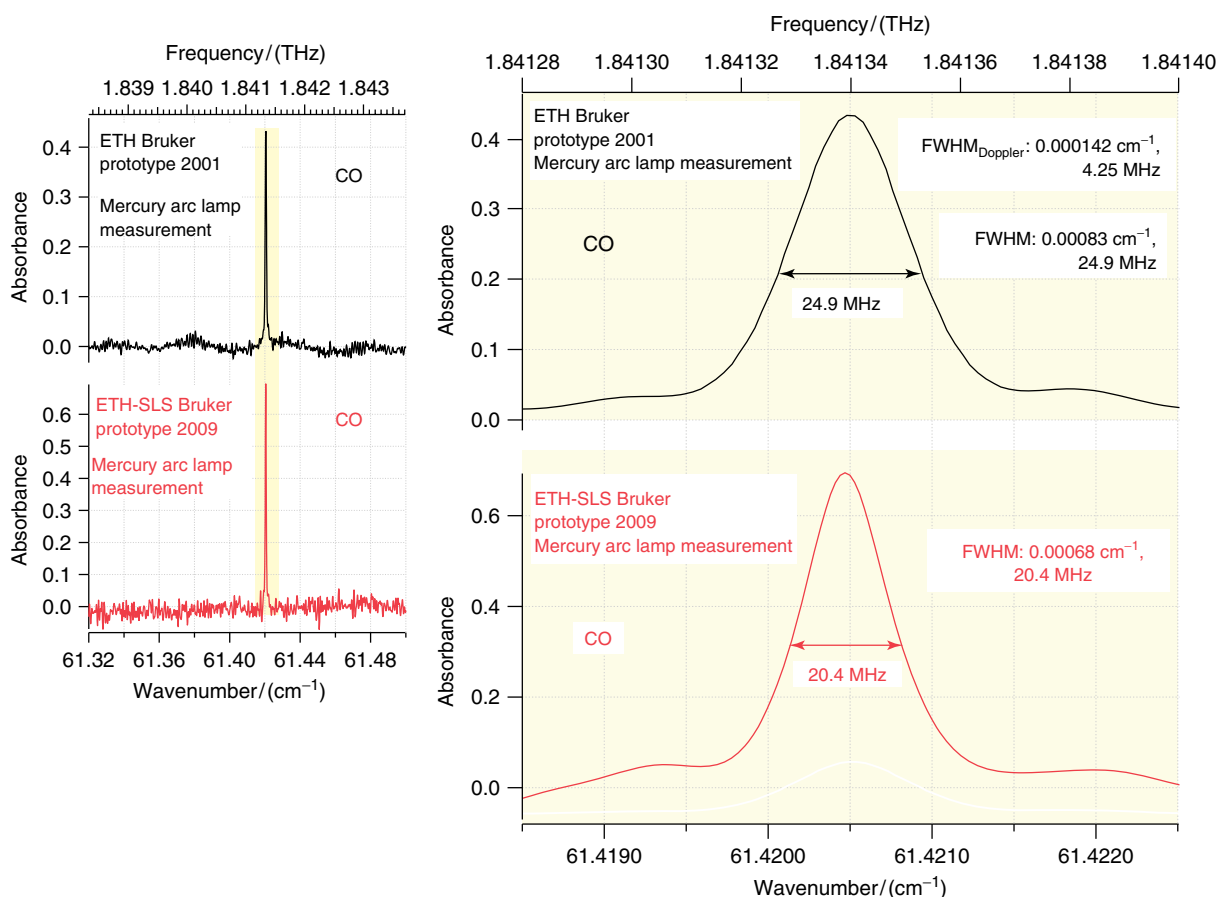


**Figure 6** A CO absorption line in the far infrared spectral region measured with the Bruker IFS 125 HR Zurich Prototype (ZP) 2001 at highest resolution ( $\Delta\tilde{\nu} = 0.00083 \text{ cm}^{-1}$ , 24.9 MHz, upper right trace) and with the Bruker ETH-SLS 2009 prototype ( $\Delta\tilde{\nu} = 0.00068 \text{ cm}^{-1}$ , 20.4 MHz, lower right trace) in a 20 cm glass cell at 295 K. A comparison of the signal-to-noise ratio is shown on the left. The absorbance shown is  $A_{10} = \lg(I_0/I)$ , see Fig. 5.

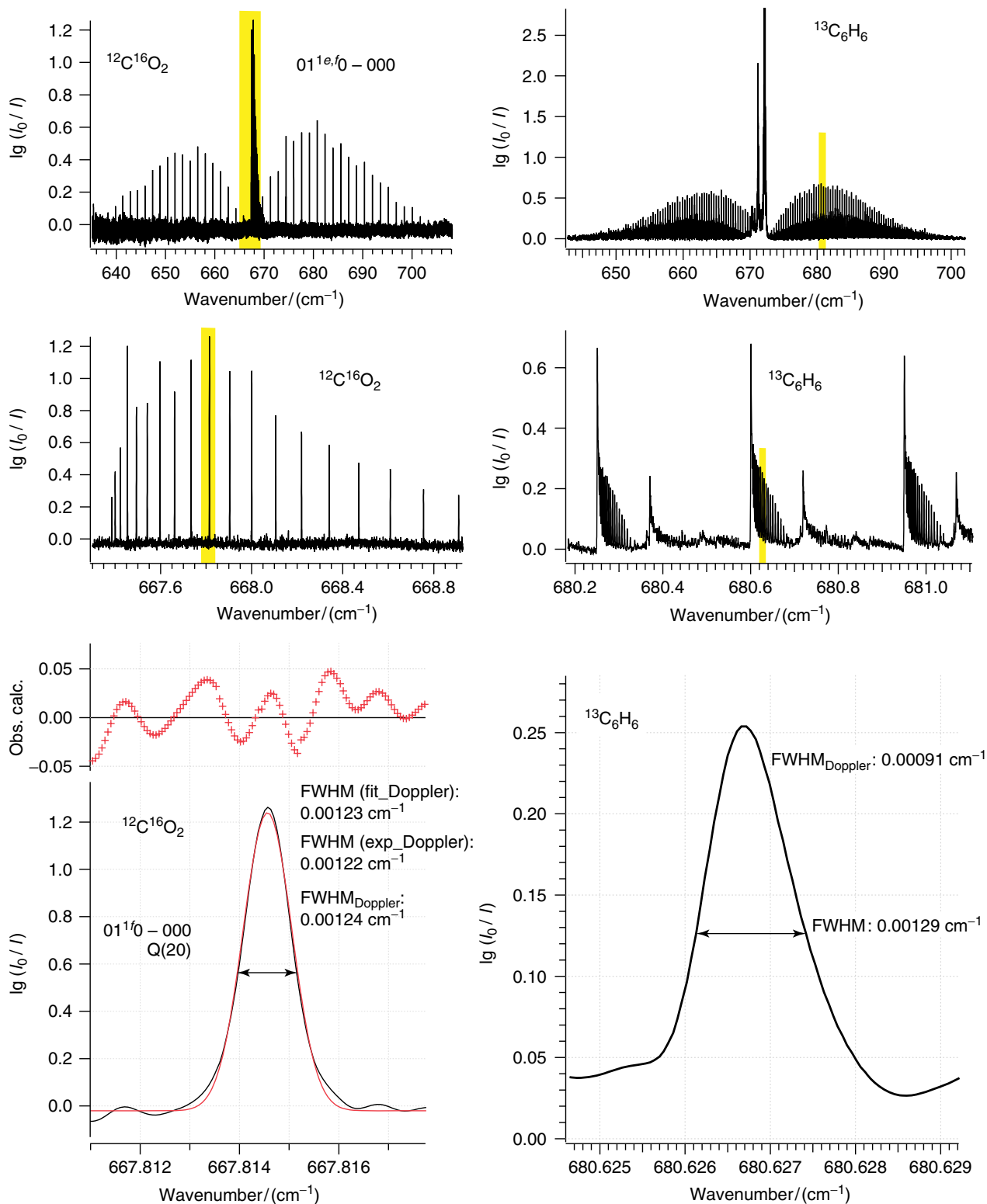
### 3.2 CO<sub>2</sub> and <sup>13</sup>C<sub>6</sub>H<sub>6</sub> FTIR Spectra in the Low-frequency Mid-infrared (Almost Doppler Limited)

Figure 7 illustrates CO<sub>2</sub> and benzene lines in the range 640–700 cm<sup>-1</sup>. The experimentally determined CO<sub>2</sub> line width  $\Delta\tilde{\nu} = 0.00122 \text{ cm}^{-1}$  recorded with an aperture diameter of 1.15 mm is a result of a convolution of Gaussian profile with Doppler width  $\Delta\tilde{\nu}_D = 0.00123 \text{ cm}^{-1}$  and with a *sinc* function with an instrumental line width  $\Delta\tilde{\nu}_S = 0.00062 \text{ cm}^{-1}$ . The broadening of the line due to the finite aperture can be neglected and only the broadening due to the *sinc* function can be considered in the first approximation. To test the influence of the instrumental line shape, the line profile was fitted to a Gaussian line profile. Figure 7 (lower trace, left) illustrates that the deviation between the fitted and measured line profile is not statistical. The fitted Doppler line width  $\Delta\tilde{\nu}_{\text{fit-D}} = 0.00122 \text{ cm}^{-1}$  corresponds to the experimentally determined line width and the calculated Doppler width  $\Delta\tilde{\nu}_D = 0.00123 \text{ cm}^{-1}$  at 295 K. Therefore,

the measured line profile is, as expected, a convolution of the Gaussian and the *sinc* profile. The  $\Delta\tilde{\nu}_S = 0.00063 \text{ cm}^{-1}$  is half of the Doppler width  $0.5\Delta\tilde{\nu}_D = 0.00062 \text{ cm}^{-1}$  and the approximation in Equation (42) is valid. The <sup>12</sup>C<sup>16</sup>O<sub>2</sub> spectrum is ideal for such tests as it has pure, isolated lines with no hyperfine structure because all nuclear spins are zero in this molecule.

For <sup>13</sup>C<sub>6</sub>H<sub>6</sub> (Figure 7, right) the recorded line width ( $\Delta\tilde{\nu} = 0.00129 \text{ cm}^{-1}$ , aperture: 1.3 mm) is larger than the Doppler width  $\Delta\tilde{\nu}_D = 0.00091 \text{ cm}^{-1}$  calculated for 295 K. The instrumental line shape must be considered due to the larger aperture and the *sinc* function. In addition, <sup>13</sup>C<sub>6</sub>H<sub>6</sub> has a more complicated spectrum and the line illustrated in Figure 7 (lower trace, right) represents more than one transition including a rich unresolved hyperfine structure from the protons and the <sup>13</sup>C nuclei.

The line widths of CO<sub>2</sub> and OCS in the 700–900 cm<sup>-1</sup> region (Figure 8, left: CO<sub>2</sub>, right: OCS) are close to the Doppler width recorded with an aperture of 1.15 mm. However, the line profile fitted as a Gaussian line shape



**Figure 7**  $\text{CO}_2$  absorption lines of the  $01^{1e,f}0-000$  fundamental band around  $670\text{ cm}^{-1}$  (left) and  $^{13}\text{C}_6\text{H}_6$  absorption lines around  $670\text{ cm}^{-1}$  (right) measured with the Bruker IFS 125 HR Zurich Prototype (ZP) 2001. The upper traces show the complete bands. The middle traces show a part of the Q branch of the  $\text{CO}_2$  band (left) and a part of the R branch of  $^{13}\text{C}_6\text{H}_6$  band (right). The lower trace shows single lines (left:  $\text{CO}_2$ ,  $01^{1f}0-000$ , Q(20) 0.03 mbar, 3.2 m path length, aperture 1.15 mm, 295 K, right:  $^{13}\text{C}_6\text{H}_6$ , 0.1 mbar, 3.2 m path length, aperture 1.15 mm, 295 K).

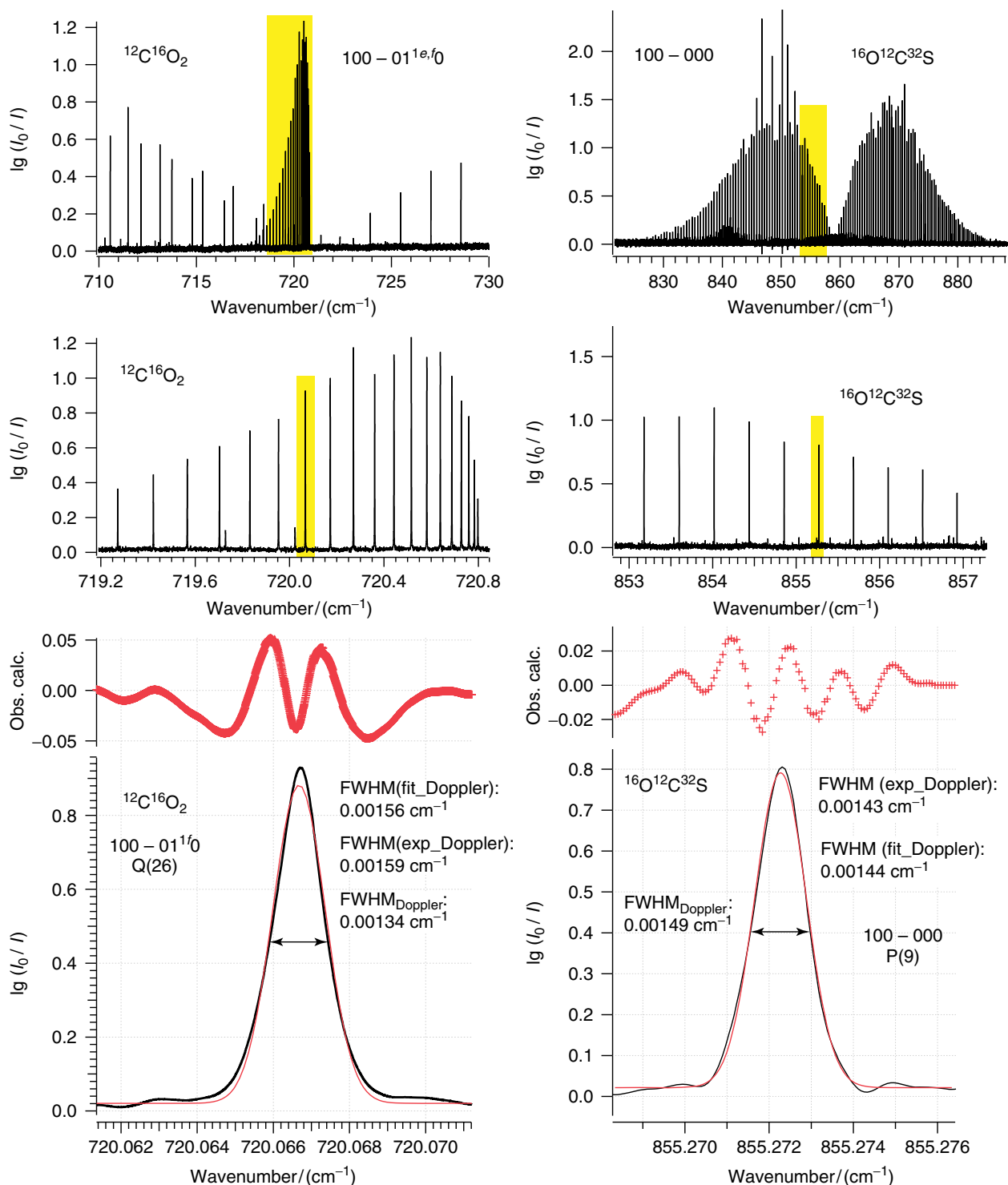


**Figure 8** CO<sub>2</sub> absorption lines of the  $100 - 01^{e,f}0$  difference band around  $720 \text{ cm}^{-1}$  (left) and OCS absorption lines of the  $100 - 000$  fundamental band around  $858 \text{ cm}^{-1}$  (right) measured with the Bruker IFS 125 HR Zurich Prototype (ZP) 2001. The upper trace shows the complete bands. Some of the OCS lines are saturated. The middle trace shows a part of the Q branch of the CO<sub>2</sub> band (left) and a part of the P branch of the OCS band. The lower trace shows single lines (left: CO<sub>2</sub>,  $100 - 01^{f}0$ , Q(26), 1.5 mbar, 20 cm path length, aperture 1.15 mm, 295 K, right: OCS,  $100 - 000$ , P(9) 0.2 mbar, 3.2 m path length, aperture 1.0 mm, 295 K).

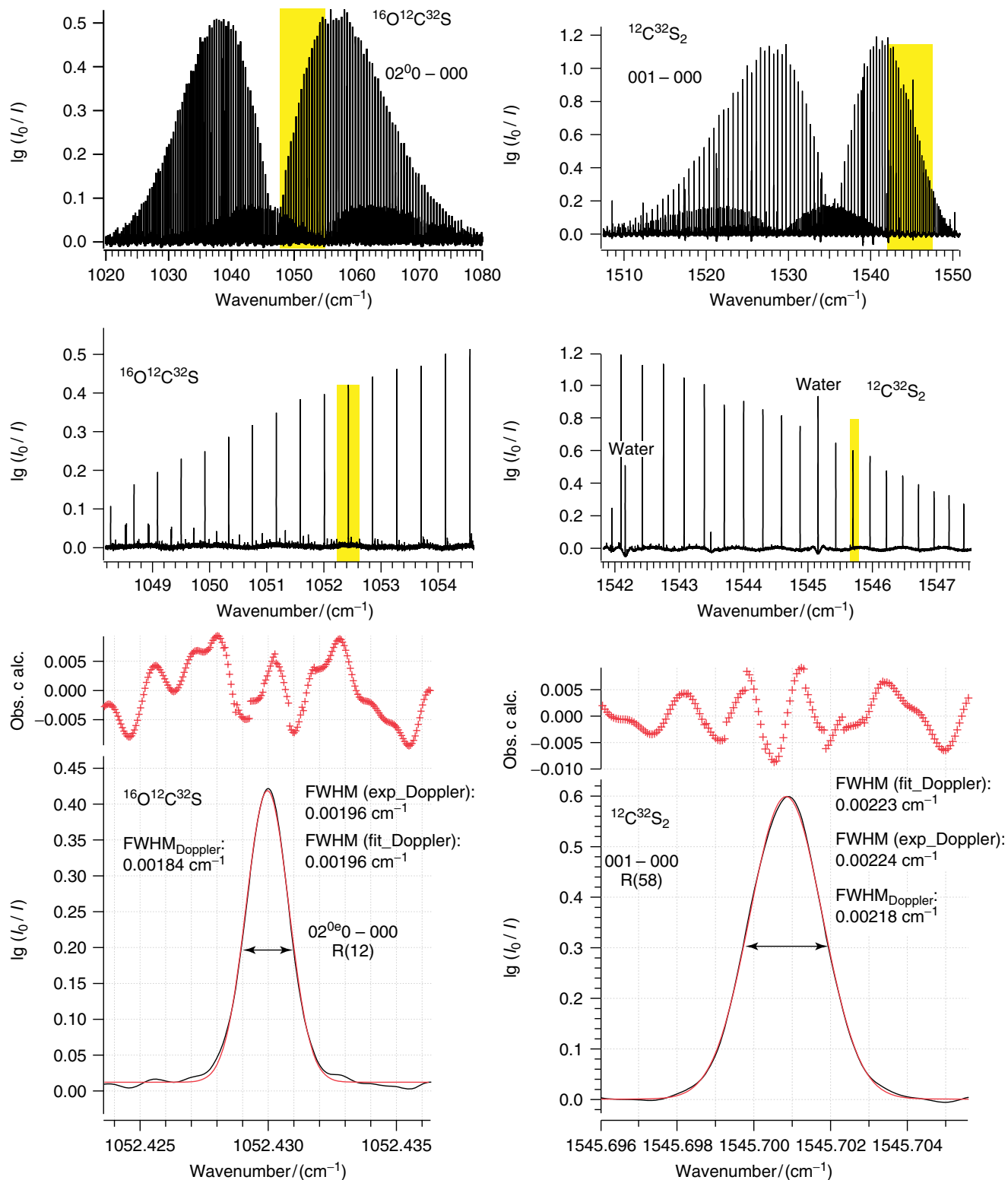


**Figure 9** OCS absorption lines of the  $02^{0e}_0 - 000$  band and corresponding hot bands around  $1050\text{ cm}^{-1}$  (left) and  $\text{CS}_2$  absorption lines of the  $001 - 000$  fundamental band around  $1550\text{ cm}^{-1}$  (right) measured with the Bruker IFS 125 HR Zurich Prototype (ZP) 2001. The upper trace shows the complete bands. The middle trace shows a part of the R branch of the OCS band (left) and a part of the R branch of the  $\text{CS}_2$  band. The lower trace shows single lines (left: OCS,  $02^{0e}_0 - 000$ , R(12), 0.5 mbar, 9.6 m path length, aperture 0.8 mm, 295 K, right:  $\text{CS}_2$ ,  $001 - 000$ , R(58) 0.1 mbar, 18 cm path length, aperture 0.8 mm, 295 K).

still shows systematic differences between the fitted and measured line shapes.

### 3.3 OCS and CS<sub>2</sub> FTIR Spectra in Fingerprint Mid-infrared Region

If we examine the OCS spectra at larger wavenumbers around 1000 cm<sup>-1</sup> and retain the same aperture, a slightly larger line width than the Doppler width is observed as shown in Figure 9 (left). In the case of CS<sub>2</sub> at 1500 cm<sup>-1</sup>, the measured line width recorded with an aperture diameter of 1 mm is actually very close to the Doppler line width as shown in Figure 9 (right). The  $d_{\text{MOPD}} = 980$  cm was used for all the measurements described here up to 1600 cm<sup>-1</sup>.

### 3.4 OCS and N<sub>2</sub>O FTIR Spectra in the High-frequency Mid-infrared Region under Truly Doppler-limited Conditions

For the region 2400–2500 cm<sup>-1</sup>, we have used an optical path difference  $d_{\text{OPD}} = 625$  cm, resulting in a line width for N<sub>2</sub>O very close to the Doppler width, as shown in Figure 10 (left). The OCS line around 3100 cm<sup>-1</sup> (Figure 10, right) illustrates a fitted line width in the range of the Doppler width. A  $d_{\text{OPD}} = 550$  cm was used. The last two measurements were done using an aperture of 0.8 mm. Pressure broadening can be neglected for all measurements described here due to the low sample pressure (0.01–0.1 mbar) used during the recordings.

### 3.5 CO and CH<sub>4</sub> FTIR Spectra under Collisional Cooling Conditions

The collisional cooling process makes it possible to fully exploit the high resolving power of our spectrometer (Albert *et al.* 2007). As an example, we show in Figure 11 CO FTIR spectra measured at low resolution 0.1 cm<sup>-1</sup> cooled down to 7 K. CO mixed in helium gas was injected into the cell and was measured at several temperatures down to 7 K. Figure 11 shows the spectra. At 15 K, an absorption band caused by CO nanoparticles is visible in addition to the absorption lines of the monomer. At 7 K, no monomer absorption lines were observed and only the nanoparticle band of CO is visible. These low-resolution measurements confirmed the measurements taken by Bauerecker *et al.* (2001). We mention here the first observation of infrared spectra of nanoparticles of HF/DF in supersonic jets by Quack *et al.* (1997).

The high-resolution advantage of our spectrometers in the higher frequency regions is illustrated using the methane

spectra (Albert *et al.* 2009b) shown in Figure 12 and in the spectra of isotopomers of methane discussed in Niederer *et al.* (2008) and Ulenikov *et al.* (2009, 2010b). Figure 12 displays the FTIR methane <sup>12</sup>CH<sub>4</sub> spectrum in the range 2700 up to 7700 cm<sup>-1</sup> recorded in the collisional cooling cell at 80 K. The resolution defined here as  $1/d_{\text{MOPD}}$  ranging from 0.0027 to 0.005 cm<sup>-1</sup> was chosen so that it was half of the Doppler width or less in the spectral range measured. A comparison of the fitted FWHM line width  $\Delta\tilde{\nu} = 0.0066$  cm<sup>-1</sup> (Gaussian profile at 80 K of an absorption line at 3871.565 cm<sup>-1</sup>) (Figure 13, top) with the Doppler width  $\Delta\tilde{\nu}_{\text{D}} = 0.0062$  cm<sup>-1</sup> illustrates the overall good agreement. The very small discrepancies can be explained by having had an effect from the instrumental line shape or having measured with a slightly higher temperature than 80 K.

Methane is the prototype of a spherical top molecule and its spectrum is now completely analyzed by Albert *et al.* (2009b) up to the octad region based on the tensor formalism developed in the Dijon group (Champion *et al.* 1992). For a more detailed understanding of the theory and analysis of the spectra, we refer to Champion *et al.* (1992), Albert *et al.* (2009b), Boudon *et al.* 2011: **Spherical Top Theory and Molecular Spectra** and the references therein. Here, we show only the very nice agreement between a part of the experimental and the simulated spectrum in the spectral region (Figure 13, bottom) and an enlarged part of the icosad region (6750–7600 cm<sup>-1</sup>) of CH<sub>4</sub> in Figure 14. The strong lines in the enlarged regions 7052–7100 cm<sup>-1</sup> and 7440–7590 cm<sup>-1</sup> display patterns. A fit of the line shape of a line at 7076.310 cm<sup>-1</sup> to a Gaussian line profile and the resulting line width of  $\Delta\tilde{\nu} = 0.0122$  cm<sup>-1</sup> is again very close to the theoretically calculated Doppler width  $\Delta\tilde{\nu}_{\text{D}} = 0.0120$  cm<sup>-1</sup>. An optical path difference of  $1/d_{\text{MOPD}} = 0.005$  cm<sup>-1</sup> was used. Smaller sections of the icosad region were measured and analyzed using supersonic jet cavity ring down laser spectroscopy (Hippler and Quack 2002 and Snels *et al.* 2011)

### 3.6 CH<sub>3</sub>D, CHD<sub>3</sub>, and CH<sub>2</sub>D<sub>2</sub> under Collisional Broadening Conditions in the Infrared

As is already clear from the general discussion and some of the examples discussed above, even for rather light molecules such as methane at low temperature, the FIR range will have instrument-limited line shapes at low pressures. For instance, between 10 and 100 cm<sup>-1</sup>, the Doppler width for the methane isotopomers is about  $1.5 \times 10^{-5}$ – $1.5 \times 10^{-4}$  cm<sup>-1</sup>, well below what can be reached with current instrumental line-shape functions from available FTIR spectrometers. However, it may be important to obtain accurate integrated line strengths, which is only

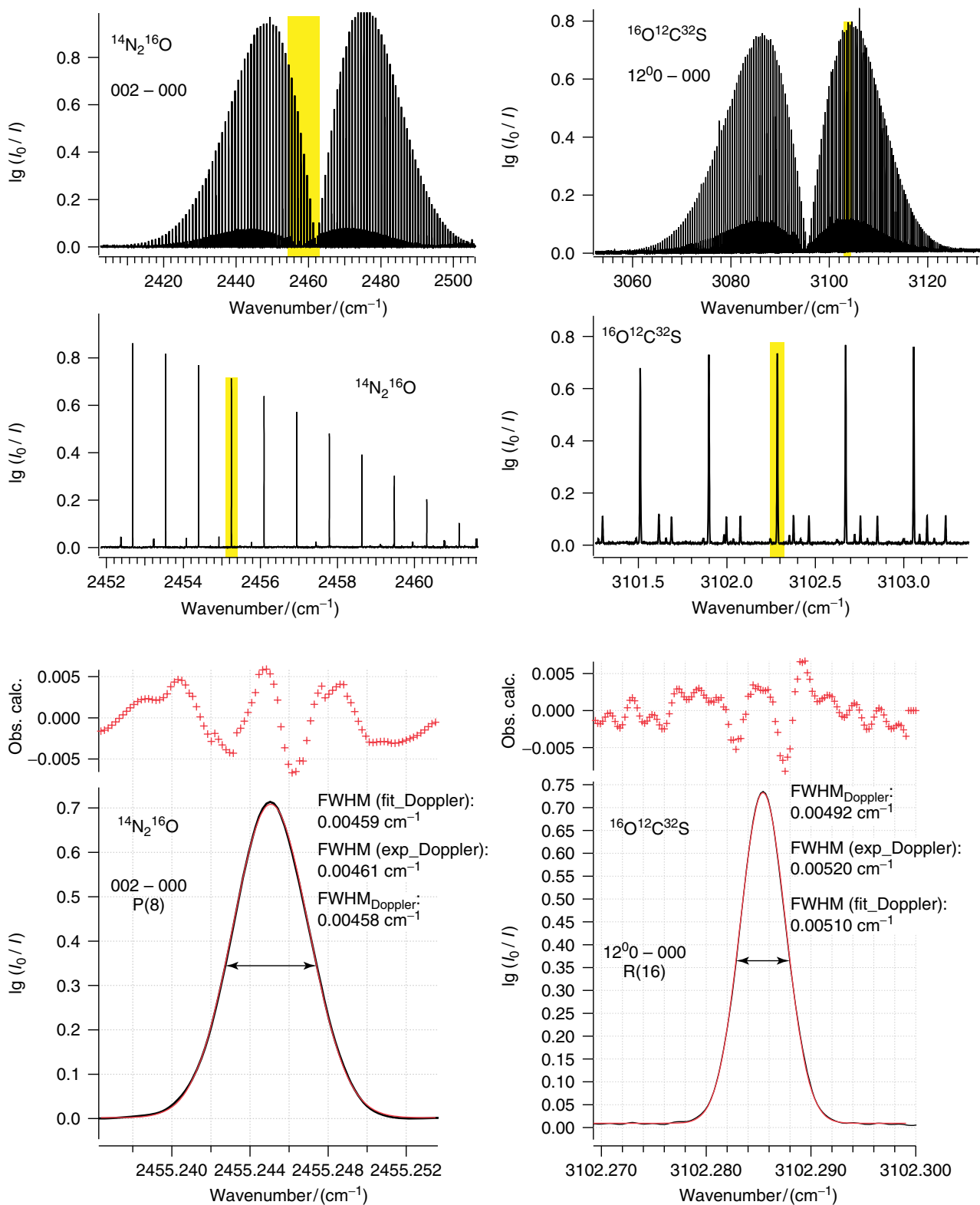


**Figure 10**  $\text{N}_2\text{O}$  absorption lines of the 002 - 000 band around  $2460\text{cm}^{-1}$  (left) and  $\text{OCS}$  absorption lines of the  $12^0 - 000$  band around  $3100\text{cm}^{-1}$  (right) measured with the Bruker IFS 125 HR Zurich Prototype (ZP) 2001. The upper trace shows the complete bands. The middle trace shows a part of the P branch of the  $\text{N}_2\text{O}$  band (left) and a part of the R branch of the  $\text{OCS}$  band (right). The lower trace shows single lines (left:  $\text{N}_2\text{O}$ , 002 - 000, P(8), 0.4 mbar, 9.6 m path length, aperture 0.8 mm, 295 K, right:  $\text{OCS}$ ,  $12^0 - 000$ , R(16) 0.3 mbar, 9.6 m path length, aperture 0.8 mm, 295 K).

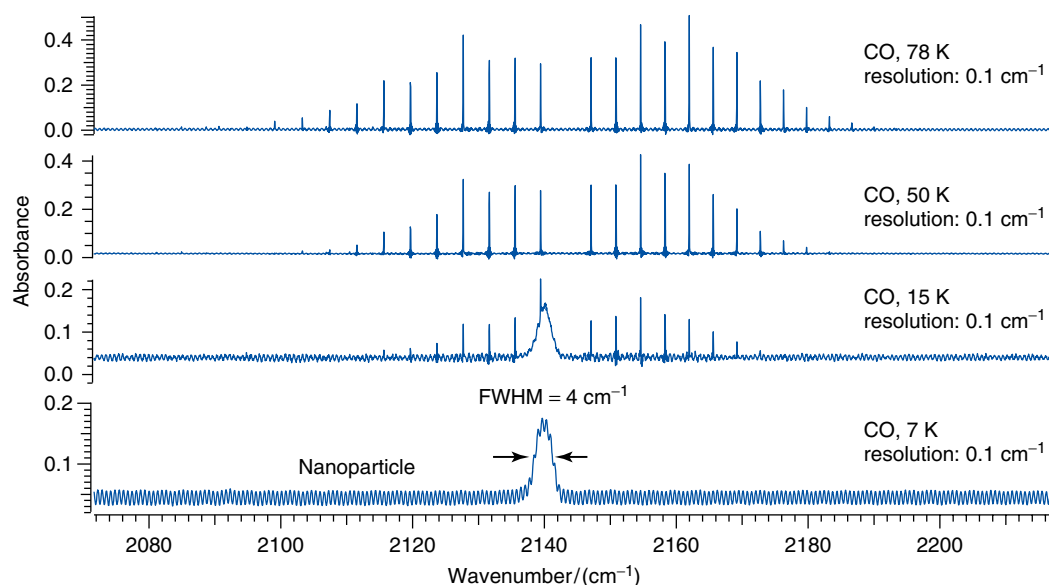


**Figure 11** Spectra of CO recorded with a path length of 10 m at different temperatures with a resolution of  $0.1\text{ cm}^{-1}$ . Top trace: The spectrum taken at 78 K shows CO monomer absorption lines. Second trace: The spectrum taken at 50 K displays CO monomer absorption lines. Third trace: The spectrum taken at 15 K shows monomer absorption lines and a nanoparticle peak of CO. Bottom trace: The spectrum taken at 7 K shows only the nanoparticle peak of CO. [Reproduced from Albert *et al.* 2007 by permission.]

possible using spectra that are not instrument limited. Here, one measures under collisionally broadened conditions. For this, with the traditional low-resolution grating spectrometers in the use of the celebrated Wilson Wells (Wilson and Wells 1946) method, one had to use quite high pressures of well above 1 bar. The advantage of high-resolution FTIR spectroscopy is obviously that gas pressures well below atmospheric pressures of 1 bar are sufficient to obtain true pressure-broadened line shapes and intensities at available resolutions.

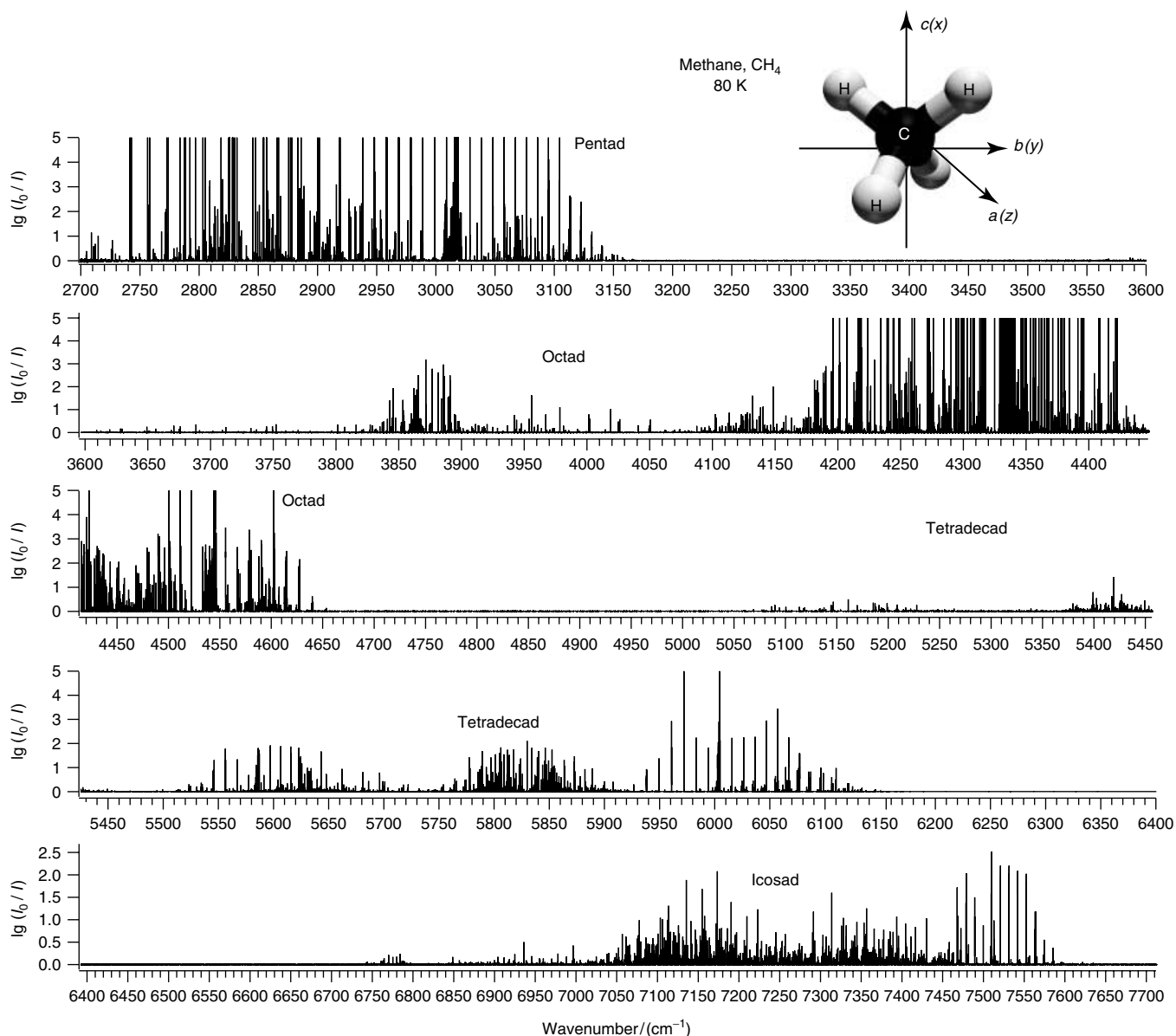
We cite here results from an application of this method to spectra and intensities of the methane isotopomers with the goal of determining the magnitude and sign of the electric dipole moment of these deuterated isotopomers. This is, in turn, related to a long-standing question concerning the CH-bond dipole moment in methane (Hollenstein *et al.* 1994, Signorell *et al.* 1996) and literature cited therein. Figure 15(a) shows the FIR spectrum of the symmetric top isotopomers  $\text{CH}_3\text{D}$  and  $\text{CHD}_3$  measured in a light pipe cell of 2.71 m path length (Quack and Suhm 1990), specially developed for the IR showing pressure broadening. The typical regularly spaced R lines from  $J = 6$  to 10 ( $\text{CD}_3\text{H}$ ) and  $J = 7$ –12 ( $\text{CHD}_3$ ) are seen in the range  $50$ – $90\text{ cm}^{-1}$  shown here.

Figure 15(b) shows the range  $30$ – $90\text{ cm}^{-1}$  for  $\text{CH}_2\text{D}_2$  under comparable conditions, showing a much more complex rotational line structure typical for an asymmetric top. Without discussing details here, we can summarize one main result of these investigations: The electric dipole moment ( $7.8 \times 10^{-3}\text{ D}$  for  $\text{CH}_2\text{D}_2$ ,  $6.6 \times 10^{-3}\text{ D}$  for  $\text{CHD}_3$ ,

and  $6.8 \times 10^{-3}$  for  $\text{CH}_3\text{D}$ ) is always toward the deuterium-containing part of the isotopomers (which has thus a positive partial charge with proper sign convention of the electric dipole moment) (*see also* Stohner and Quack 2011: **Conventions, Symbols, Quantities, Units and Constants for High-resolution Molecular Spectroscopy**, this handbook). This result is, in turn, related to a CH-bond dipole model in methane corresponding to a partial charge distribution  $\text{C}^{\delta-}-\text{H}^{\delta+}$ . We note that this resolution of a five decade long controversy starting with the paper by Coulson (1942) was obtained using IR intensities from the spectrum shown and combining this with numerous NIR intensity measurements and theoretical results in terms of a multi-dimensional electric dipole hypersurface (Hollenstein *et al.* 1994, Marquardt and Quack 1998). We refer to the original papers for a more detailed discussion, leading to this now well-established result (*see also* Marquardt and Quack 2004).

### 3.7 Characteristics and Setup of the Nine-chamber Zürich FTIR spectrometer Bruker IFS120/125 Prototype 2001

The influence of the aperture is nicely illustrated in Figure 16. Part of the absorption spectra of the  $\nu_3$  band of  $\text{CDBrClF}$  recorded with different apertures is shown. Reducing the aperture from 1.15 m (Figure 16, upper trace) to 0.8 mm (lower trace) leads to much better-resolved features. Even lines with peak distances of  $0.0008\text{ cm}^{-1}$  can



**Figure 12** Overview spectrum of methane  $^{12}\text{CH}_4$  between  $2700$  and  $7700\text{ cm}^{-1}$  recorded at  $80\text{ K}$ . The different polyads are labeled. [See Albert *et al.* 2009b.]

be resolved. However, because of the smaller aperture, the signal-to-noise ratio decreases.

The second effect of a finite aperture is the shift of the wavenumber scale. This effect is shown on an OCS line around  $882\text{ cm}^{-1}$  in Figure 17. Reduction of the aperture leads to a larger shift versus the reference line position. In addition, one can see the narrowing of the line due to the reduction of the aperture and the increase of the noise.

To illustrate the excellent details of the recorded spectra and the improvement of the spectral resolution, we show a part of the CDBrClF spectrum in the  $\nu_3$  region in Figure 18, recorded with different spectral resolutions. The upper trace shows the CDBrClF spectrum recorded

with a resolution of  $0.004\text{ cm}^{-1}$ , corresponding to the first generation of highly resolving Fourier transform spectrometers, the Bomem DA 002 series. As one can see, a line-by-line assignment is quite impossible. The middle trace shows the spectrum recorded with a resolution of  $0.0016\text{ cm}^{-1}$ , which was the maximum resolution of the first prototype of the Bruker IFS 120 HR series. At this resolution, more absorption features are resolved and an initial line-by-line assignment is possible. However, many overlapping and coalescent line features exist even here, rendering a complete assignment difficult or impossible. Finally, the lowest trace shows the spectrum recorded with the Bruker IFS 125 HR Zurich prototype 2001. Compared

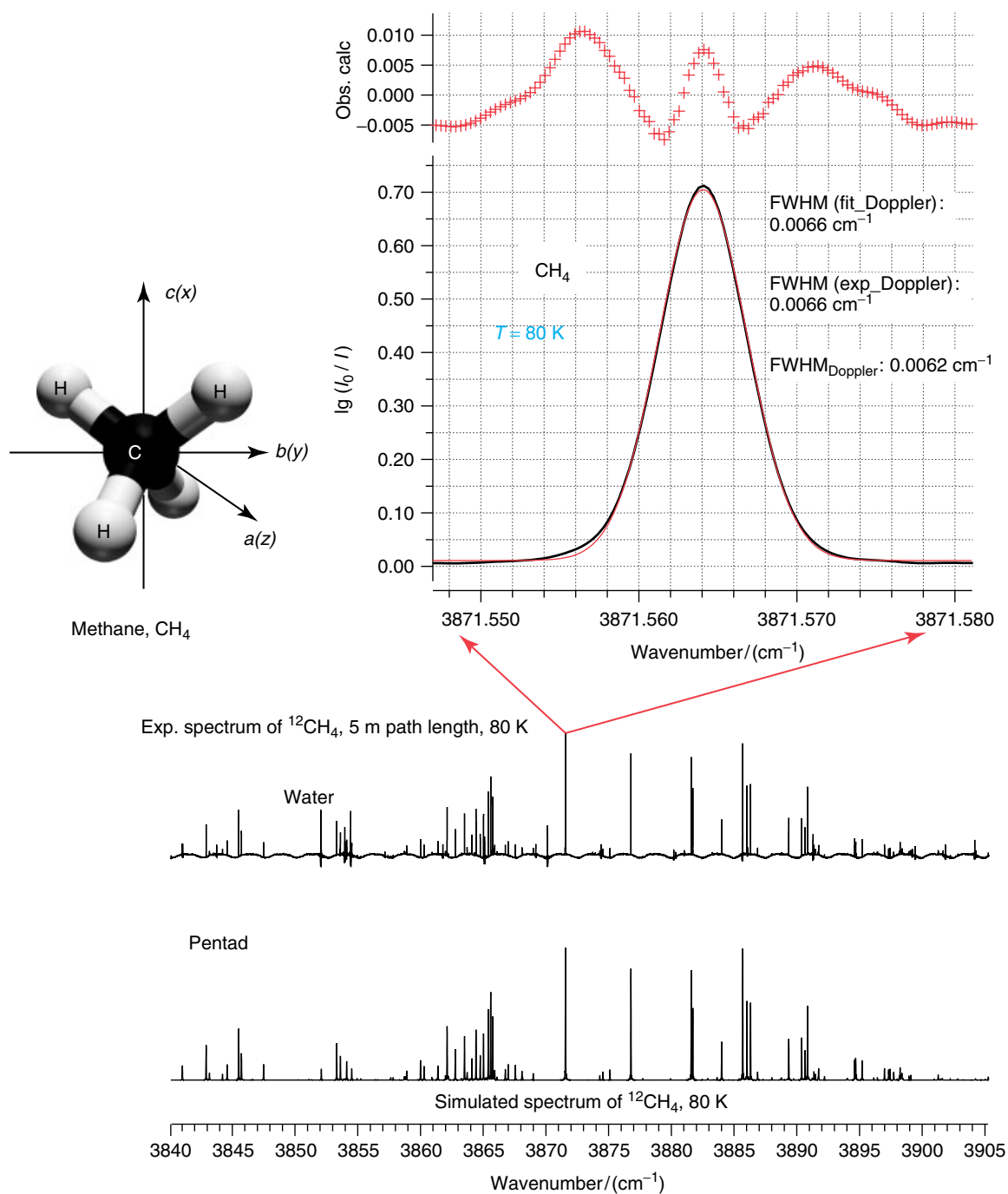


**Figure 13** Top: Experimental and fitted line profile of a Gaussian shape absorption line of methane at  $3871.565\text{ cm}^{-1}$  recorded at 80 K and with path length of 10 m. Bottom: Comparison of part of the measured (upper trace) and simulated methane spectrum (lower trace). [See Albert *et al.* 2009b.]

to the first spectrometer of the IFS 120 HR series, we achieve roughly a better instrumental resolution by a factor of two. The Doppler width of CDBrClF in this spectral region is about  $0.0009\text{ cm}^{-1}$ . We record completely resolved absorption lines, in part, and therefore are even able to detect close rovibrational resonances in the spectrum. Thus, the higher resolution indeed opens the route

for the complete rovibrational analysis of a whole new set of heavier polyatomic molecules, like chiral and aromatic molecules.

In addition to the commercially available glass, White-type multireflection cell with a base length of 0.8 m and maximum optical path length of 41.6 m, our spectrometer is equipped with two other external absorption cells. One of

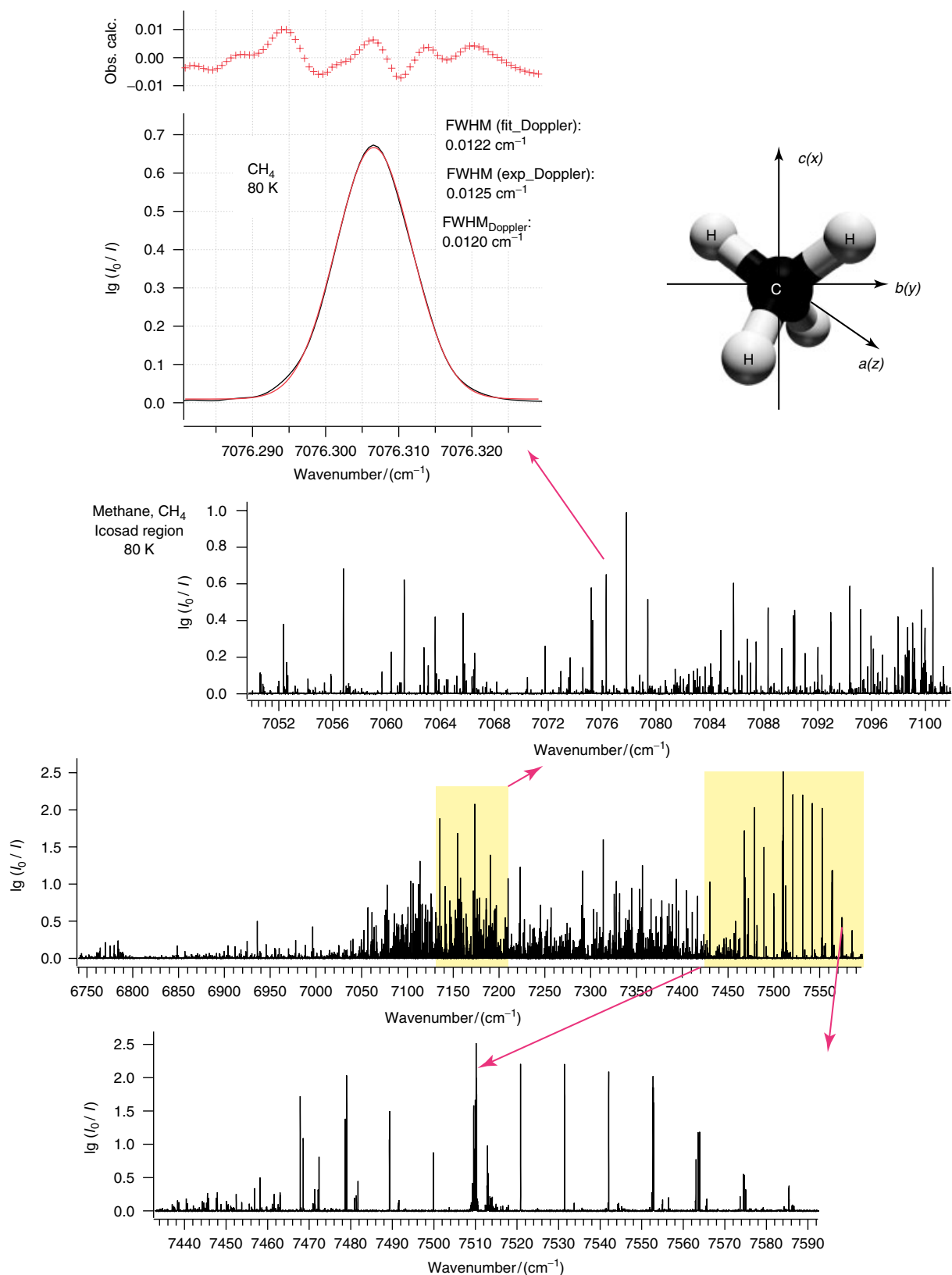


**Figure 14** Cold (80 K) methane spectrum in the icosad region (6750–7600 cm<sup>-1</sup>, path length 10 m) Top: Experimental and fitted line profile of a Gaussian shape absorption line of methane at 7076.310 cm<sup>-1</sup>. Middle and bottom: Enlargements of the methane icosad spectrum in the ranges 7052–7100 cm<sup>-1</sup> and 7440–7590 cm<sup>-1</sup>. [See Albert *et al.* 2009b.]

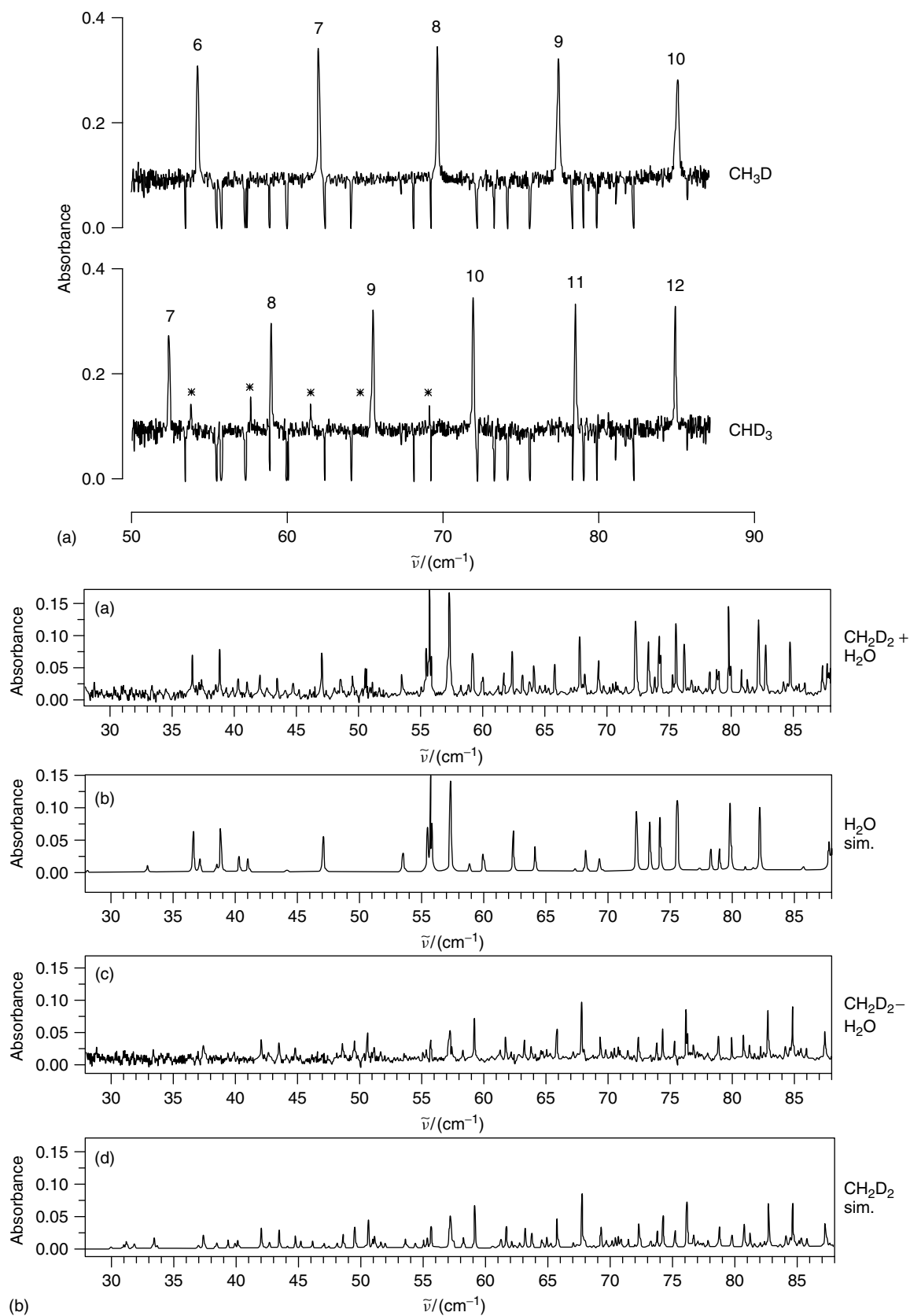


**Figure 15** Far infrared spectra of (a)  $\text{CH}_3\text{D}$ ,  $\text{CHD}_3$  and  $\text{CH}_2\text{D}_2$  (b). [Reproduced from Hollenstein *et al.* 1994 and Signorell *et al.* 1996 with permission.] (see these references for further details and conditions).

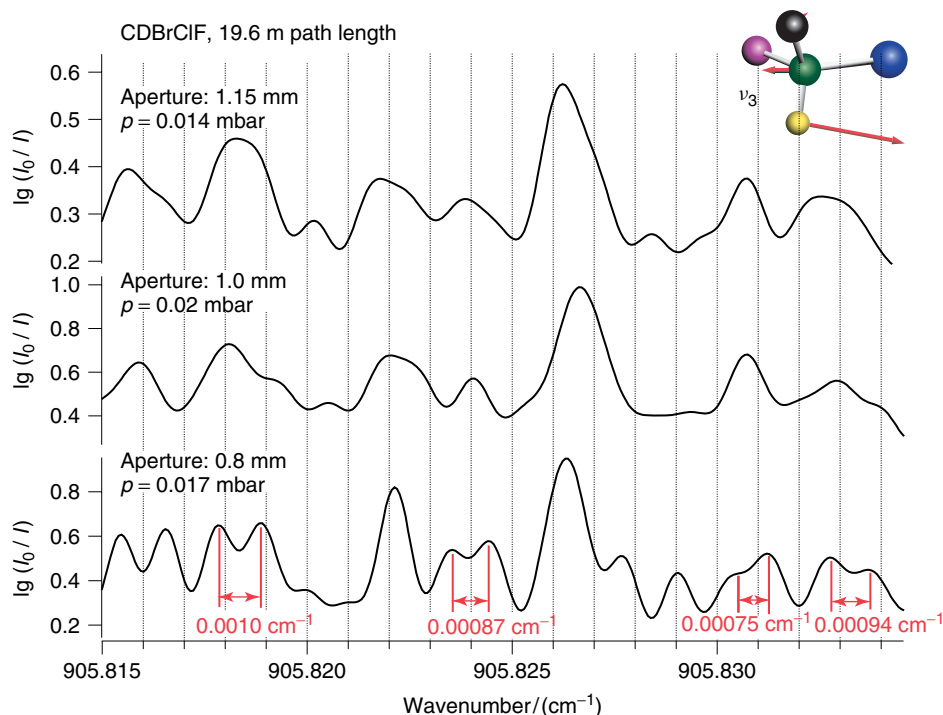


**Figure 16** The influence of the aperture on the resolution illustrated in part of the CDBrClF spectrum around  $900\text{ cm}^{-1}$ . The CDBrClF spectrum was measured with a path length of 19.6 m, a pressure of 0.014 mbar, and an aperture with a diameter of 1.15 mm (upper trace), with a pressure of 0.02 mbar and an aperture with a diameter of 1.00 mm (middle trace) and with a pressure of 0.017 mbar and an aperture with a diameter of 0.80 mm (lower trace).

them is an enclosive cooling cell (Albert *et al.* 2007, Buch *et al.* 2004, Bauerecker *et al.* 1995, 2001, Bauerecker 2005). Spectra can be recorded at temperatures down to 4 K by helium cooling in this cell. It is also optically designed as a multireflection cell with a maximum optical path of 20 m. This enclosive cooling cell is connected via transfer optics to the parallel output beam of the Bruker spectrometer. The other external cell is a 3 m glass cell. It can be used to record the spectra of reactive and unstable species.

The FTIR spectra of the molecules presented here have been recorded in the region  $50$  to  $7800\text{ cm}^{-1}$ . The unapodized instrumental resolution ranged from  $0.00061$  to  $0.002\text{ cm}^{-1}$ . About 150 to 300 spectra were co-added in each spectral region. The White-type cell with path lengths ranging from 3.2 up to 19.6 m and the 3 m glass cell were used for the room temperature measurements. The cold measurements of  $\text{CHCl}_2\text{F}$  and methane were carried out in a collisional cooling cell with a path length of 17.5 m. The sample pressure was varied from 0.01 to 1 mbar. All spectra were self-apodized and were recorded close to or below the Doppler limit for the conditions of the experiment. Apertures of 0.8–1.3 mm were used. The frequency measurements were calibrated with OCS and  $\text{N}_2\text{O}$  lines (Maki and Wells 1991). For FTIR spectroscopy of supersonic jets, we refer to the review by

Snels *et al.* 2011: **High-resolution FTIR and Diode Laser Spectroscopy of Supersonic Jets**, this handbook.

## 4 ASSIGNMENT AND ANALYSIS OF COMPLEX HIGH-RESOLUTION FTIR SPECTRA

### 4.1 Overview

The five molecules presented here,  $\text{CH}^{35}\text{Cl}_2\text{F}$ , CDBrClF, pyrimidine, pyridine and naphthalene, are asymmetric top molecules. As illustrated in Figure 19 (for naphthalene see Figure 31, top left), they have three principal axes  $a$ ,  $b$ , and  $c$ , with different rotational constants  $A$ ,  $B$ , and  $C$  and energy levels characterized by rotational quantum numbers  $J$ ,  $K_a$ , and  $K_c$  (Herzberg 1945, Zare 1988).

A resolved rovibrational spectrum in a typical frequency range defined by an optical filter range consists normally of 5000–10000 absorption lines for the heavier molecules discussed here. To deal with such a large amount of information, interactive pattern-recognition programs are used. These programs plot the line positions as a function of one of the rotational constants. As a result, absorption lines belonging to the same  $K_a$  or  $K_c$  values appear

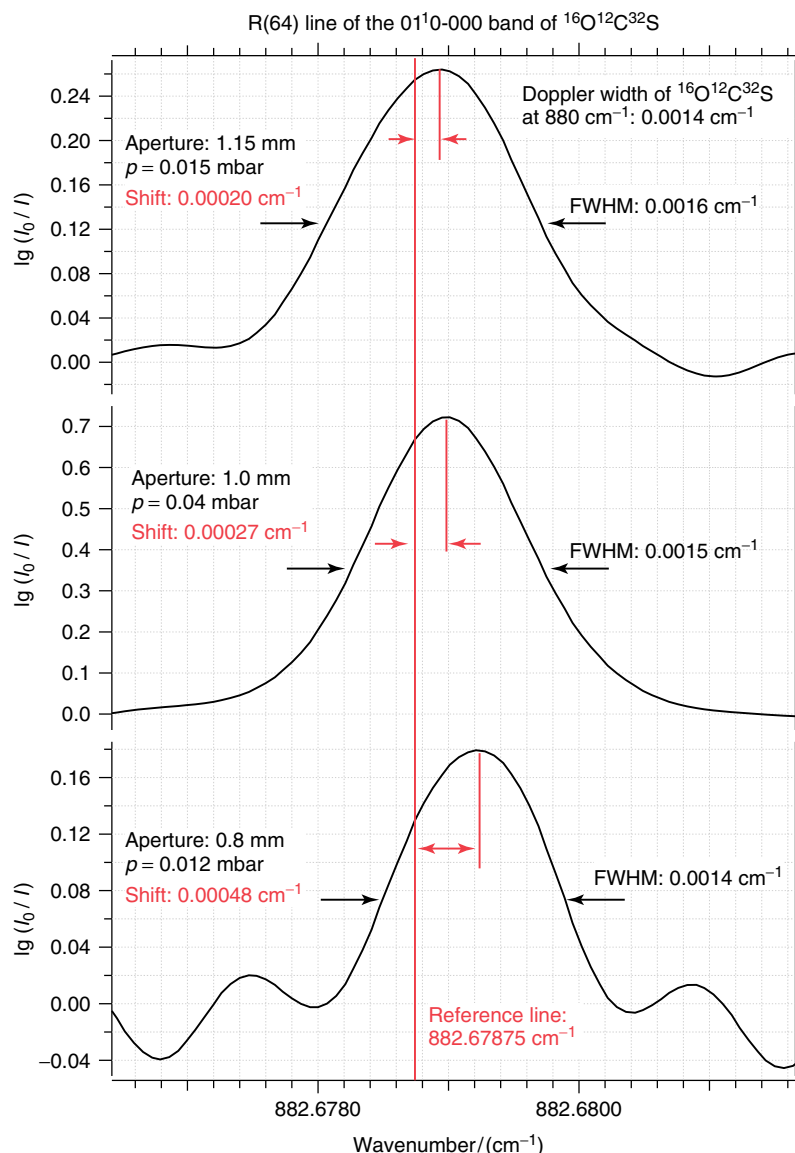


**Figure 17** Shift of the OCS line R(64) at  $882.67875\text{ cm}^{-1}$  (Maki and Wells 1991) due to the change of aperture. Upper trace: An aperture of 1.15 mm leads to a shift of  $0.00020\text{ cm}^{-1}$ , an aperture of 1.0 mm to a shift of  $0.00027\text{ cm}^{-1}$  (middle trace) and an aperture of 0.8 mm leads to a shift of  $0.00048\text{ cm}^{-1}$  compared to the OCS reference line R(64).

as series. One of the first general pattern-recognition programs of this kind was the Giessen Loomis–Wood assignment program (Loomis and Wood 1928, Winnemisser *et al.* 1989). Figure 20a shows a Loomis–Wood diagram of the  $\nu_4$  band of benzene as an example of an oblate symmetric top and Figure 20b of the  $\nu_{11}$  band of pyridine as an example of an oblate asymmetric top. The  $J$  quantum number is shown as a function of the effective  $B$  rotational constant. The different  $K$  series of benzene are clearly visible (Figure 20a). The lower trace illustrates an enlargement of the Loomis–Wood plot of benzene and shows the series up to  $K \leq 15$ . The Loomis–Wood plot of pyridine (Figure 20b, upper picture) shows the  $K_c$  series,

$c$ -type transitions, up to  $K_c \leq 6$ . The asymmetric splitting at lower  $J$  levels is visible. The lower picture in Figure 20b shows an enlargement of part of the Loomis–Wood plot of pyridine illustrating the  $K_c$  series between  $K_c = 10$  and  $K_c = 35$ .

In the meantime, several other assignment programs have become available. We refer to the recently developed CAAARS (Medvedev *et al.* 2005) and AABS (Kisiel *et al.* 2005) program packages; besides, there exist, of course, local versions of the Loomis–Wood assignment programs within various research groups, including our own, developed for specific purposes (*see also* Albert *et al.* 2011: **Fundamentals of Rotation–Vibration Spectra**, this

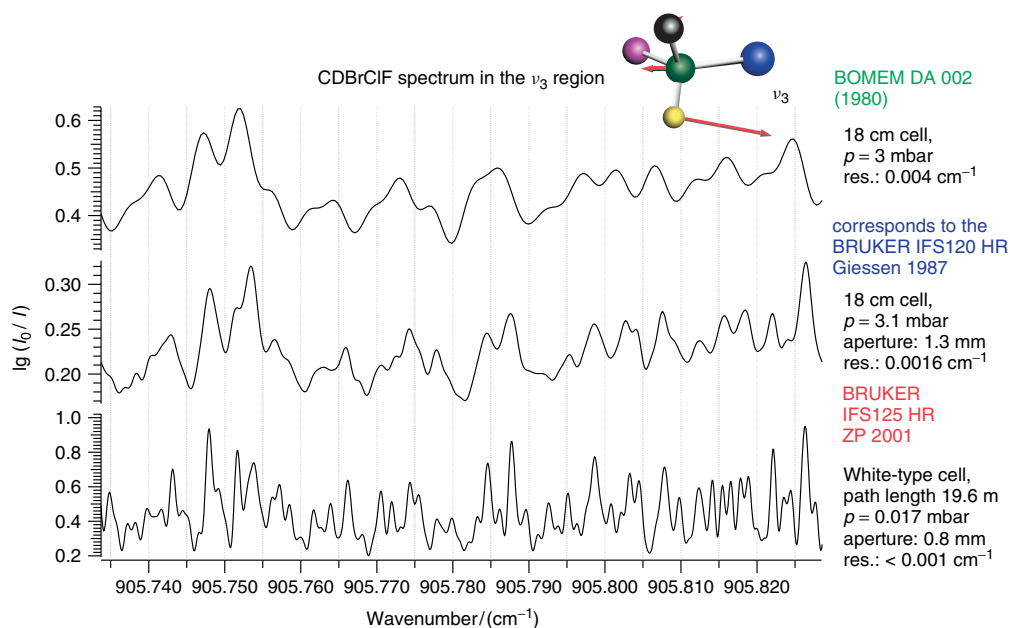


**Figure 18** Comparison of recordings of the spectra of CDBrClF at room temperature obtained with different resolution, demonstrating progress in resolution achieved over the 20-year period of FTIR spectroscopy. Upper trace: CDBrClF spectrum obtained with a resolution of  $0.004\text{ cm}^{-1}$  corresponding to the apodized resolution of a 1982 Bomem DA 002 with MOPD = 250 cm (path length = 18 cm,  $p = 3$  mbar). Middle trace: CDBrClF spectrum recorded with a resolution of  $0.0016\text{ cm}^{-1}$  with MOPD = 500 cm corresponding to the resolution of the Giessen 1987 Bruker IFS 120 HR (path length = 18 cm,  $p = 3.1$  mbar). Lower trace: CDBrClF spectrum recorded with a resolution of  $0.001\text{ cm}^{-1}$  with MOPD = 970 cm corresponding to the resolution of the Bruker IFS 125 HR Zurich prototype (ZP) 2001 (path length = 19.6 m,  $p = 0.017$  mbar).

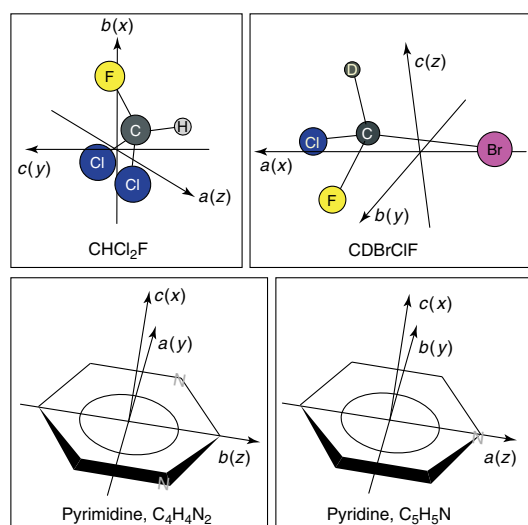


**Figure 19** The molecules  $\text{CHCl}_2\text{F}$ ,  $\text{CDBrClF}$ , pyridine ( $\text{C}_5\text{H}_5\text{N}$ ), and pyrimidine ( $\text{C}_4\text{H}_4\text{N}_2$ ) in their molecule-fixed center-of mass-axis systems. The principal inertial axes  $a$ ,  $b$ , and  $c$  correspond to the rotational constants  $A$ ,  $B$ , and  $C$  and three principal moments of inertia  $I_A$ ,  $I_B$ , and  $I_C$ . The definition of the Cartesian axes  $x$ ,  $y$ ,  $z$  corresponds to the convention used for labeling the vibrational modes in pyridine. For the rotational analyses, relabeling is sometimes necessary (see text and Snels *et al.* 1997).

handbook). The Giessen Loomis–Wood program, originally designed only for linear molecules (Albert *et al.* 1996, 1997a,b, 1998a, 2001b, Schulze *et al.* 2000), has been used successfully in our group for several asymmetric top molecules:  $\text{CHCl}_2\text{F}$  (Albert *et al.* 2004c),  $\text{CH}^{35}\text{Cl}_2\text{F}$  (Albert *et al.* 2004a),  $\text{CDBrClF}$  (Albert *et al.* 2003b),  $\text{C}_2\text{H}_3\text{DO}$  (Albert *et al.* 2003a), pyridine (Albert *et al.* 2005), chloro- and fluorobenzene (Albert and Quack 2006), phenol, aniline, and naphthalene (Albert *et al.* 2010).

After the assignment of absorption lines, the rovibrational analysis is carried out with Watson's reduced effective Hamiltonian in the  $A$  or  $S$  reduction up to sextic centrifugal distortion constants (Watson 1978, Papoušek and Aliev 1982):

$$\begin{aligned} \hat{H}_{\text{rot}}^{v,v} = & A_v \hat{J}_z^2 + B_v \hat{J}_x^2 + C_v \hat{J}_y^2 \\ & - \Delta_v^v \hat{J}^4 - \Delta_{JK}^v \hat{J}^2 \hat{J}_z^2 - \Delta_K^v \hat{J}_z^4 \\ & - \frac{1}{2} \left[ (\delta_J^v \hat{J}^2 + \delta_K^v \hat{J}_z^2), (\hat{J}_+^2 + \hat{J}_-^2) \right]_+ + \Phi_J^v (\hat{J}^2)^3 \\ & + \Phi_{JK}^v (\hat{J}^2)^2 \hat{J}_z^2 + \Phi_{KJ}^v \hat{J}^2 \hat{J}_z^4 + \Phi_K^v \hat{J}_z^6 \\ & + \frac{1}{2} \left[ (\phi_J^v (\hat{J}^2)^2 + \phi_{JK}^v \hat{J}^2 \hat{J}_z^2 + \phi_K^v \hat{J}_z^4), (\hat{J}_+^2 + \hat{J}_-^2) \right]_+ \end{aligned} \quad (47)$$

The angular momentum operators are given by  $\hat{J}^2 = \hat{J}_x^2 + \hat{J}_y^2 + \hat{J}_z^2$  and  $\hat{J}_{\pm} = \hat{J}_x \pm i\hat{J}_y$ .

Effective rotational Hamiltonians that couple different vibrational states  $v'$  and  $v$  may be considered in the case of accidental degeneracies. Taking into account terms up to quartic interactions, this Hamiltonian may be written in the form (Luckhaus and Quack 1989)

$$\hat{H}_{\text{rot}}^{v'v} = i\xi_{\alpha}^{v'v} \hat{J}_{\alpha} + \eta_{\beta\gamma}^{v'v} [\hat{J}_{\beta}, \hat{J}_{\gamma}]_{+} \quad (\alpha \neq \beta \neq \delta) \quad (48)$$

The spectroscopic data of the asymmetric top molecules discussed here were analyzed using the Zurich WANG program described in detail by Luckhaus and Quack (1989) (see also Albert *et al.* 2011: **Fundamentals of Rotation–Vibration Spectra**, this handbook). Table 2 lists the rotational constants of the rovibrational bands discussed here. The WANG program was designed to allow, in principle, inclusion of all types of rovibrational interactions in the analysis, without the need for fundamental changes in the program. There are also other programs available

that adjust the constants of an effective asymmetric top Hamiltonian (Pickett 1991). Symmetric rotor programs like that described by Graner (1993) are also available.

## 4.2 Rovibrational Spectra of $\text{CHCl}_2\text{F}$

$\text{CHCl}_2\text{F}$  is a prolate asymmetric top molecule of  $C_s$  symmetry for identical chlorine isotopes with nine normal modes of symmetry  $A'$  and  $A''$  for the symmetric isotopomer.  $\text{CHCl}_2\text{F}$  exists in three isotopomers with a natural abundance of approximately 9 : 6 : 1 ( $\text{CH}^{35}\text{Cl}_2\text{F}$  :  $\text{CH}^{35}\text{Cl}^{37}\text{ClF}$  :  $\text{CH}^{37}\text{Cl}_2\text{F}$ ). The mixed  $^{35}\text{Cl}^{37}\text{Cl}$  isotopomer is chiral with  $C_1$  point group symmetry. We have recorded and analyzed the FTIR spectrum of  $\text{CHCl}_2\text{F}$  at 170 K and at room temperature in the range 1800–3600  $\text{cm}^{-1}$  (Albert *et al.* 2004b, 2007) at essentially Doppler-limited resolution. The rovibrational spectra of  $\text{CH}^{35}\text{Cl}_2\text{F}$  and  $\text{CH}^{35}\text{Cl}^{37}\text{ClF}$  have been studied in (Snels and Quack 1991) and (Albert *et al.* 2004a) in some detail. The ground state

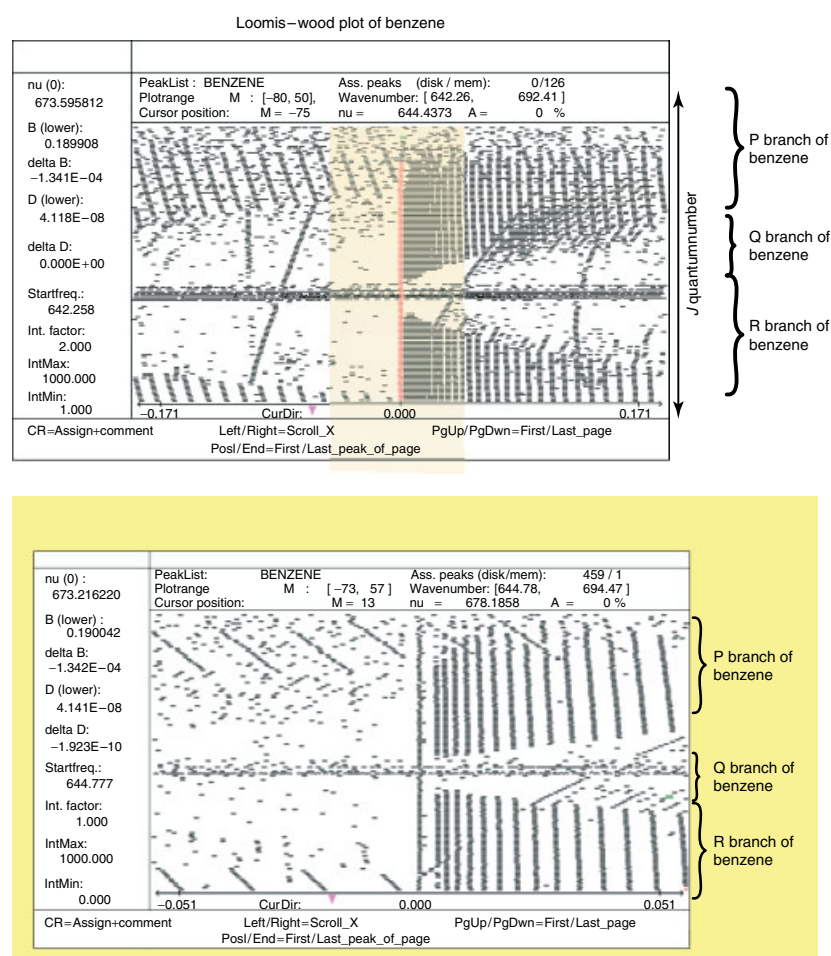


**Figure 20** (a) Loomis–Wood diagram of absorption transitions of the  $\nu_4$  band of benzene (top) in the P and R branch region. The different  $K$  series are visible. The lower frame illustrates a smaller part of the band and shows the benefit of the high resolution.

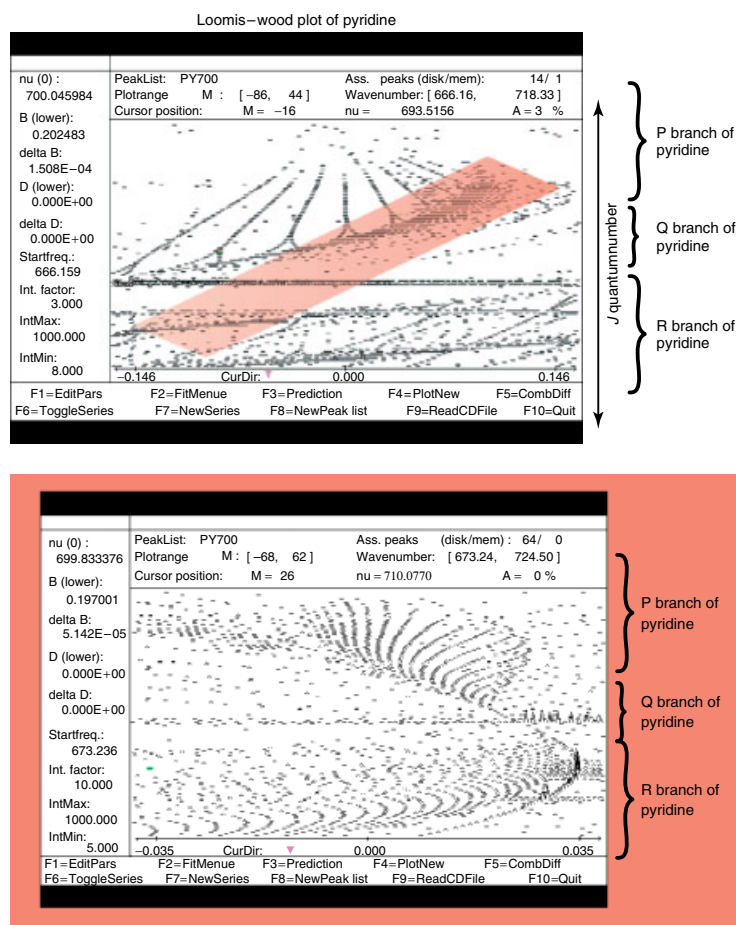


**Figure 20** (b) Loomis–Wood diagram of pyrimidine. The shaded area in the upper part appears enlarged in the lower part. The different  $K_c$  series are visible.

of  $\text{CHCl}_2\text{F}$  has been investigated using microwave (McLay 1964) and submillimeter wave spectroscopy (Luis *et al.* 1997, Lopez *et al.* 2002).

Because of the two heavy atoms and the presence of several isotopomers, the rotational structure of the bands is dense and congested. Only hybrid bands have been observed in the spectrum. For two reasons we discuss here the analysis of the  $2\nu_3$  band of  $\text{CH}^{35}\text{Cl}_2\text{F}$  and  $\text{CH}^{35}\text{Cl}^{37}\text{ClF}$  recorded at room temperature and at 170 K. First, we can demonstrate that the detailed rovibrational analysis of overtone spectra of relatively heavy molecules is now possible, which will lead to the identification and characterization of much more complicated resonance systems than those present in quasi-linear systems (Albert *et al.* 1996) or analyzed for  $\text{CHCl}_2\text{F}$  and related systems at lower resolution (Quack 1990, Dübal and Quack 1984). This provides much more insight into complicated rovibrational dynamics and energy transfers upon excitation. One can also relate this to recent results on the slightly lighter molecule  $\text{CHClF}_2$  (Albert *et al.* 2004c, 2006c). Second, the  $2\nu_3$  band provides the opportunity to study an overtone band of an isotopically

chiral molecule, on which quasis resonant two-photon  $\text{CO}_2$  laser spectroscopy can be carried out in order to experimentally detect parity violation (Albert *et al.* 2007). Finally, the spectroscopy of  $\text{CHCl}_2\text{F}$  is of obvious interest in the framework of studies of trace gases in the Earth's atmosphere.

A-type transitions of the  $2\nu_3$  band of  $\text{CHCl}_2\text{F}$  up to  $J \leq 90$ ,  $K_a \leq 9$  and c-type transitions up to  $J \leq 65$ ,  $K_c \leq 23$  were assigned in the room-temperature spectrum. The a-type series were identified as P and R branches with  $J \pm 1$ ,  $K_a$ ,  $K_c = J \pm 1 - K_a \leftarrow J$ ,  $K_a$ ,  $K_c = J - K_a$ . All three rotational constants, all five quartic distortion constants, and the sextic distortion constants  $\Phi_J$ ,  $\Phi_{KJ}$ ,  $\phi_J$ , and  $\phi_K$  were determined. The  $2\nu_3$  band of  $\text{CH}^{35}\text{Cl}_2\text{F}$  is relatively free of perturbations. However, the determination of sextic constants indicates a weak global interaction, probably with the  $\nu_3 + \nu_6 + \nu_8$  state. The  $2\nu_3$  band of  $\text{CH}^{35}\text{Cl}^{37}\text{ClF}$  is more perturbed. In spite of these perturbations, a simulation performed using the optimized spectroscopic constants represents the spectrum fairly well. A comparison of the  $2\nu_3$  band measured at room temperature with a simulation of the  $2\nu_3$  bands of  $\text{CH}^{35}\text{Cl}_2\text{F}$  and  $\text{CH}^{35}\text{Cl}^{37}\text{ClF}$ ,

**Table 2** Rotational constants and spectroscopic parameters of  $\text{CHCl}_2\text{F}$ ,  $\text{CDBrClF}$ , pyridine, and pyrimidine.

Molecule	Number of modes	Isotopomers	Molecular mode mass/Da	$\tilde{\nu}_0/\text{cm}^{-1}$	$A/\text{cm}^{-1}$	$B/\text{cm}^{-1}$	$C/\text{cm}^{-1}$	Perturbations	
<b><math>\text{CHCl}_2\text{F}</math></b>	9	3							
Albert <i>et al.</i> (2007)		$^{12}\text{CH}^{35}\text{Cl}_2\text{F}$	101.94	$2\nu_3$	2140.084 560 (48)	0.231 449 59 (13)	0.110 349 95 (21)	0.078 232 286 (66)	Weak global interaction
		$^{12}\text{CH}^{35}\text{Cl}^{37}\text{ClF}$	103.94	$2\nu_3$	2139.991 790 (63)	0.229 948 40 (19)	0.107 421 85 (43)	0.076 590 29 (19)	Weak global interaction
<b><math>\text{CDBrClF}</math></b>	9	4							
Albert <i>et al.</i> (2003b)		$^{12}\text{CD}^{79}\text{Br}^{35}\text{ClF}$	146.90	$\nu_4$	1082.811 560 (22)	0.207 968 2 (38)	0.067 242 9 (23)	0.053 237 41 (82)	Interactions not detectable
		$^{12}\text{CD}^{81}\text{Br}^{35}\text{ClF}$	148.90	$\nu_4$	1082.796 250 (23)	0.207 825 8 (49)	0.066 580 5 (19)	0.052 793 35 (82)	Interactions not detectable
<b>Pyridine</b>	27	1							
Albert <i>et al.</i> (2005, 2006b)		$^{12}\text{C}_6\text{H}_5^{14}\text{N}$	91.04	$\nu_{18a}$	1071.887 80 (64)	0.201 389 7 (96)	0.193 849 4 (86)	0.098 765 (93)	Strong Coriolis resonance with $\nu_{18b}$
		$^{12}\text{C}_6\text{H}_5^{14}\text{N}$	91.04	$\nu_{15}$	1143.537 400 (37)	0.201 553 023 (43)	0.193 539 66 (13)	0.098 737 62 (16)	Weak Coriolis resonance with $\nu_4 + \nu_{16b}$
<b>Pyrimidine</b>	24	1							
Albert and Quack (2007b)		$^{12}\text{C}_4\text{H}_4^{14}\text{N}_2$	80.00	$\nu_4$	718.541 112 (12)	0.209 826 260 (47)	0.202 415 99 (52)	0.102 920 77 (35)	No interaction observed

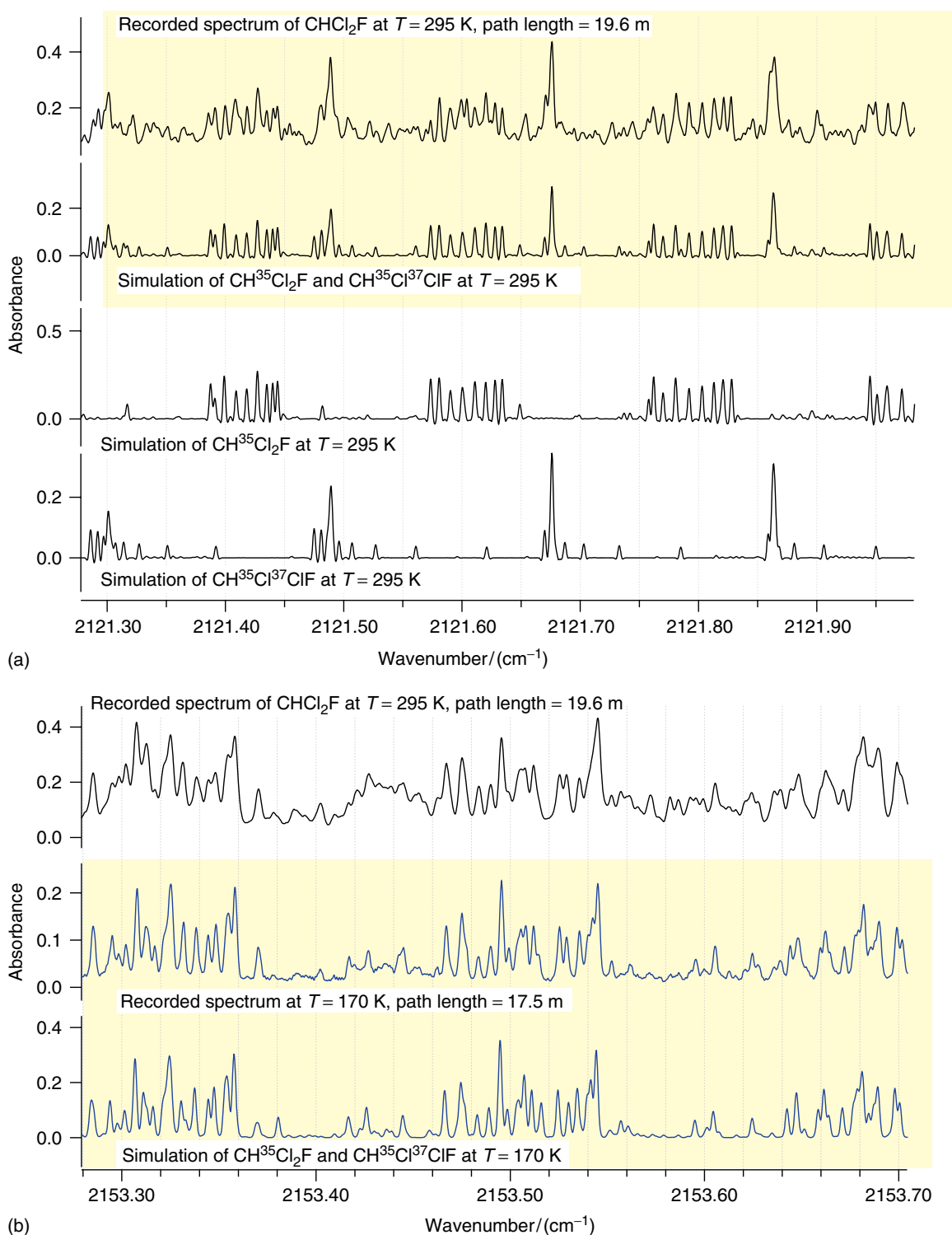


**Figure 21** (a) A comparison of the  $2\nu_3$  band of  $\text{CHCl}_2\text{F}$  measured at  $295\text{ K}$  and at a pressure of  $0.9\text{ mbar}$  (a, first trace, path length =  $19.6\text{ m}$ , instrumental resolution =  $0.0011\text{ cm}^{-1}$ ) with a simulation of the  $2\nu_3$  band at  $295\text{ K}$  of the two major isotopomers  $\text{CH}^{35}\text{Cl}_2\text{F}$  and  $\text{CH}^{35}\text{Cl}^{37}\text{ClF}$  (a, second trace); simulation of the  $2\nu_3$  band of  $\text{CH}^{35}\text{Cl}_2\text{F}$  at  $295\text{ K}$  (a, third trace); simulation of the  $2\nu_3$  band of  $\text{CH}^{35}\text{Cl}^{37}\text{ClF}$  at  $295\text{ K}$  (a, bottom trace). (b) A comparison of part of the  $2\nu_3$  band of  $\text{CHCl}_2\text{F}$  measured at  $295\text{ K}$  and at a pressure of  $0.9\text{ mbar}$  (b, first trace, path length =  $19.6\text{ m}$ , instrumental resolution =  $0.0011\text{ cm}^{-1}$ ) with a recorded cold spectrum (b, second trace,  $170\text{ K}$ ,  $17.5\text{ m}$  path length,  $0.8\text{ mbar}$  pressure, instrumental resolution =  $0.0011\text{ cm}^{-1}$ ) and with a simulation of the  $2\nu_3$  band at  $170\text{ K}$  of the two major isotopomers  $\text{CH}^{35}\text{Cl}_2\text{F}$  and  $\text{CH}^{35}\text{Cl}^{37}\text{ClF}$  (b, third trace). [Reproduced from Albert *et al.* 2007 with permission.]

calculated with the adjusted spectroscopic constants, is shown in Figure 21(a). It illustrates a selected part of the room-temperature spectrum in the region of the *c*-type P branches (a, top trace). One can clearly see by comparison of experiment (a, first trace) with the simulation (a, second trace) how the two major species  $\text{CH}^{35}\text{Cl}_2\text{F}$  (a, third trace) and  $\text{CH}^{35}\text{Cl}^{37}\text{ClF}$  (a, fourth trace) combine to form the spectrum of the  $2\nu_3$  band of  $\text{CHCl}_2\text{F}$ . The agreement between the recorded (a, first trace) and simulated (a, second trace) spectra in Figure 21 is quite good. The remaining differences can be attributed to hot bands and the minor isotopic species  $\text{CH}^{37}\text{Cl}_2\text{F}$ .

An even better agreement is possible if the cold spectrum (21b, second trace) measured at 170 K is compared to a simulation at 170 K containing the two major isotopomers  $\text{CH}^{35}\text{Cl}_2\text{F}$  and  $\text{CH}^{35}\text{Cl}^{37}\text{ClF}$  (b, third trace). In addition, the advantage of measuring a spectrum under cooling conditions is visible. A comparison of the  $\text{CH}^{35}\text{Cl}_2\text{F}$  spectrum taken at room temperature (b, first trace) with

the spectrum taken at 170 K (b, second trace) illustrates the better resolution of the spectra with features in the cold spectrum.

### 4.3 Rovibrational Spectra of CDBrClF

CDBrClF exists in four major isotopomers with a natural abundance of 0.380 ( $\text{CD}^{79}\text{Br}^{35}\text{ClF}$ ) : 0.369 ( $\text{CD}^{81}\text{Br}^{35}\text{ClF}$ ) : 0.122 ( $\text{CD}^{79}\text{Br}^{37}\text{ClF}$ ) : 0.118 ( $\text{CD}^{81}\text{Br}^{37}\text{ClF}$ ). Because of the two heavy atoms and their isotopomers, the rotational structure of the bands in this molecule also is dense and congested, as is that for  $\text{CHCl}_2\text{F}$ . Because of the low symmetry of the molecule, hybrid bands have been observed in the spectrum. The FIR spectrum of CDBrClF recorded at room temperature has been measured with instrumental resolutions between  $0.0008$  and  $0.0012\text{ cm}^{-1}$  and has been analyzed within the  $\nu_6$  (CBr-stretch),  $\nu_5$  (CCl-stretch),  $\nu_4$  (CF-stretch), and  $\nu_3$  (CDF-bend) regions (Albert and Quack 2001, Albert *et al.* 2001a, 2003b). Figure 22

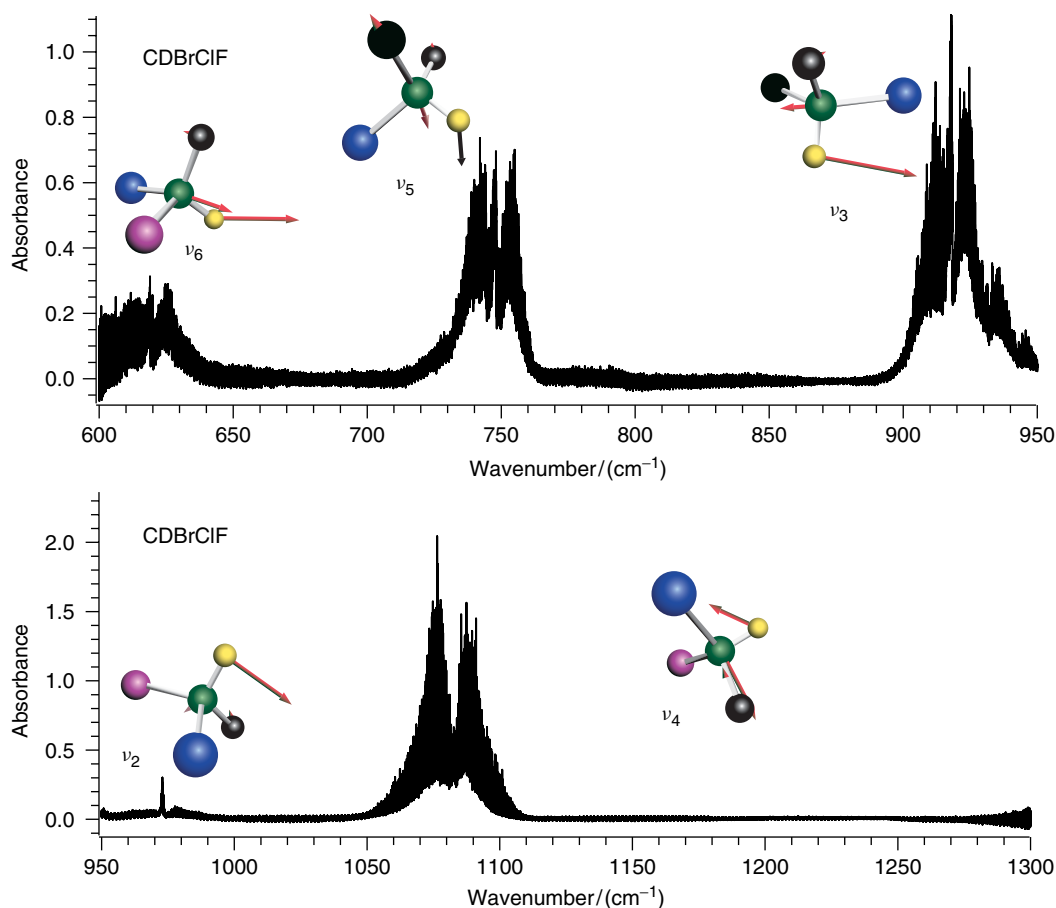


**Figure 22** Survey spectrum of CDBrClF in the range  $600\text{--}1300\text{ cm}^{-1}$  with the normal modes  $\nu_6$  (CBr-stretch),  $\nu_5$  (CCl-stretch),  $\nu_3$  (CDF-bend),  $\nu_2$  (CDF-bend), and  $\nu_4$  (CF-stretch) recorded at room temperature with a path length of 3.2 m and a pressure of 0.08 mbar. [See Albert *et al.* 2003b.]

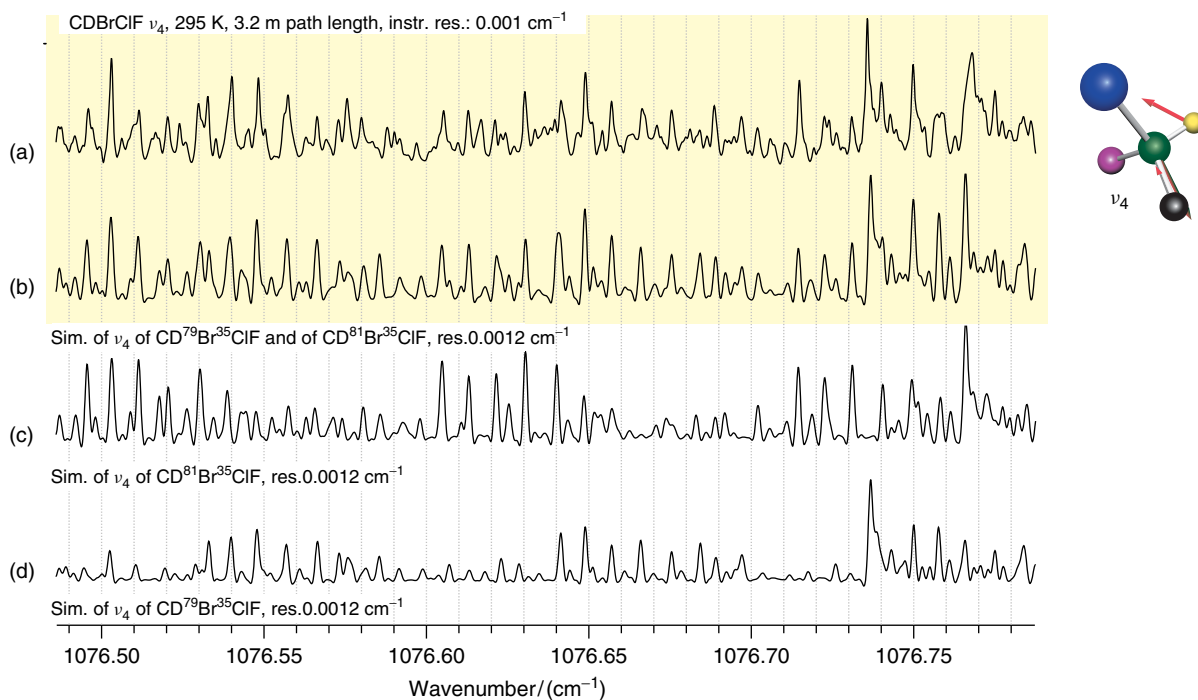


**Figure 23** A comparison of the  $\nu_4$  band of CDBrClF within the  $c$ -type P branches measured at 295 K (a trace, path length = 3.2 m, pressure = 0.08 mbar), with a simulation of the  $\nu_4$  band at 295 K of the two major isotopomers  $\text{CD}^{79}\text{Br}^{35}\text{ClF}$  and  $\text{CD}^{81}\text{Br}^{35}\text{ClF}$  (b trace); simulation of the  $\nu_4$  band of  $\text{CD}^{81}\text{Br}^{35}\text{ClF}$  at 295 K (c trace); and simulation of the  $\nu_4$  band of  $\text{CD}^{79}\text{Br}^{35}\text{ClF}$  at 295 K (d trace). Resolution =  $0.001\text{ cm}^{-1}$  for all. [See also Albert *et al.* 2003b.]

displays a survey spectrum of CDBrClF between  $600$  and  $1300\text{ cm}^{-1}$  recorded at room temperature, showing the fundamentals  $\nu_2$ ,  $\nu_3$ ,  $\nu_4$ ,  $\nu_5$ , and  $\nu_6$ . All the bands shown except  $\nu_2$  have been rotationally resolved and analyzed in our work.

As an example of an analysis of a rovibrational band, we present here in Figure 23 the CF-stretching fundamental  $\nu_4$  (Albert and Quack 2001), which occurs near  $1100\text{ cm}^{-1}$  as shown in Figure 22. The absorption lines of the two major isotopomers  $\text{CD}^{79}\text{Br}^{35}\text{ClF}$  and  $\text{CD}^{81}\text{Br}^{35}\text{ClF}$  have been assigned. Despite the congestion of the spectrum at room temperature, it was not necessary to decrease the rotational temperature of the sample in order to simplify the spectra. There were no rotational constants available for the ground state or any other vibrationally excited state. For this reason, additional vibrational bands of CDBrClF ( $\nu_3$ ,  $\nu_5$ ,  $\nu_6$ ) were assigned and analyzed to determine the spectroscopic constants of the ground state for the isotopomers  $\text{CD}^{79}\text{Br}^{35}\text{ClF}$  and  $\text{CD}^{81}\text{Br}^{35}\text{ClF}$  by means of ground-state combination differences. Two types of subbands ( $a$ - and  $c$ -types) were assigned in the spectrum.

The simulation of the  $\nu_4$  band for  $\text{CD}^{79}\text{Br}^{35}\text{ClF}$  and  $\text{CD}^{81}\text{Br}^{35}\text{ClF}$  can be based on the adjusted spectroscopic constants. Figure 23 provides an example for a comparison between the observed and simulated spectra of a part of the  $\nu_4$  fundamental band for  $\text{CD}^{79}\text{Br}^{35}\text{ClF}$  and  $\text{CD}^{81}\text{Br}^{35}\text{ClF}$ .

This part of the spectrum contains the  $c$ -type P branch lines. As can be seen from the spectrum (a trace) and the simulation for the two major isotopomers (b trace),  $\text{CD}^{81}\text{Br}^{35}\text{ClF}$  (c trace), and  $\text{CD}^{79}\text{Br}^{35}\text{ClF}$  (d trace), there is good agreement between the experimental and calculated spectra. Obviously, the agreement cannot be perfect because lines of the two minor isotopomers  $\text{CD}^{79}\text{Br}^{37}\text{ClF}$  and  $\text{CD}^{81}\text{Br}^{37}\text{ClF}$  are not assigned, and because hot bands visible at room temperature are not considered in the simulation. These remain to be studied.

## 4.4 Rovibrational Spectrum of Pyrimidine

### 4.4.1 General Aspects

Pyrimidine is a molecule of  $C_{2v}$  symmetry. The coordinate system for the symmetry assignment of the  $C_{2v}$  normal modes was chosen so that the twofold rotational axis, the  $z$ -axis, goes through the C atom between the two N atoms, the  $y$ -axis lies perpendicular not only to  $z$  but also in the plane of the molecule, and the  $x$ -axis intersects the center of gravity perpendicular to the  $z$ - and  $y$ -axes (Figure 19 lower left). Pyrimidine has 24 normal modes. Among these, nine modes have  $A_1$  symmetry, eight modes have  $B_2$  symmetry, five modes have  $B_1$  symmetry, and two modes have  $A_2$  symmetry. All modes except the  $A_2$  modes are IR active.

**Table 3** The symmetry classes for the normal modes of benzene, pyridine, D1-benzene and pyrimidine according to Wilson's notation (Snels *et al.* 1997, Kline and Turkevich 1944, Albert *et al.* 2005, 2006b, Wilson 1934, Innes *et al.* 1988).

Benzene	D1-Benzene	Pyridine	Pyrimidine
$A_{1g}$ { 1 } (-, -)	1 982.1	1 991	1 991
$B_{1u}$ { 2 } (-, -)	2 3068.0	2 3094	2 3074
$E_g^+$ { 6a, 7a, 8a, 9a } (R, -)	6a 603.1 7a 3087 8a 1591.1 9a 1175.6	6a 601 8a 1584 9a 1218	6a 677 7a 8a 1570 9a 1147
$E_u^-$ { 3, 8a, 9a } (-, IR)	3 2277.8 8a 1034.6 9a 1480.5	3 3073 18a 1071.87780 19a 1483	3 3052 18a 19a 1398
$E_u^-$ { 18, 19, 20 } (-, IR)	18 3087 19 20	20a 3030 T <sub>z</sub>	20a 3038 T <sub>z</sub>
$E_u^-$ { 18, 19, 20 } (-, IR)	18 3087 19 20	20a 3030 T <sub>z</sub>	20a 3038 T <sub>z</sub>
$B_{2u}$ { 14, 15 } (-, -)	14 1292 15 1158.2	14 1362 15 1143.537400	14 1225 15 1159
$A_{2g}$ { 3 } (-, -)	3 1332.7	3 1227	3 1370
$B_{2g}$ { 4, 5 } (-, -)	4 697.7 5 984.3	4 744.006597 5 1007	4 718.541112 5 980
$A_{2u}$ { 11 } (-, IR)	11 607.1	11 700.252875	11 803.979476
$E_u^+$ { 16, 17 } (-, -)	16b 377.9 17b 924.2	16b 403.3 17b 937	16b 344 17b 955
$E_g^-$ { 10 } (R, -)	10a 849.9 16a 398 17a 970	10a 871 16a 373 17a 966	10a 16a 399 17a 927

For the axes notation see Figure 19. The  $T_{x,y,z}$  are the translations along the  $x, y, z$  axes and  $R_{x,y,z}$  are the rotations around the  $x, y, z$  axes.

**Table 4** Character table for the  $C_{2v}$  and  $S_2^*(M_{S4})$  symmetry groups relating to axes definitions in the bottom part of Figure 19.

$C_{2v}$	$S_2^*(M_{S4})$	$E$	$C_2$ ( $\alpha\beta$ )	$\sigma_{xy}$ ( $\alpha\beta$ ) <sup>*</sup>	$\sigma_{yz}$ $E^*$	$\mu$	$J$	$K_a K_c$	$n_{\Gamma_v}$	$g$
<b>Pyrimidine (C<sub>4</sub>H<sub>4</sub>N<sub>2</sub>)</b>										
$A_1$	$A^+$	1	1	1	1	$\mu_z$		$ee$	9	15
$A_2$	$A^-$	1	1	-1	-1		$J_z$	$eo$	2	21
$B_1$	$B^-$	1	-1	1	-1	$\mu_x$	$J_y$	$oo$	5	15
$B_2$	$B^+$	1	-1	-1	1	$\mu_y$	$J_x$	$oe$	8	21
<b>Pyridine (C<sub>5</sub>H<sub>5</sub>N)</b>										
$A_1$	$A^+$	1	1	1	1	$\mu_z$		$ee$	10	60
$A_2$	$A^-$	1	1	-1	-1		$J_z$	$eo$	3	60
$B_1$	$B^-$	1	-1	1	-1	$\mu_x$	$J_y$	$oo$	5	36
$B_2$	$B^+$	1	-1	-1	1	$\mu_y$	$J_x$	$oe$	8	36

For the molecular symmetry group  $M_{S4}$  ( $\alpha\beta$ ) corresponds to the permutation of the equivalent parts of the molecule and the upper right index of the symmetry species indicates parity (+ or -) (Quack 1977, Puttkamer and Quack 1987, Puttkamer *et al.* 1988, Riedle *et al.* 1994).

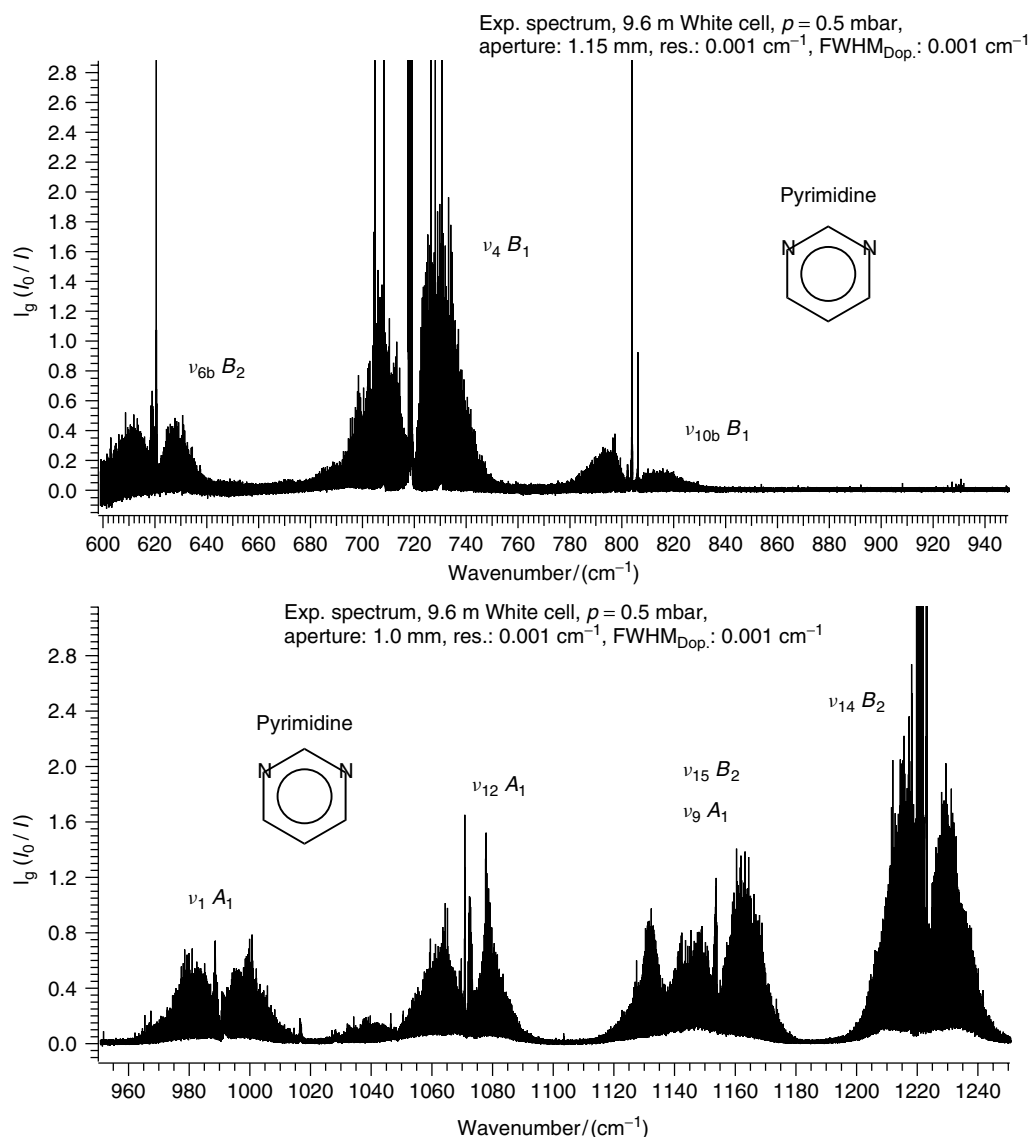


**Figure 24** Overview spectrum of pyrimidine in the range 600–1250  $\text{cm}^{-1}$ .

The  $A_1$  modes show  $b$ -type transitions in the IR spectra, the  $B_1$  modes  $c$ -type transitions, and the  $B_2$  modes  $a$ -type transitions. Table 3 provides an overview of the normal modes of pyrimidine according to the labeling of Innes *et al.* (Innes *et al.* 1988) and their correlation with the normal modes of benzene, deuterated benzene, and pyridine (Lord *et al.* 1957, Kline and Turkevich 1944, Snels *et al.* 1997) according to Lord's (Lord *et al.* 1957) notation, which is based on Wilson's benzene notation (Wilson 1934). However, it should be mentioned that with an increased number of nitrogen atoms and a decreased number of normal modes, the correlation to the benzene modes is not always unambiguous. For this reason, the mode at 803  $\text{cm}^{-1}$  is labeled as  $\nu_{10b}$  by Innes *et al.* (1988) and as  $\nu_{11}$  by Billes *et al.* (1998).

We have recorded and analyzed the FTIR spectrum of pyrimidine in the range 600 to 1250  $\text{cm}^{-1}$  shown in Figure 24 at essentially Doppler-limited resolution (Albert and Quack 2007b). The  $\nu_4$  mode discussed in this article is an out-of-plane mode of the aromatic ring of  $B_1$  species, ( $x$ -polarized in the present convention). For the sake of clarity, Table 4 (upper part) shows the  $C_{2v}$  character table in relation to the  $S_2^*$  molecular symmetry group  $M_{S4}$  (Quack 1977, Puttkamer and Quack 1987, Puttkamer *et al.* 1988, Riedle *et al.* 1994), giving the relevant species, as well as the related parity (+ or – as exponent to the  $S_2^*$  symmetry species), the components of the electric dipole moment vector  $\mu$  in the molecule-fixed axis system, the components of the rotational angular momentum  $J$ , and the reduction  $n_{\Gamma_v}$  of the vibrational species in  $C_{2v}$  for

pyrimidine as well as the spin statistical weights. The overall electric dipole rovibronic selection rule is

1. parity change ( $+ \leftrightarrow -$ );
2. conservation of nuclear spin symmetry (i.e.,  $A \leftrightarrow B$ )

Table 4, together with the usual asymmetric rotor functions and nuclear spin functions, thus defines the relevant transitions. The upper part in Table 4 represents the pyrimidine molecule and the lower part the pyridine molecule.

#### 4.4.2 The $\nu_4$ Mode of Pyrimidine

The  $\nu_4$  band has  $B_1$  symmetry and shows  $c$ -type transitions, which were assigned up to  $J \leq 76$ ,  $K_c \leq 47$  in the spectrum. No important perturbations were observed. The  $c$ -type series were identified as P and R branches with  $J \pm 1$ ,  $K_a = J \pm 1 - K_c$ ,  $K_c \leftarrow J$ ,  $K_a = J - K_c$ ,  $K_c$ . The spacing between two transitions of a series is approximately  $2A$ . The assignments were checked by comparison of the combination differences of the ground state calculated from the assignments of the  $\nu_4$  and  $\nu_{10b}$  fundamental bands.

All constants for the ground state up to the sextic distortion constants of pyrimidine were fixed to the values

of Kisiel *et al.* (1999). All absorption lines up to  $J \leq 76$  were used for the fit of the spectroscopic constants of the  $\nu_4$  ( $B_1$  symmetry) state of pyrimidine. All three rotational constants, all five quartic distortion constants, and the sextic distortion constants  $\Phi_J$ ,  $\Phi_{KJ}$ ,  $\Phi_K$ , and  $\phi_J$  in the  $A$ -reduction and  $I'$  representation were determined. The values of the other sextic constants were held to the values of the ground state. Using the  $S$ -reduction and  $III'$  representation, all constants used to describe the ground state were determined for the  $\nu_4$  state. The  $d_{rms}$  was  $0.00018 \text{ cm}^{-1}$  for both representations. There were small correlations between the determined sextic constants in the  $A$ -reduction and  $I'$  representation. These correlations were reduced to one small correlation between  $H_J$  and  $D_J$  by the use of the  $S$ -reduction and  $III'$  representation. A comparison of the recorded spectrum with the simulated spectrum calculated with the spectroscopic constants partially shown in Table 2, including the spin statistical weights according to Table 4 in the  $\nu_4$  region, illustrates a very good agreement, as is shown by the enlargement of the Q branch region of the  $\nu_4$  band of pyrimidine in Figure 25, which shows the overall agreement in this range as well as the agreement

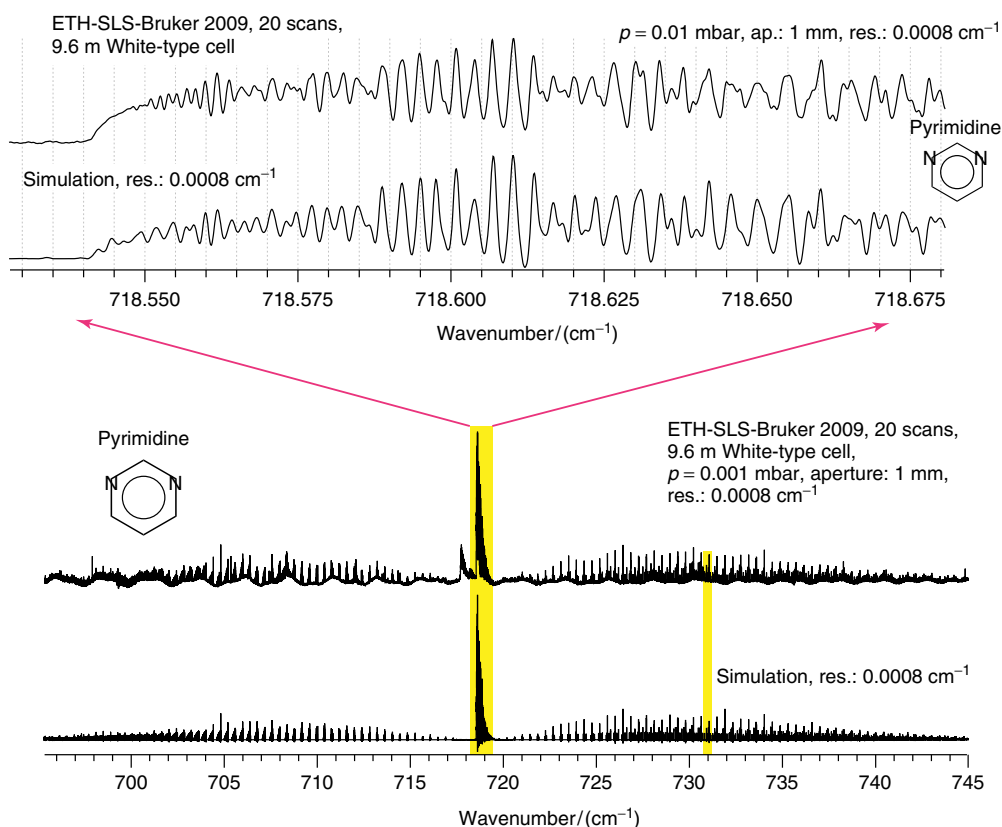


**Figure 25** Comparison of recorded and simulated spectrum of the  $\nu_4$  band of pyrimidine: The top figure is an enlargement of the Q branch region. The  $\nu_4$  band of pyrimidine measured at 295 K in a 9.6 m White-type cell with  $p = 0.01$  mbar and resolution =  $0.0008 \text{ cm}^{-1}$  (top traces,  $\text{FWHM}_{\text{Dop}} = 0.001 \text{ cm}^{-1}$ ) is shown together with a simulation of the  $\nu_4$  band of pyrimidine at 295 K (lower traces, resolution =  $0.0008 \text{ cm}^{-1}$ ). [see also Albert and Quack 2007b.]

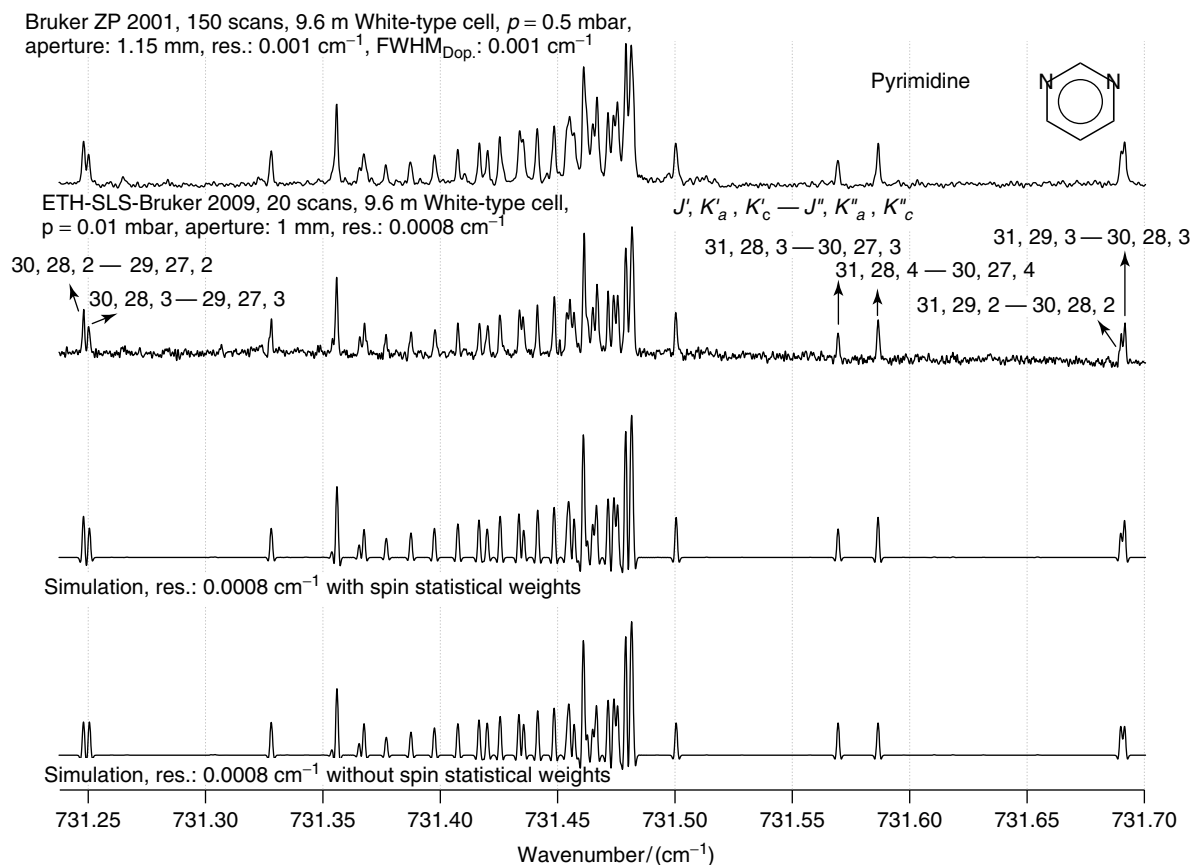


**Figure 26** Comparison of part of the spectrum of the  $\nu_4$  band of pyrimidine recorded with the Bruker ZP2001 (top trace, 9.6 m path length, 1.15 mm aperture, 0.5 mbar pressure, resolution  $0.001\text{ cm}^{-1}$ ), measured with the ETH-SLS Bruker 2009 (second trace, 9.6 m path length, 1 mm aperture, 0.001 mbar pressure, resolution  $0.0008\text{ cm}^{-1}$ ) with a simulation including spin statistical weights (third trace) and a simulation neglecting spin statistical weights (bottom trace).

in detail. Even the absorption features of incompletely resolved absorption lines can be reproduced.

Because of the spin statistical weights  $ee/eo/oo/oe = 15/21/15/21$  of pyrimidine, the intensity alternation of the  $c$ -type transitions can only be observed if the asymmetric splitting can be resolved. For this reason, we have measured the  $\nu_4$  band of pyrimidine, a sum of twenty scans, with our new Bruker ETH-SLS spectrometer again using the synchrotron source and a resolution of  $0.0008\text{ cm}^{-1}$  at low pressure (0.01 mbar). As seen from Figure 26 (top and second trace), the ETH-SLS recording (second trace) leads to a slightly better resolution compared to the Bruker ZP2001 measurement (top trace) and therefore slightly better-resolved asymmetric splitting. A simulation with spin statistical weights is shown in Figure 26 (third trace). The agreement is excellent and illustrates again the very high resolving power of our spectrometers. As a comparison, a simulation without spin statistical weights is also shown (bottom trace). The discrepancies are clearly visible.

## 4.5 Rovibrational Spectra of Pyridine

### 4.5.1 General Aspects

Pyridine is also a molecule of  $C_{2v}$  symmetry and has 27 normal modes. Among these, 10 modes have  $A_1$  symmetry, 9 modes have  $B_2$  symmetry, 5 modes have  $B_1$  symmetry, and 3 modes have  $A_2$  symmetry (Kline and Turkevich 1944). In assigning the symmetry species of the  $C_{2v}$  point group, we follow here the axis convention in which the  $z$ -axis goes through the N atom corresponding to the  $a$  axis, the  $y$ -axis lies perpendicular to  $z$  in the plane of the molecule, corresponding to the  $b$  axis, and the  $x$ -axis ( $c$  axis) intersects the center of gravity perpendicular to the ring plane spanned by the  $z$ - and  $y$ -axes (Figure 19). The rovibrational analysis was carried out with the  $A$ -reduced Watson Hamiltonian in the  $\text{III}'$  representation, which requires relabeling of the axis ( $x' = a$ ,  $y' = -b$ ,  $z' = c$ ; see Snels *et al.* 1997). All modes except the  $A_2$  modes are IR active. The  $A_1$  modes show  $a$ -type transitions in the IR spectra, the  $B_1$  modes  $c$ -type transitions, and the  $B_2$  modes  $b$ -type transitions. Table 3 summarizes the fundamental frequencies of pyridine and

relates the conventional spectroscopic numbering to the Wilson notation (Kline and Turkevich 1944, Wilson 1934), which is derived from the symmetric  $C_6H_6$   $D_{6h}$  case. By lowering the symmetry, the  $C_6H_6$  modes split into nondegenerate modes labeled as  $A$  and  $B$  in isotopomers such as  $C_6H_5D$  (Snels *et al.* 1997). Pyridine has one atom and three vibrational degrees of freedom less than benzene. In Table 4, the character table for pyridine is given including the spin statistical weights. A comparison with pyrimidine illustrates the difference. As an example, we show here a part of the  $\nu_{11}$  band of pyridine fully analyzed in Albert *et al.* (2005). According to the spin statistical weights, it is not necessary to resolve the asymmetric splitting in order to observe intensity alternation. As Figure 27 illustrates, the intensity alternation is observed for  $ee$  and  $oo$  transitions (top trace, left part) or for  $eo$  and  $oe$  transitions (top trace, right part). The agreement with the simulation that includes the spin statistical weights (Figure 27, middle trace) is again excellent. A simulation for comparison without spin statistical weights is shown in Figure 27

(lower trace). The intensity discrepancies are again clearly visible.

In addition, we present here the rovibrational analysis of the fundamentals  $\tilde{\nu}_{18a} = 1071.887\ 80\text{ cm}^{-1}$  and  $\tilde{\nu}_{15} = 1143.537\ 400\text{ cm}^{-1}$  of pyridine (Albert *et al.* 2005, 2006b, Albert and Quack 2007a). An overview spectrum of these region  $960\text{--}1240\text{ cm}^{-1}$  is shown in Figure 28. A complete analysis of these bands including the  $\nu_{9a}$ ,  $\nu_1$ , and  $\nu_{12}$  is reported in (Albert *et al.* 2006b). These two bands are examples of perturbed transitions. The analysis of these bands illustrates the importance of including the interaction of dark states.

#### 4.5.2 The $\nu_{18a}$ Mode of Pyridine

This mode of pyridine has  $A_1$  symmetry. It was assigned in the spectrum as P and R branches for  $a$ -type transitions ( $J < 60$ ,  $K_a < 55$ ). The  $\nu_{18a}$  band is perturbed by a  $z$ -Coriolis resonance between the  $\nu_{18a}$  and  $\nu_{18b}$  ( $B_2$ ) states.

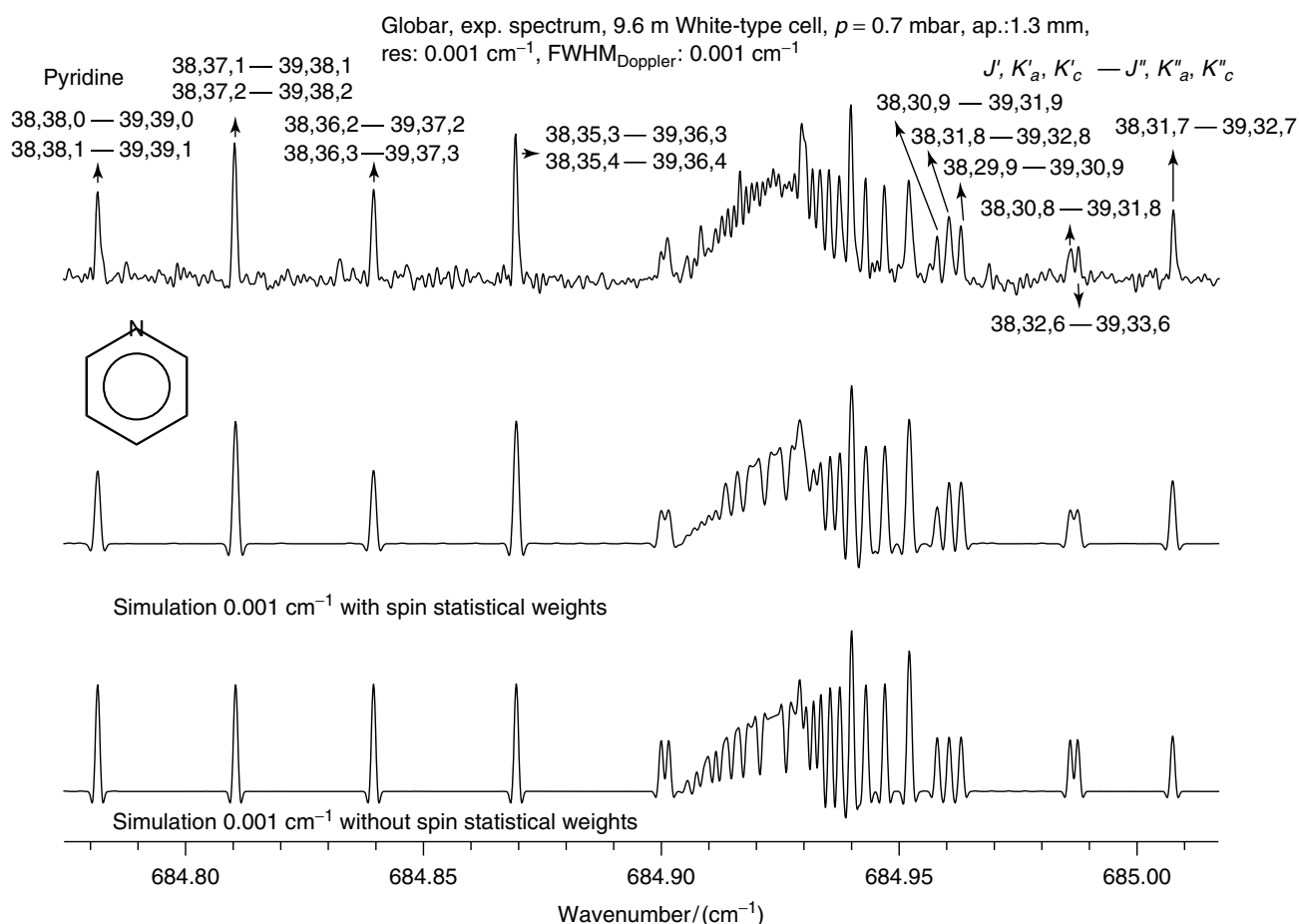


**Figure 27** Comparison of part of the spectrum of the  $\nu_{11}$  band of pyridine recorded with the Bruker ZP2001 (top trace, 9.6 m path length, 1.3 mm aperture, 0.7 mbar pressure, resolution  $0.001\text{ cm}^{-1}$ ) with a simulation including spin statistical weights (middle trace) and a simulation neglecting spin statistical weights (bottom trace).

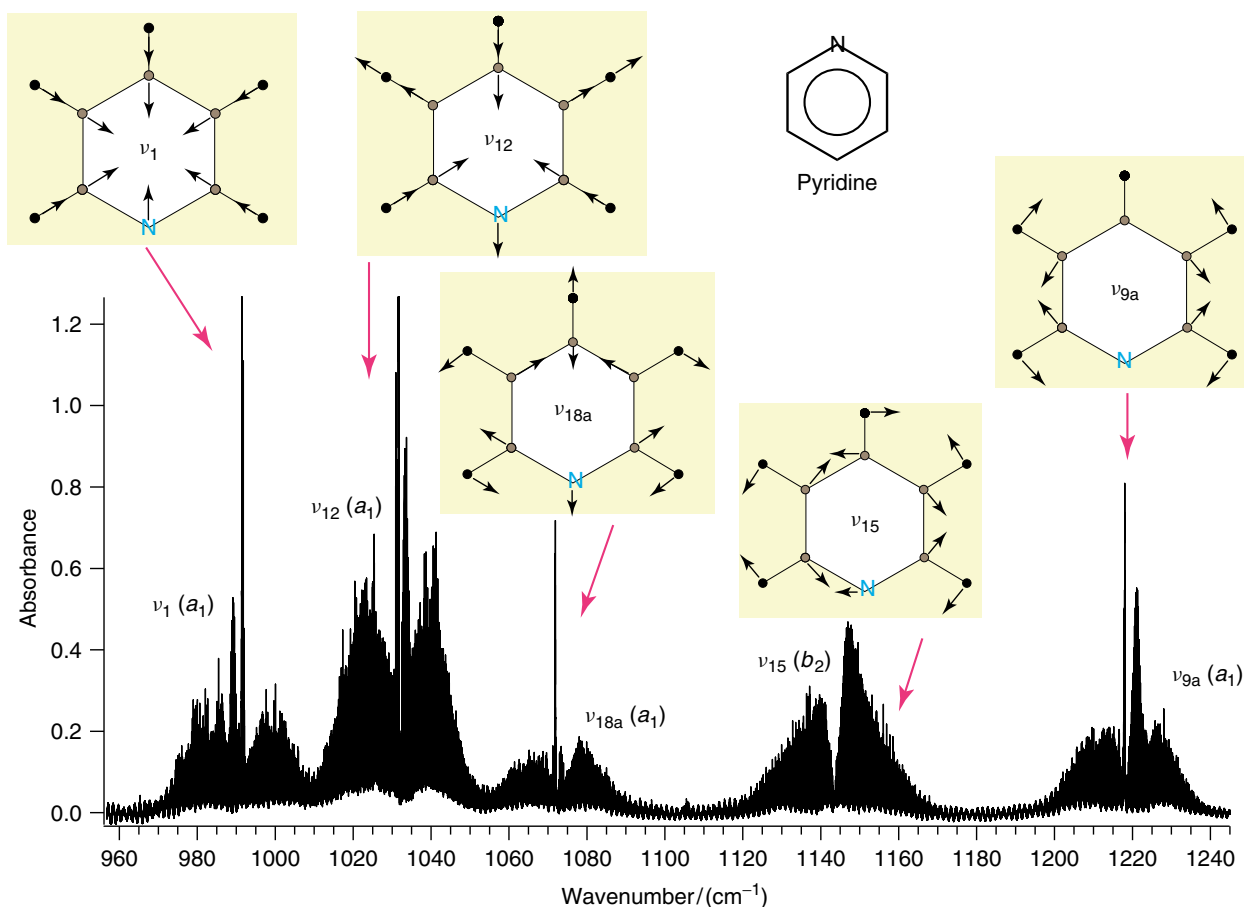


**Figure 28** Overview spectrum of pyridine in the range 940–1240  $\text{cm}^{-1}$  (decadic absorbance  $\lg(I_0/I)$  is shown).

Because of the lower symmetry of pyridine, the degenerate mode  $\nu_{18}$  ( $E_u$ -symmetry) of benzene splits into two different vibrations of pyridine  $\nu_{18a}$  and  $\nu_{18b}$ . Both vibrations are strongly coupled by a  $J$ -dependent Coriolis resonance. The rotational, quartic, and some sextic distortion constants of the  $\nu_{18a}$  state were determined. Because of the strong coupling, the band center  $\nu_0 = 1075.28 \text{ cm}^{-1}$  of the dark state  $\nu_{18b}$  and the Coriolis parameter  $\xi_z = 0.037 \text{ cm}^{-1}$  were determined. The rotational constants of the dark state  $\nu_{18b}$  were fixed to the values for the ground state except for the rotational constants  $B$  and  $C$ . Figure 29 shows a comparison of the recorded band to a simulation using the fitted constants of an effective Hamiltonian. The upper trace of each set shows the spectrum recorded in a 3 m cell with aperture 1.15 mm and a pressure of 0.8 mbar, the middle trace of each set the spectrum recorded in a White-type cell with 9.6 m path length with aperture 1 mm and a pressure of 0.3 mbar, and the lowest trace of each set shows the simulation of the pyridine spectrum with a resolution of  $0.0014 \text{ cm}^{-1}$ . As one can see, the reduction of the aperture and the pressure yields a slightly more highly resolved spectrum. A few  $\text{NH}_3$  absorption lines are visible at large path

length. These lines can be used for an internal wavenumber calibration of the measured spectrum. The enlargements of parts of the spectrum in Figure 29 illustrate the good agreement between the recorded and the simulated spectrum, which is excellent for such a complex molecule.

#### 4.5.3 The $\nu_{15}$ Mode of Pyridine

This mode of pyridine has  $B_2$  symmetry. It was assigned in the spectrum as P and R branches for  $b$ -type transitions ( $J < 55$ ). The  $\nu_{15}$  band is perturbed by a  $z$ -Coriolis resonance between the  $\nu_{15}$  and a dark state with the preliminary assignment  $\nu_4 + \nu_{16b}$  ( $A_1$ ). According to an estimation of the vibrational levels, the state  $\nu_4 + \nu_{16b}$  is the closest state to the  $\nu_{15}$  state ( $\Delta\nu_c \approx 7 \text{ cm}^{-1}$ ). The rotational and quartic distortion constants of the  $\nu_{15}$  state were determined. The spectroscopic constants of the dark state  $\nu_4 + \nu_{16b}$  were fixed to the values of the ground state, except for the rotational constant  $B$ . The Coriolis parameter  $\xi_z$  was determined to be  $0.006 \text{ cm}^{-1}$  and the band center of this vibrational band as  $1147.08 \text{ cm}^{-1}$ . Figure 30 shows a comparison of the recorded band to a simulation using the adjusted constants of an effective Hamiltonian. Again, the

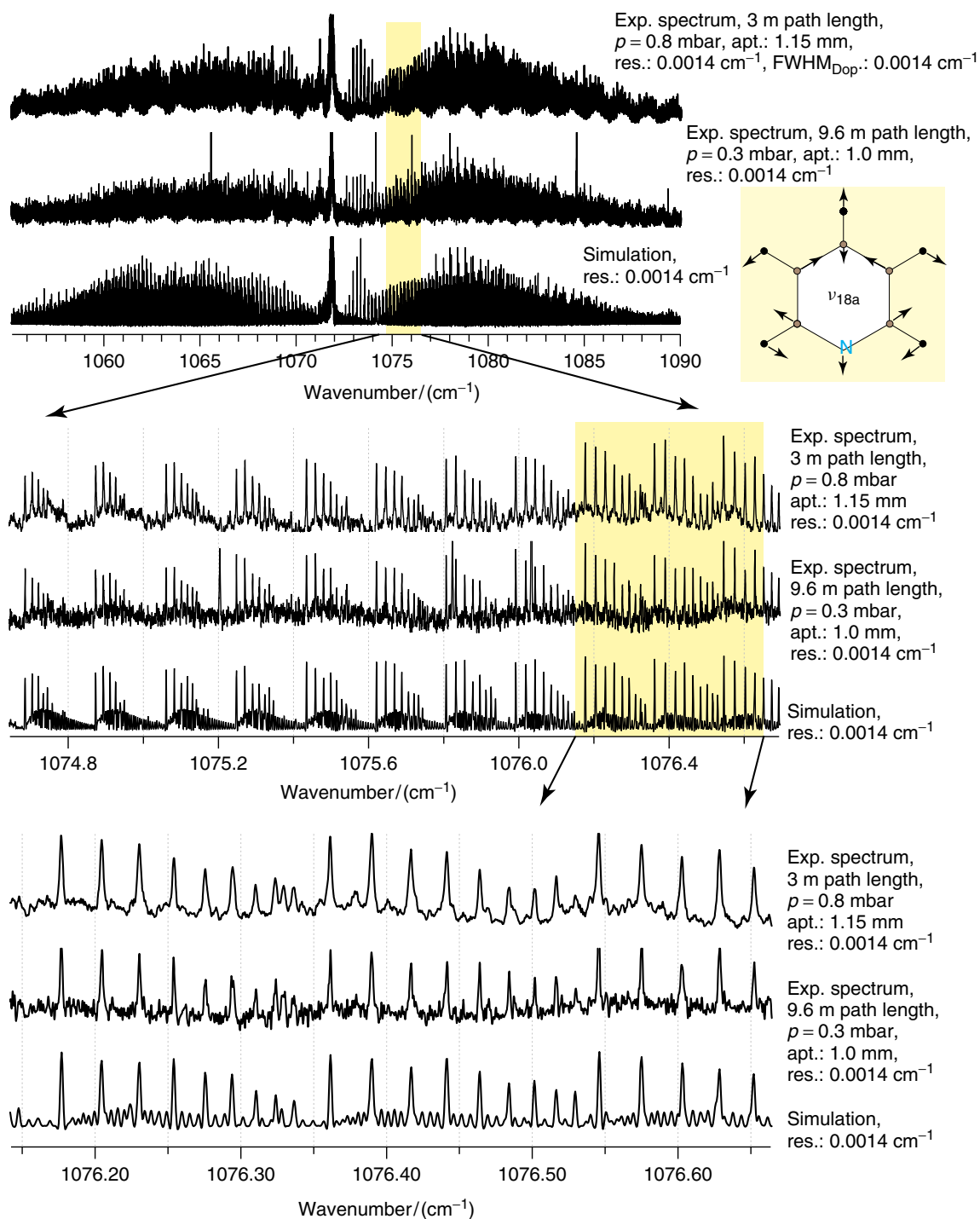


**Figure 29** Comparison of recorded and simulated spectra of the  $\nu_{18a}$  band of pyridine: the middle and bottom figures are enlargements of the shaded parts of the spectra shown above. The  $\nu_{18a}$  band of pyridine measured at 295 K in a 3 m glass cell with  $p = 0.8$  mbar and resolution =  $0.0014\text{ cm}^{-1}$  (top traces,  $\text{FWHM}_{\text{Dop}} = 0.0014\text{ cm}^{-1}$ ) and at 295 K in a 9.6 m White-type cell,  $p = 0.3$  mbar and a resolution =  $0.0014\text{ cm}^{-1}$  (middle traces,  $\text{FWHM}_{\text{Dop}} = 0.0014\text{ cm}^{-1}$ ) is shown together with a simulation of the  $\nu_{18a}$  band of pyridine at 295 K (lower traces, resolution =  $0.0014\text{ cm}^{-1}$ ).  $\text{NH}_3$  absorption lines are visible in the middle traces of the top two spectra sets that are recorded at large path length. These  $\text{NH}_3$  lines can be used for internal calibration of the measured spectrum. [Reproduced by permission from Albert and Quack 2007b.]

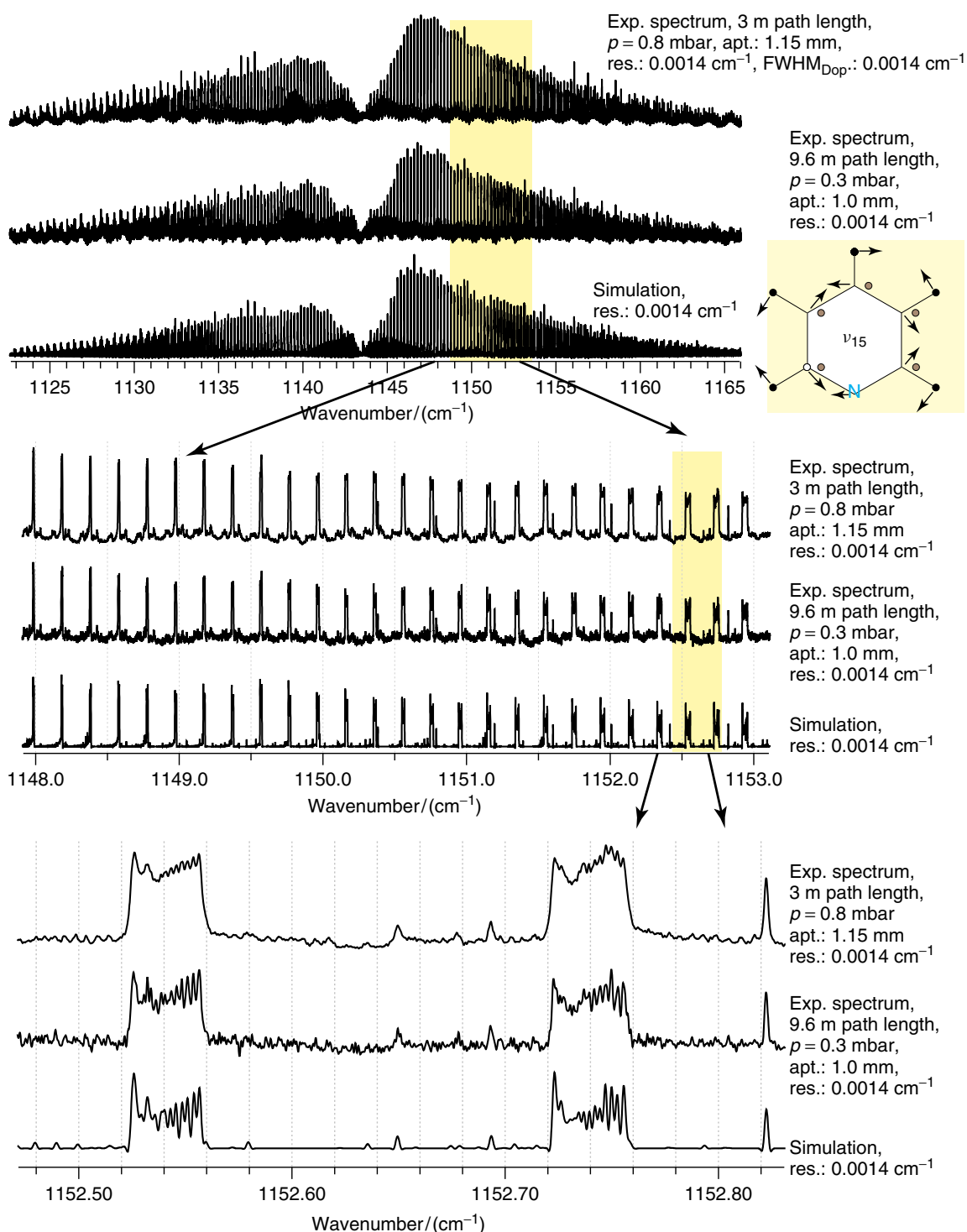


**Figure 30** Comparison of recorded and simulated spectra of the  $\nu_{15}$  band of pyridine: the middle figure is an enlargement of a part of the top figure and the bottom figure is an enlargement of a part of the middle figure. The  $\nu_{15}$  band of pyridine measured at 295 K in a 3 m glass cell with  $p = 0.8$  mbar and resolution =  $0.0014\text{ cm}^{-1}$  (top traces,  $\text{FWHM}_{\text{Dop}} = 0.0014\text{ cm}^{-1}$ ) and at 295 K in a 9.6 m White-type cell,  $p = 0.3$  mbar and a resolution =  $0.0014\text{ cm}^{-1}$  (middle traces,  $\text{FWHM}_{\text{Dop}} = 0.0014\text{ cm}^{-1}$ ) is shown together with a simulation of the  $\nu_{15}$  band of pyridine at 295 K (lower traces, resolution =  $0.0014\text{ cm}^{-1}$ ). [Reproduced by permission from Albert and Quack 2007b.]

upper two traces of each set represent the recorded spectra. It is obvious that a pressure reduction and the use of a slightly smaller aperture lead to a more highly resolved spectrum. This is essential for the rovibrational analysis of this congested band, as the enlargements in Figure 30 illustrate. Considering perturbations and extra bands, the agreement between the simulated and recorded spectrum is quite good.

Table 2 summarizes some of the parameters of the bands analyzed here. Several factors determine the complexity of a rovibrational spectrum: the molecular moments of inertia, the size and complexity of the molecule, the symmetry and floppiness of the molecule, the number of isotopomers, and the presence of accidental resonances. The molecular mass distribution determines the magnitude of the rotational constants; the larger the number of heavy atoms, the smaller the rotational constants, and the higher the density of absorption lines, as a rule. However, the symmetry of the molecule must also be considered. Roughly speaking, the higher the symmetry of the molecule, the fewer the absorption lines. The floppiness of a molecule, expressed by large amplitude motions such as torsion and inversion modes, leads to low-lying modes. These modes increase the density of lines considerably through the presence of hot bands related to a fundamental mode. In addition, the density of the lines is increased by the number of isotopomers. CDBrCIF has a low symmetry and has four important isotopomers in natural abundance. It has smaller rotational constants than  $\text{CHCl}_2\text{F}$ , which has three important isotopomers. Therefore, the rovibrational spectrum of  $\text{CHCl}_2\text{F}$  is less congested than that of CDBrCIF. However, this does not imply that the  $\text{CHCl}_2\text{F}$  spectrum is less complicated. Another factor must be considered, namely, the presence of “accidental” resonances or perturbations. One can estimate that an increasing number of vibrational modes increases the probability of accidental resonances, at least at higher frequencies. Pyridine and pyrimidine are the lightest of the four molecules investigated and both have only one important isotopomer compared to CDBrCIF and  $\text{CHCl}_2\text{F}$ , which have several. However, the pyridine and pyrimidine spectra are more complicated than the spectra of CDBrCIF and  $\text{CHCl}_2\text{F}$  owing to the large number of normal modes and the appearance of accidental perturbations. Even the vibrational state  $\nu_4$  of pyridine at  $744\text{ cm}^{-1}$  is strongly perturbed by the  $2\nu_{16a}$  state (Albert *et al.* 2005). The lowest frequency modes, however, should in general be unperturbed or less perturbed. Interactions with excited rotational states of the vibrational ground state are, in principle, possible even for the lowest frequency mode (Quack and Suhm 1990).

## 4.6 Rovibrational Spectra of Naphthalene

Naphthalene is of symmetry  $D_{2h}$  as shown in Figure 31 (top left) and has 48 normal modes (Albert *et al.* 2010). Only modes with  $b_{1u}$ ,  $b_{2u}$ , and  $b_{3u}$  symmetry are IR active. These generate  $a$ -,  $b$ -, and  $c$ -type bands, respectively. The  $\nu_{46}$  band is of  $b_{3u}$  symmetry and shows  $c$ -type transitions in the spectrum. The spin statistical weights for each line ( $K_a$ ,  $K_c$ ) are  $ee : eo : oe : oo = 76 : 60 : 60 : 60$ . The  $c$ -type bands were identified as P and R branches up to  $J < 95$ ,  $K_a < 44$ , and  $K_c < 66$ . The different  $c$ -type series are clearly visible in the Loomis–Wood diagram and are grouped into three groups as shown in Figure 31 (lower left). The rovibrational analysis was carried out with Watson’s  $A$  reduced effective Hamiltonian in the  $III'$  representation up to sextic centrifugal distortion constants. The spectroscopic constants of the  $\nu_{46}$  band of naphthalene were fitted according to the  $A$  reduction, resulting in a standard deviation of  $d_{rms} = 0.000327\text{ cm}^{-1}$ . The spectroscopic constants for the ground state were fixed to the values given in Kabir *et al.* (2003). No perturbation was observed despite the large density of states. A comparison between the experimental spectrum and a simulation of part of the  $\nu_{46}$  band is shown in Figure 31 (right). The agreement between simulated and experimental spectrum is very good considering the large number of hot bands.

## 5 CONCLUSIONS

We have summarized the current experimental principles, progress, and new possibilities of high-resolution Fourier transform spectroscopy. As the rovibrationally resolved IR spectra of the selected molecules illustrate, it is now possible to investigate the rovibrational spectrum of large molecules consisting of 10 and more atoms including also many “heavy”, i.e., nonhydrogen or deuterium atoms. The further improved resolution of the new Bruker 125 series (ETH-SLS Bruker 2009 11-chamber prototype system) in combination with a bright synchrotron source allows the investigation of PAHs, which are of fundamental interest for astrochemistry, as the analysis of naphthalene demonstrates. A detailed and systematic rovibrational analysis of such highly resolved IR spectra provides several important opportunities:

1. It gives a deeper and complementary insight into the rovibrational dynamics and intramolecular rovibrational energy redistribution including also weaker interactions and longer time scales. As the analysis of the pyridine spectra illustrates, numerous weaker perturbations such as Coriolis interactions have to be considered in order to successfully simulate the

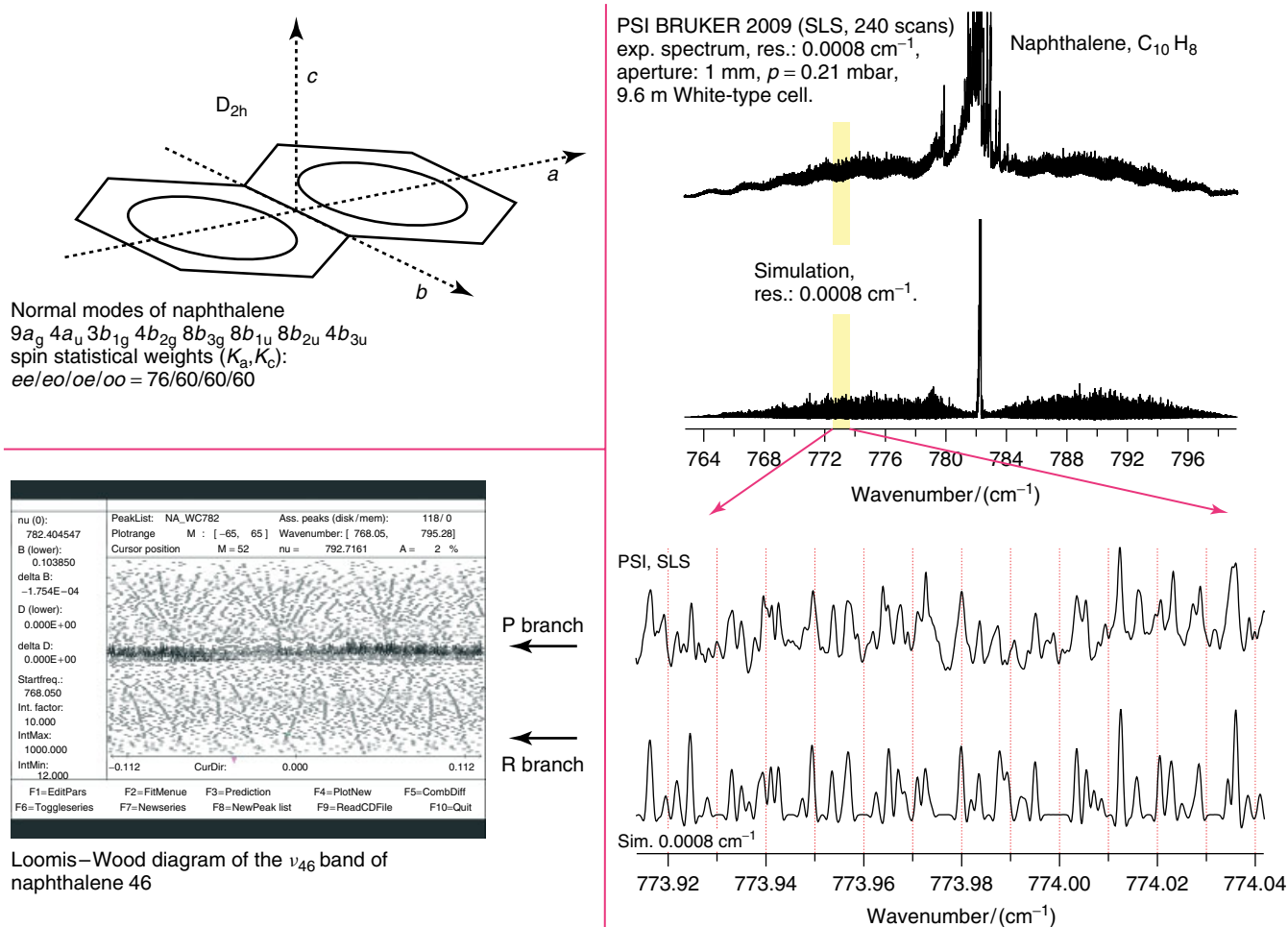


**Figure 31** Top left: Molecular fixed coordinate system for Naphthalene with  $D_{2h}$  symmetry. Bottom left: Loomis–Wood diagram of the out-of-plane mode  $\nu_{46}$  of naphthalene. Right top: The  $\nu_{46}$  band of naphthalene (upper trace) compared to simulation (lower trace). Right bottom: Enlargement of a part of the P branch region (see Albert *et al.* 2010).

experimental spectra. Similar observations apply, of course, to  $\text{CHCl}_2\text{F}$  and  $\text{CDBrClF}$ . Further quantum dynamical analysis will then be able to provide ultimately full dimensional quantum wavepacket descriptions of primary processes of intramolecular energy flow (Quack 1990, 2001, Beil *et al.* 2000, Marquardt and Quack 2001, Marquardt *et al.* 2003). The high-resolution analysis performed here will greatly extend the dynamical range of femtosecond processes analyzed before (Dübal and Quack 1984) and is a complement to the femtosecond pump–probe approaches to study intramolecular energy flow (Krylov *et al.* 2004, 2007).

- High-resolution analysis of IR spectra of complex molecules has the potential to lead to an identification of molecules that are relevant for interstellar chemistry and chemistry of the Earth's and planetary atmospheres. On the basis of the assignments of the  $\nu_{11}$

mode of pyridine, it may be possible to identify this molecule in protoplanetary nebulae.

- High-resolution analyses of the IR spectra of chiral molecules are still very scarce. They provide a necessary first step toward further experiments designed for detecting molecular parity violation as discussed in Quack (1986, 1989b, 2002, 2006), Daussy *et al.* (1999), Laerdahl *et al.* (2000), Hollenstein *et al.* (1997), Quack and Stohner (2000, 2003, 2005), Gross *et al.* (1998), Quack and Willeke (2006), Berger and Quack (2000a,b). This kind of effort provides a connection between molecular spectroscopy and fundamental high-energy physics. There remains even the speculative possibility of a connection to biomolecular homochirality (Quack 1989b, 2002, 2006, Berger and Quack 2000a,b, *see also* the review by Quack *et al.* (2008) and by Quack 2011: **Fundamental Symmetries and Symmetry Violations from High-resolution Spectroscopy**, this handbook).

In future developments, one of the major goals will be the rovibrational analysis of the IR spectra of biomolecules. We think that an analysis of the rovibrational spectra of the DNA bases and base pairs should be possible in the near future based on the techniques discussed here, especially in consideration of the possible applications of the new ETH-SLS interferometer in combination with the SLS synchrotron light source. Many relevant vibrational bands lie in the low-frequency range often called the *terahertz (THz) region* of the electromagnetic spectrum, 10–1000  $\text{cm}^{-1}$  corresponding to 0.3–30 THz. In this frequency range, intensity and noise limitations are important and we can make use of the brilliance of the SLS in this spectral region. In particular, below 2 THz, we gain a 10–100 times better signal-to-noise ratio compared to conventional thermal sources. An alternative in this spectral region is the use of backward wave oscillators based on phase-locked BWOs and the FASST Scanning Submillimeter Spectroscopic Technique (FASST) technology (Petkie *et al.* 1997, Lewen *et al.* 1998, Albert *et al.* 1998b, Albert and De Lucia 2001, De Lucia 2010). It will be possible using these techniques to record and analyze rovibrationally resolved low-lying modes of weak absorbers like large aromatic systems and hydrogen-bridged biomolecules in the electronic ground state. High-resolution FTIR spectroscopy also offers many possibilities for “combination techniques”, for instance, by combination with supersonic jets or molecular beams and with laser technology, some of which we describe elsewhere in this handbook (Snels *et al.* 2011 and Hippler *et al.* 2011).

## ACKNOWLEDGMENTS

We thank Sigurd Bauerecker, Veronika Horka-Zelenkova, Hans Hollenstein, Phillipe Lerch, Carine Manca Tanner, Roberto Marquardt, Hans-Martin Niederer, Luca Quaroni, Georg Seyfang, Jürgen Stohner, Martin Suter, and Martin Willeke for help and discussions. The spectroscopic work reviewed here has furthermore profited from a number of past and present collaborations as cited in part in the list of references, in particular with A. Amrein, V. Boudon, A. Bauder, A. Beil, R.P.A. Bettens, H. Bürger, H.R. Grassi, H. Gross, Z. Guennoun, E. Herbst, M. Hippler, A. Keens, F.C. De Lucia, D. Luckhaus, O. Monti, D. Pochert, S. Picirillo, R. Pfab, M. Snels, A. Steinlin, M. Suhm, B.P. Winnewisser, M. Winnewisser, and R.N. Zare. Our work is financially supported by the Schweizerischer Nationalfonds and the ETH Zürich (including AGS, CSCS and C<sup>4</sup>).

## ABBREVIATIONS AND ACRONYMS

FASST	FASt Scanning Submillimeter Spectroscopic Technique
FFT	Fast Fourier Transform
FIR	Far Infrared
FTIR	Fourier transform infrared
FWHM	full width at half maximum
IVR	intramolecular vibrational redistribution
NIR	near infrared
NMR	nuclear magnetic resonance
PAH	polycyclic aromatic hydrocarbon
SLS	Swiss Light Source
UIB	unidentified infrared band

## REFERENCES

- Albert, S. and De Lucia, F.C. (2001) Fast scan submillimeter spectroscopy technique (FASST): a new analytical tool for the gas phase. *Chimia*, **55**(1/2), 29–34.
- Albert, S. and Quack, M. (2001) A high resolution infrared study of CDBrCIF: analysis of the ground state and the  $\nu_4$  state. *Chimia*, **55**, 651.
- Albert, S. and Quack, M. (2002) Rovibrational analysis of the  $\nu_3$  band of CDBrCIF. *Chimia*, **56**, 374.
- Albert, S. and Quack, M. (2006) High resolution infrared spectroscopy of aromatic compounds, in *Contributions, 15th Symposium on Atomic and Surface Physics and Related Topics, Obergurgl, Österreich, 4.-9.2.2006*, Grill, V. and Mark, T.D. (eds), Innsbruck University Press, Innsbruck, pp. 213–216.
- Albert, S. and Quack, M. (2007a) High resolution rovibrational spectroscopy of chiral and aromatic compounds. *ChemPhys Chem*, **8**, 1271–1281.
- Albert, S. and Quack, M. (2007b) High resolution rovibrational spectroscopy of pyrimidine. Analysis of the  $B_1$  modes  $\nu_{10b}$  and  $\nu_4$  and the  $B_2$  mode  $\nu_{6b}$ . *Journal of Molecular Spectroscopy*, **243**, 280–291.
- Albert, S. and Quack, M. (2008) The high resolution infrared spectrum of phenol: first rovibrational analysis of the modes  $\nu_4$  and  $\nu_{17b}$ . *Chimia*, **62**, 657.
- Albert, S., Winnewisser, M., and Winnewisser, B.P. (1996) Networks of anharmonic resonance systems in the rovibrational overtone spectra of the quasilinear molecule HCNO. *Berichte der Bunsengesellschaft für Physikalische Chemie*, **100**, 1876–1896.
- Albert, S., Winnewisser, M., and Winnewisser, B.P. (1997a) The colorful world of quasilinearity as revealed by high resolution molecular spectroscopy. *Microchimica Acta*, **14**, 79–88.
- Albert, S., Winnewisser, M., and Winnewisser, B.P. (1997b) The  $\nu_1, \nu_2, 2\nu_3, \nu_2 + \nu_3$  band systems and the overtone region of HCNO above 4000  $\text{cm}^{-1}$ : a networks of resonance systems. *Berichte der Bunsengesellschaft für Physikalische Chemie*, **101**, 1165–1186.
- Albert, S., Albert, K., Winnewisser, M., and Winnewisser, B.P. (1998a) The rovibrational overtone spectrum of  $\text{H}^{13}\text{CNO}$  up

- to 3600  $\text{cm}^{-1}$ : a network of resonance systems. *Berichte der Bunsengesellschaft für Physikalische Chemie*, **102**, 1428–1448.
- Albert, S., Petkie, D.T., Bettens, R.P.A., Belov, S.P., and De Lucia, F.C. (1998b) FASSST: a new gas-phase analytical tool. *Analytical Chemistry*, **70**(21), 719A–727A.
- Albert, S., Boudon, V., and Quack, M. (2001a) The infrared spectrum of CDBrClF: a rovibrational analysis of the  $\nu_5$  band. *Chimia*, **55**, 654.
- Albert, S., Winnewisser, M., and Winnewisser, B.P. (2001b) The FT-IR spectrum of  $\text{H}^{13}\text{C}^{15}\text{NO}$  between 1800–3600  $\text{cm}^{-1}$  and 6300–7000  $\text{cm}^{-1}$ . *Journal of Molecular Structure*, **599**, 347–369.
- Albert, K.K., Albert, S., Quack, M., Stohner, J., Trapp, O., and Schurig, V. (2003a) Analysis of the high resolution infrared spectrum of monodeuterated ethylene oxide between 850–950  $\text{cm}^{-1}$ , in *Proceedings of the Eighteenth Colloquium on High Resolution Molecular Spectroscopy*, Dijon, p. 202, and to be published, paper F38.
- Albert, S., Albert, K.K., and Quack, M. (2003b) Very high resolution studies of chiral molecules with a Bruker IFS 120 HR: the rovibrational spectrum of CDBrClF in the range 600 – 2300  $\text{cm}^{-1}$ . *Trends in Optics and Photonics*, **84**, 177–180.
- Albert, S., Albert, K., and Quack, M. (2004a) Rovibrational analysis of the  $\nu_4$  and  $\nu_5 + \nu_9$  bands of  $\text{CHCl}_2\text{F}$ . *Journal of Molecular Structure*, **695–696**, 385–394.
- Albert, S., Bauerecker, S., Quack, M., and Steinlin, A. (2004b) Rovibrational overtone spectroscopy of  $\text{CHCl}_2\text{F}$  at 150 K. *Chimia*, **58**, 538.
- Albert, S., Hollenstein, H., Quack, M., and Willeke, M. (2004c) Doppler-limited FTIR spectrum of the  $\nu_3(a')/\nu_b(a'')$  Coriolis resonance dyad of  $\text{CHClF}_2$ : analysis and comparison with ab initio calculations. *Molecular Physics*, **102**, 1671–1686.
- Albert, S., Albert, K.K., Quack, M., Bettens, R.P.A., and De Lucia, F.C. (2005) The high resolution FTIR spectrum of pyridine: a rovibrational analysis of the fundamental Coriolis perturbed bands  $\nu_{11}$ ,  $\nu_4$ ,  $\nu_{12}$ ,  $\nu_{15}$  and  $\nu_{18a}$ , *Proceedings of the Nineteenth Colloquium on High Resolution Molecular Spectroscopy*, Salamanca, p. 443, paper P6 and to be published.
- Albert, S., Albert, K.K., and Quack, M. (2006a) High resolution rovibrational spectroscopy of halogenated aromatic compounds. *Chimia*, **60**, 463.
- Albert, S., Guennoun, Z., Albert, K.K., and Quack, M. (2006b) Rovibrational analysis of the  $\nu_{9a}$ ,  $\nu_{15}$  and  $\nu_{18a}$  modes of pyridine. *Chimia*, **60**, 469.
- Albert, S., Hollenstein, H., Quack, M., and Willeke, M. (2006c) Rovibrational analysis of the  $\nu_4$ ,  $2\nu_6$  Fermi resonance band of  $\text{CH}^{35}\text{ClF}_2$  by means of a polyad Hamiltonian involving the vibrational levels  $\nu_4$ ,  $2\nu_6$ ,  $\nu_6 + \nu_9$  and  $2\nu_9$ , and comparison with ab initio calculations. *Molecular Physics*, **104**(16–17), 2719–2735.
- Albert, S., Bauerecker, S., Quack, M., and Steinlin, A. (2007) Rovibrational analysis of the  $2\nu_3$ ,  $3\nu_3$  and  $\nu_1$  bands of  $\text{CHCl}_2\text{F}$  measured at 170 and 298 K by high-resolution FTIR spectroscopy. *Molecular Physics*, **105**, 541–558.
- Albert, K.K., Albert, S., Quack, M., and Stohner, J. (2008a) High resolution infrared spectroscopy of small heterocyclic chiral biomolecular precursor molecules. *Chimia*, **62**, 656.
- Albert, S., Albert, K.K., Bauerecker, S., and Quack, M. (2008b) CHBrF and molecular parity violation: first high resolution rovibrational analysis of the CF-stretching mode, in *Contributions, 16th Symposium on Atomic and Surface Physics and Related Topics, Les Diablerets, Switzerland, 20.-25.1.2008 ISBN 978-902571-31-1*, Beck, R.D., Drabbels, M., and Rizzo, T.R. (eds), Innsbruck University Press, Innsbruck, pp. 79–82.
- Albert, S., Albert, K.K., Bauerecker, S., and Quack, M. (2008c) Steps toward experimental detection of molecular parity violation in CHBrF: High resolution rovibrational analysis of the  $\nu_6$  mode. *Chimia*, **62**, 655.
- Albert, K.K., Albert, S., Quack, M., and Stohner, J. (2009a) High resolution infrared spectroscopy of oxirane carbonitrile. *Chimia*, **63**, 477.
- Albert, S., Bauerecker, S., Boudon, V., Brown, L.R., Champion, J.P., Loete, M., Nikitin, A., and Quack, M. (2009b) Global analysis of the high resolution infrared spectrum of methane  $^{12}\text{CH}_4$  in the region from 0 to 4800  $\text{cm}^{-1}$ . *Chemical Physics*, **356**(1–3), 131–146.
- Albert, S., Albert, K.K., Lerch, P., and Quack, M. (2010) Synchrotron-based highest resolution FTIR spectroscopy of naphthalene ( $\text{C}_8\text{H}_{10}$ ): rovibrational analysis of the  $\nu_{46}$  band, in *Proceedings of the 17th Symposium on Atomic, Cluster and Surface Physics (SASP 2010), Obergurgl, Austria, 24th to 29th January 2010, ISBN 978-3-902719-52-2*, Milewski, I., Kendl, A., and Scheier, P. (eds), Innsbruck University Press, Innsbruck, pp. 134–137. see also Faraday Disc **150** (2011) DOI.
- Albert, S., Albert, K.K., Hollenstein, H., Tanner, C.M., and Quack, M. (2011) Fundamentals of rotation–vibration spectra, in *Handbook of High-resolution Spectroscopy*, Quack, M. and Merkt, F. (eds), John Wiley & Sons, Ltd., Chichester, UK.
- Amano, T. (2011) High-resolution microwave and infrared spectroscopy of molecular cations, in *Handbook of High-resolution Spectroscopy*, Quack, M. and Merkt, F. (eds), John Wiley & Sons, Ltd., Chichester, UK.
- Amrein, A., Luckhaus, D., Merkt, F., and Quack, M. (1988a) High-Resolution FTIR Spectroscopy of  $\text{CHClF}_2$  in a Supersonic Free Jet Expansion. *Chemical Physics Letters*, **152**(4,5), 275–280.
- Amrein, A., Quack, M., and Schmitt, U. (1988b) High resolution interferometric Fourier transform infrared absorption spectroscopy in supersonic free jet expansions: carbon monoxide, nitric oxide, methane, ethyne, propyne and trifluoromethane. *The Journal of Physical Chemistry*, **92**, 5455–5466.
- Amrein, A., Quack, M., and Schmitt, U. (1987a) High resolution interferometric Fourier transform infrared absorption spectroscopy in a supersonic free jet expansion. The interacting states  $\nu_2$ ,  $\nu_5$  and  $\nu_3 + \nu_6$  of trifluoromethane. *Molecular Physics*, **60**(1), 237–248.
- Amrein, A., Quack, M., and Schmitt, U. (1987b) High resolution interferometric Fourier transform infrared absorption spectroscopy in a supersonic free jet expansions. A new technique for ultracold gaseous samples. *Zeitschrift für Physikalische Chemie (N.F.)*, **154**, 59–72.
- Barone, V. (2004) Accurate vibrational spectra of large molecules by density functional computations beyond the harmonic approximation: the case of azabenzene. *Journal of Physical Chemistry A*, **108**(18), 4146–4150.

- Basterretxea, F.J. and Escribano, R. (2004) The  $\nu_{19a}$  band of fluorobenzene. *Journal of Molecular Spectroscopy*, **223**(1), 80–83.
- Bauder, A. (2011) Fundamentals of rotational spectroscopy, in *Handbook of High-resolution Spectroscopy*, Quack, M. and Merkt, F. (eds), John Wiley & Sons, Ltd., Chichester, UK.
- Bauder, A., Beil, A., Luckhaus, D., Müller, F., and Quack, M. (1997) Combined high resolution infrared and microwave study of bromochlorofluoromethane. *Journal of Physical Chemistry*, **106**(18), 7558–7570.
- Bauerecker, S. (2005) Self-diffusion in core-shell composite  $^{12}\text{CO}_2/^{13}\text{CO}_2$  nanoparticles. *Physical Review Letters*, **94**, 33404.
- Bauerecker, S., Taraschewski, M., Weitkamp, C., and Cammenga, H. (2001) Liquid-helium temperature long-path infrared spectroscopy of molecular clusters and supercooled molecules. *The Review of Scientific Instruments*, **72**, 3946–3955.
- Bauerecker, S., Taucher, F., Weitkamp, C., Michaelis, W., and Cammenga, H. (1995) Spectral simplification by enclosive flow cooling I. FTIR-spectroscopy of supercooled gases. *Journal of Molecular Structure*, **348**, 243–248.
- Beil, A., Hollenstein, H., Monti, O., Quack, M., and Stohner, J. (2000) Vibrational spectra and intramolecular vibrational redistribution in highly excited deuterobromochlorofluoromethane CDBrClF: experiment and theory. *Journal of Chemical Physics*, **113**, 2701–2718.
- Beil, A., Luckhaus, D., Marquardt, R., and Quack, M. (1994a) Discussion contributions on molecular chirality and anharmonic vibrational dynamics of chiral molecules. *Journal of the Chemical Society Faraday Discussions*, **99**, 96–97.
- Beil, A., Luckhaus, D., Marquardt, R., and Quack, M. (1994b) Intramolecular energy transfer and vibrational redistribution in chiral molecules: experiment and theory. *Journal of the Chemical Society Faraday Discussions*, **99**, 49–76.
- Beil, A., Luckhaus, D., and Quack, M. (1996) Fermi resonance structure and femtosecond quantum dynamics of a chiral molecule from the analysis of vibrational overtone spectra of CHBrClF. *Berichte der Bunsengesellschaft für Physikalische Chemie*, **100**(11), 1853–1875.
- Beil, A., Luckhaus, D., Quack, M., and Stohner, J. (1997) Intramolecular vibrational redistribution and unimolecular reaction: concepts and new results on the femtosecond dynamics and statistics in CHBrClF. *Berichte der Bunsengesellschaft für Physikalische Chemie*, **101**(3), 311–328.
- Bell, R.J. (1972) *Introductory Fourier Transform Spectroscopy*, Academic Press, New York.
- Berger, R., Laubender, G., Quack, M., Sieben, A., Stohner, J., and Willeke, M. (2005) Isotopic chirality and molecular parity violation. *Angewandte Chemie (International ed. in English)*, **44**, 3623–3626.
- Berger, R. and Quack, M. (2000a) Electroweak quantum chemistry of alanine: parity violation in gas and condensed phases. *ChemPhysChem*, **1**, 57–60.
- Berger, R. and Quack, M. (2000b) Multiconfiguration linear response approach to the calculation of parity violating potentials in polyatomic molecules. *Journal of Chemical Physics*, **112**(7), 3148–3158.
- Billes, F., Mikosch, H., and Holly, S. (1998) A comparative study on the vibrational spectroscopy of pyridazine, pyrimidine and pyrazine. *Journal of Molecular Structure*, **423**(3), 225–234.
- Birk, M., Winnewisser, M., and Cohen, E.A. (1989) The rotational-torsional spectrum of carbodiimide: a probe for the unusual dynamics. *Journal of Molecular Spectroscopy*, **136**(2), 402–445.
- Boese, A.D. and Martin, J.M.L. (2004) Vibrational spectra of the azabenzenes revisited: anharmonic force fields. *Journal of Physical Chemistry A*, **108**, 3085–3096.
- Boudon, V., Champion, J.-P., Gabard, T., Loëte, M., Rotger, M., and Wenger, C. (2011) Spherical top theory and molecular spectra, in *Handbook of High-resolution Spectroscopy*, Quack, M. and Merkt, F. (eds), John Wiley & Sons, Ltd., Chichester, UK.
- Bowling Barnes, R., Gore, R.C.B., Liddel, U., and Willams, V.Z. (1944) Infrared spectroscopy, in *Industrial and Engineering Chemistry*, Reinhold, New York, pp. 1–113.
- Brault, J.W. (1985) Fourier transform spectrometry, in *Proceedings of the Fifteenth Advanced Course of the Swiss Society of Astronomy and Astrophysics*, Benz, A.O., Huber, M.C.E., and Mayor, M. (eds), Sauverny, Observatoire de Geneve, Switzerland, Saas Fee, pp. 1–61.
- Brault, J. (1987) Fourier transform spectrometry. *Mikrochimica Acta*, **3**, 215–227.
- Breidung, J. and Thiel, W. (2011) Predictions of vibrational spectra from ab initio theory, in *Handbook of High-resolution Spectroscopy*, Quack, M. and Merkt, F. (eds), John Wiley & Sons, Ltd., Chichester, UK.
- Breda, S., Reva, I.D., Lapinski, L., Nowak, M.J., and Fausto, R. (2006) Infrared spectra of pyrazine, pyrimidine and pyridazine in solid argon. *Journal of Molecular Structure*, **786**(2–3), 193–206.
- Brownlie, I.A. (1950) Infrared spectroscopic measurements of substituted pyrimidines. *Part II. Journal of the Chemical Society* 3062–3072.
- Bruker, C. (1989) *IFS 120 HR User's Manual*, Bruker Analytische Meßtechnik GmbH, Karlsruhe, Germany. Version 25.10.89.
- Buch, V., Bauerecker, S., Devlin, J., Buck, U., and Kazimirski, J. (2004) Water clusters in the size range of tens-thousands of molecules: a combined computational/spectroscopic outlook. *International Reviews in Physical Chemistry*, **23**, 375.
- Buijs, H. (1979) A class of high resolution ruggedized Fourier transform spectrometers. *Proceedings of the Society of Photo-Optical Instrumentation Engineering*, **191**, 116.
- Caminati, W. (2011) Microwave spectroscopy of large molecules and molecular complexes, in *Handbook of High-resolution Spectroscopy*, Quack, M. and Merkt, F. (eds), John Wiley & Sons, Ltd., Chichester, UK.
- Carr, G.L., Smith, R.J., Mihaly, L., Zhang, H., Reitze, D.H., and Tanner, D.B. (2008) High-resolution far-infrared spectroscopy at NSLS beamline U12IR. *Infrared Physics and Technology*, **51**(5), 404–406.
- Cernicharo, J., Heras, A.M., Tielens, A.G.G.M., Pardo, J.R., Herpin, F., Guélin, M., and Waters, L. (2001) Infrared space observatory's discovery of  $\text{C}_4\text{H}_2$ ,  $\text{C}_6\text{H}_2$  and benzene in CRL 618. *Astrophysical Journal*, **546**, L123–L126.

- Chamberlain, J. (1979) *The Principles of Interferometric Spectroscopy*, Wiley, Chichester.
- Champion, J.-P., Loete, M., and Pierre, G. (1992) Spherical top spectra, in *Spectroscopy of the Earth's Atmosphere and Interstellar Medium*, Rao, K.N. and Weber, A. (eds), Academic Press, San Diego, pp. 339–422.
- Chimdi, T., Robertson, E.G., Puskar, L., Thompson, C.D., Tobin, M.J., and McNaughton, D. (2008) High resolution synchrotron FTIR spectroscopy of the far infrared  $\nu_{10}$  and  $\nu_{11}$  bands of R152a ( $\text{CH}_3\text{CHF}_2$ ). *Chemical Physics Letters*, **465**(4–6), 203–206.
- Chukalina, E.P., Popova, M.N., Bezmaternykh, L.N., and Gudimb, I.A. (2010) Spectroscopic study of the magnetic ordering in  $\text{SmFe}_3(\text{BO}_3)_4$ . *Physics Letters A*, **374**, 1790–1792.
- Connes, J. (1961) Recherche sur la spectroscopie par transformation de Fourier. *Revue d'Optique*, **40**(2), 45–79.
- Connes, P. (1970) Astronomical Fourier spectroscopy. *Annual Review of Astronomy and Astrophysics*, **8**(1), 209–230.
- Coulson, C.A. (1942) The dipole moment of the C-H bond. *Transactions of the Faraday Society*, **38**, 433–444.
- Daussy, C., Marrel, T., Amy-Klein, A., Nguyen, C.T., Bordé, C.J., and Chardonnet, C. (1999) Limit on the parity nonconserving energy difference between the enantiomers of a chiral molecule by laser spectroscopy. *Physical Review Letters*, **83**(8), 1554–1557.
- Davis, S.P., Abrams, M.C., and Brault, J.W. (2001) *Fourier Transform Spectrometry*, Academic Press, San Diego.
- De Lucia, F.C. (2010) The submillimeter: a spectroscopist's view. *Journal of Molecular Spectroscopy*, **261**, 1–17.
- Demtröder, W. (2011) Doppler-free laser spectroscopy, in *Handbook of High-resolution Spectroscopy*, Quack, M. and Merkt, F. (eds), John Wiley & Sons, Ltd., Chichester, UK.
- Dicke, R.H. (1953) The effect of collisions upon the Doppler width of spectral lines. *Physical Review*, **89**(2), 472.
- Diem, M. and Burow, D.F. (1976) Vibrational spectra and normal coordinate analysis of bromochlorofluoromethane. *Journal of Chemical Physics*, **64**, 5179–5185.
- Diem, M. and Burow, D.F. (1977) A Urey-Bradley force field for bromochlorofluoromethane. *Journal of Physical Chemistry*, **81**(5), 476–479.
- Diem, M., Nafie, L.A., and Burow, D.F. (1978) Analysis of the gas phase infrared spectrum of bromochlorofluoromethane: calculated and observed band contours and intensities. *Journal of Molecular Spectroscopy*, **71**(1–3), 446–457.
- DiLella, D.P. (1980) Vibrational spectra of  $C_{2v}$  deuterium substituted pyridines 3. *Journal of Raman Spectroscopy*, **9**(4), 239–246.
- Dolph, C.L. (1946) A current distribution for broadside arrays which optimizes the relationship between beam width and side-lobe level. *Proceedings of the IRE*, **34**, 335–348.
- Domenech, J.L., Junttila, M.L., and Pine, A.S. (1991) Molecular-beam spectrum of the 3.3- $\mu\text{m}$   $\nu_{12}$ -band of benzene. *Journal of Molecular Spectroscopy*, **149**, 391–398.
- Dübal, H.-R. and Quack, M. (1984) Vibrational overtone spectra and vibrational dynamics of  $\text{CFHCl}_2$  and  $(\text{CH}_3)_2\text{CFH}$ . *Molecular Physics*, **53**(1), 257–264.
- Dübal, H.-R., Quack, M., and Schmitt, U. (1984) High resolution interferometric infrared spectroscopy of  $\text{CO}_2$  and  $\text{CH}_4$  vapour at low temperatures near 10 K: collisional cooling in supersonic jets and nuclear spin symmetry conservation. *Chimia*, **38**(12), 438–439.
- Eikema, K.S.E. and Ubachs, W. (2011) Precision laser spectroscopy in the extreme ultraviolet, in *Handbook of High-resolution Spectroscopy*, Quack, M. and Merkt, F. (eds), John Wiley & Sons, Ltd., Chichester, UK.
- Ernst, R.R., Bodenhausen, G., and Wokaun, A. (1987) *Principles of Nuclear Magnetic Resonance in One and Two Dimensions*, Clarendon Press, Oxford.
- Eschenmoser, A. (1997) Towards a chemical etiology of nucleic acid structure. *Origins of Life and Evolution of the Biosphere*, **27**(5–6), 535–553.
- Fellgett, P. (1958) Spectromètre interférentiel multiplex pour mesures infra-rouges sur les étoiles. *Journal de Physique et Le Radium*, **19**(3), 237–240.
- Fischer, G., Cai, Z.L., Reimers, J.R., and Wormell, P. (2003) Singlet and triplet valence excited states of pyrimidine. *The Journal of Physical Chemistry A*, **107**(17), 3093–3106.
- Flaud, J.-M. and Oelhaf, H. (2004) Infrared spectroscopy and the terrestrial atmosphere. *Comptes Rendus Physique*, **5**, 259–271.
- Flaud, J.-M. and Orphal, J. (2011) Spectroscopy of the Earth's atmosphere, in *Handbook of High-resolution Spectroscopy*, Quack, M. and Merkt, F. (eds), John Wiley & Sons, Ltd., Chichester, UK.
- Frey, H.-M., Kummli, D., Lobsiger, S., and Leutwyler, S. (2011) High-resolution rotational Raman coherence spectroscopy with femtosecond pulses, in *Handbook of High-resolution Spectroscopy*, Quack, M. and Merkt, F. (eds), John Wiley & Sons, Ltd., Chichester, UK.
- Genzel, L. (1998) Far-infrared Fourier transform spectroscopy, in *Topics in Applied Physics, Vol. 74, Millimeter and Submillimeter Wave Spectroscopy*, Gruener, G. (ed.), Springer, Berlin, pp. 169–220.
- Grabow, J.-U. (2011) Fourier transform microwave spectroscopy measurement and instrumentation, in *Handbook of High-resolution Spectroscopy*, Quack, M. and Merkt, F. (eds), John Wiley & Sons, Ltd., Chichester, UK.
- Graner, G. (1993) About hot bands and paper bands in spectra of  $C_{3v}$ -symmetrical-top molecules. *Journal of Molecular Spectroscopy*, **161**(1), 58–79.
- Gross, H., Grassi, G., and Quack, M. (1998) The synthesis of 2- $^2\text{H}_1$  thiirane-1-oxide and 2,2- $^2\text{H}_2$  thiirane-1-oxide and the diastereoselective infrared laser chemistry of 2- $^2\text{H}_1$  thiirane-1-oxide. *Chemistry. A European Journal*, **4**(3), 441–448.
- Guelachvili, G. (1978) High-accuracy Doppler-limited 106 samples Fourier transform spectroscopy. *Applied Optics*, **17**, 1322–1326.
- Guennoun, Z. and Maier, J.P. (2011) Electronic spectroscopy of transient molecules, in *Handbook of High-resolution Spectroscopy*, Quack, M. and Merkt, F. (eds), John Wiley & Sons, Ltd., Chichester, UK.
- Hamm, P. (2011) 2D-infrared spectroscopy, in *Handbook of High-resolution Spectroscopy*, Quack, M. and Merkt, F. (eds), John Wiley & Sons, Ltd., Chichester, UK.

- Häber, T. and Kleinerhanns, K. (2011) Multiphoton resonance spectroscopy of biological molecules, in *Handbook of High-resolution Spectroscopy*, Quack, M. and Merkt, F. (eds), John Wiley & Sons, Ltd., Chichester, UK.
- Hartmann, J.M., Boulet, C., and Robert, D. (2008) *Collisional Effects on Molecular Spectra: Laboratory Experiments and Models, Consequences for Applications*, Elsevier, Amsterdam.
- Havenith, M. and Birer, Ö. (2011) High resolution IR-laser jet spectroscopy of formic acid dimer, in *Handbook of High-resolution Spectroscopy*, Quack, M. and Merkt, F. (eds), John Wiley & Sons, Ltd., Chichester, UK.
- Hegelund, F., Larsen, R.W., Aitken, R.A., and Palmer, M.H. (2005a) A high-resolution infrared study of five bands of 1,2,5-thiadiazole in the range 750–1250  $\text{cm}^{-1}$ , together with ab initio and DFT studies. *Journal of Molecular Spectroscopy*, **233**(2), 256–268.
- Hegelund, F., Larsen, R.W., Nicolaisen, F.M., and Palmer, M.H. (2005b) The high-resolution infrared spectrum of isoxazole vapor between 800 and 1700  $\text{cm}^{-1}$ . *Journal of Molecular Spectroscopy*, **229**(2), 244–256.
- Henry, L., Valentin, A., Lafferty, W.J., Hougen, J.T., Devi, V.M., Das, P.P., and Rao, K.N. (1983) Analysis of the high-resolution Fourier-transform and diode laser spectra of the  $\nu_9$  band of ethane. *Journal of Molecular Spectroscopy*, **100**, 260–289.
- Herman, M. (2011) High-resolution infrared spectroscopy of acetylene: theoretical background and research trends, in *Handbook of High-resolution Spectroscopy*, Quack, M. and Merkt, F. (eds), John Wiley & Sons, Ltd., Chichester, UK.
- Herzberg, G. (1945) *Molecular Spectra and Molecular Structure, Vol. II*, van Nostrand, Toronto.
- Herzberg, G. (1966) *Molecular Spectra and Molecular Structure, Vol. III*, van Nostrand, Toronto.
- Herzberg, G. (1991) *Molecular Spectra and Molecular Structure, II. Infrared and Raman Spectra of Polyatomic Molecules*, Krieger Publishing Company, Malabar Florida.
- Hewett, K.B., Shen, M., Brummel, C.L., and Philips, L.A. (1994) High resolution infrared spectroscopy of pyrazine and naphthalene in a molecular beam. *Journal of Chemical Physics*, **100**(6), 4077–4086.
- Hippler, M. and Quack, M. (2002) High-resolution FTIR and cw-diode laser cavity ring-down spectroscopy of the  $\nu_2 + 2\nu_3$  band of methane near 7510  $\text{cm}^{-1}$  in slit jet expansions and at room temperature. *The Journal of Chemical Physics*, **116**, 6045–6055.
- Hippler, M. and Quack, M. (2005) Isotope selective infrared spectroscopy and intramolecular dynamics, in *Isotope Effects in Chemistry and Biology, Part III, Isotope Effects in Chemical Dynamics, Chapter 10*, Kohen, A. and Limbach, H.-H. (eds), Marcel Dekker Inc., New York.
- Hippler, M., Miloglyadov, E., Quack, M., and Seyfang, G. (2011) Mass and isotope-selective infrared spectroscopy, in *Handbook of High-resolution Spectroscopy*, Quack, M. and Merkt, F. (eds), John Wiley & Sons, Ltd., Chichester, UK.
- Hippler, M., Oeltjen, M., and Quack, M. (2007) High-resolution continuous-wave-diode laser cavity ring-down spectroscopy of the hydrogen fluoride dimer in a pulsed slit jet expansion: two components of the  $N = 2$  Triad near 1.3  $\mu\text{m}$ . *Journal of Physical Chemistry A*, **111**, 12659–12668.
- Hippler, M., Pfab, R., and Quack, M. (2003) Isotopomer-selective overtone spectroscopy of jet-cooled benzene by ionization detected IR+UV double resonance: the  $N = 2$  CH-chromophore absorption of  $^{12}\text{C}_6\text{H}_6$  and  $^{13}\text{C}^{12}\text{C}_5\text{H}_6$  near 6000  $\text{cm}^{-1}$ . *Journal of Physical Chemistry*, **107**, 10743–10752.
- van't Hoff, J.H. (1899) *Vorlesungen über Theoretische und Physikalische Chemie, Band 2*, Vieweg, Braunschweig.
- Hollenstein, H., Luckhaus, D., Pochert, J., Quack, M., and Seyfang, G. (1997) Synthesis, Structure, High Resolution Spectroscopy and laser-chemistry of fluorooxirane and 2,2-Dideutero-fluorooxirane. *Angewandte Chemie (International ed. in English)*, **36**, 140–143.
- Hollenstein, H., Marquardt, R., Quack, M., and Suhm, M.A. (1994) Dipole moment function and equilibrium structure of methane in an analytical, anharmonic nine-dimensional potential surface related to experimental rotational constants and transition moments by quantum Monte Carlo calculations. *Journal of Chemical Physics*, **101**(5), 3588–3602.
- Hollenstein, H., Piccirillo, S., Quack, M., and Snels, M. (1990) High-resolution infrared spectrum and analysis of the  $\nu_{11}$ ,  $A_{2u}(B_2)$  fundamental band of  $^{12}\text{C}_6\text{H}_6$  and  $^{13}\text{C}^{12}\text{C}_5\text{H}_6$ . *Molecular Physics*, **71**(4), 759–768.
- Innes, K.K., Ross, I.G., and Moomaw, W.R. (1988) Electronic states of azabenzenes and azanaphthalenes: a revised and extended critical review. *Journal of Molecular Spectroscopy*, **132**(2), 492–544.
- Ito, M., Shimada, R., Kuraishi, T., and Mizushima, W. (1956) Vibrational Spectra of Diazines. *Journal of Chemical Physics*, **25**(3), 597–598.
- Jacquinot, P. (1954) The luminosity of spectrometers with prisms, gratings, or Fabry-Pérot etalons. *Journal of the Optical Society of America*, **44**(10), 761–765.
- Jäger, W. and Xu, Y. (2011) Fourier transform microwave spectroscopy of doped helium clusters, in *Handbook of High-resolution Spectroscopy*, Quack, M. and Merkt, F. (eds), John Wiley & Sons, Ltd., Chichester, UK.
- Kabir, M.H., Kasahara, S., Demtroder, W., Tatamitani, Y., Doi, A., Kato, H., and Baba, M. (2003) Doppler-free laser polarization and optical-optical double resonance polarization labeling spectroscopies of a large molecule: Naphthalene. *Journal of Chemical Physics*, **119**(7), 3691–3698.
- Kauppinen, J. (1979) Working resolution of 0.010  $\text{cm}^{-1}$  between 20  $\text{cm}^{-1}$  and 1200  $\text{cm}^{-1}$  by a Fourier spectrometer. *Applied Optics*, **18**, 1788–1796.
- Kauppinen, J. and Partanen, J. (2001) *Fourier Transforms in Spectroscopy*, Wiley-VCH, Berlin.
- Keens, A. (2004) A tribute to the Winnewissers or how science meets technology. *Journal of Molecular Structure*, **695–696**, 379–384.
- Kendall, D.J.W., Buijs, H.L., and Johns, J.W.C. (1982) A very high resolution Fourier transform spectrophotometer system for Doppler-limited studies. *Journal of Molecular Structure*, **79**, 39–42.
- Kisiel, Z., Białkowska-Jaworska, E., and Pszczółkowski, L. (2005) The millimeter-wave rotational spectrum of fluorobenzene. *Journal of Molecular Spectroscopy*, **232**(1), 47–54.

- Kysiel, Z., Pszczolkowski, L., Lopez, J.C., Alonso, J.L., Maris, A., and Caminati, W. (1999) Investigation of the rotational spectrum of pyrimidine from 3 to 337 GHz: molecular structure, nuclear quadrupole coupling, and vibrational satellites. *Journal of Molecular Spectroscopy*, **195**(2), 332–339.
- Kline, C.H. and Turkevich, J. (1944) The vibrational spectrum of pyridine and the thermodynamic properties of pyridine vapors. *Journal of Chemical Physics*, **12**(7), 300–309.
- Klots, T.D. (1998) Raman vapor spectrum and vibrational assignment for pyridine. *Spectrochimica Acta*, **54**, 1481–1498.
- Konings, J.A., Majewski, W.A., Matsumoto, Y., Pratt, D.W., and Meerts, W.L. (1988) Ultra high-resolution fluorescence excitation spectrum of  $^1\text{B}_1$  pyrimidine in a molecular beam. Structural assignments, analysis of singlet-triplet perturbations, and implications for intersystem crossing in the isolated molecule. *Journal of Chemical Physics*, **89**(4), 1813–1826.
- Krylov, V., Kushnarenko, A., Miloglyadov, E., Quack, M., and Seyfang, G. (2007) High sensitivity femtosecond gas phase pump-probe experiments using a hollow waveguide: intramolecular redistribution processes in  $\text{CH}_3\text{I}$ . *Proceedings of SPIE Vol. 6460. Poster Report at Conference: Photonics West 2007, Commercial and Biomedical Applications of Ultrafast Lasers VII*, San Jose, CA, USA, 21 January, 2007), pp. 64601D–646011.
- Krylov, V., Nikitchenko, M., Quack, M., and Seyfang, G. (2004) Femtosecond intramolecular dynamics after near-IR excitation of  $\text{CH}_3\text{F}$ ,  $\text{C}_2\text{H}_5\text{I}$ ,  $\text{CF}_3\text{CHFI}$ , and  $\text{C}_7\text{H}_8$  molecules in the gas phase and in solution. *Proceedings of SPIE*, **5337**, 178–189.
- Laerdahl, J.K., Schwerdtfeger, P., and Quiney, H.M. (2000) Theoretical analysis of parity-violating energy differences between the enantiomers of chiral molecules. *Physical Review Letters*, **84**, 3811–3814.
- Lavorel, B., Tran, H., Hertz, E., Faucher, O., Joubert, P., Motzkus, M., Buckup, T., Lang, T., Skenderovi, H., and Knopp, G. (2004) Femtosecond Raman time-resolved molecular spectroscopy. *Comptes Rendus Physique*, **5**(2), 215–229.
- Lewen, F., Gendriesch, R., Pak, I., Paveliev, D., Hepp, M., Schieder, R., and Winnewisser, G. (1998) Phase locked backward wave oscillator pulsed beam spectrometer in the submillimeter wave range. *Review of Scientific Instruments*, **69**, 32.
- Lewerenz, M. (1987) *Spektroskopie und Dynamik hoch Angeregter Schwingungszustände des CH-Chromophors in Vielatomigen Molekülen: Experiment und ab Initio-Theorie*, Doctoral thesis, Eidgenössische Technische Hochschule Zürich, diss ETH Nr. 8470.
- Lin, M.-F., Dyakov, Y.A., Tseng, C.-M., Mebel, A.M., Lin, S.H., Lee, Y.T., and Ni, C.-K. (2006) Photodissociation dynamics of pyrimidine. *Journal of Chemical Physics*, **124**(8), 84303–84308.
- Loomis, F. and Wood, R. (1928) The rotational structure of the Blue-Green bands of  $\text{Na}_2$ . *Physical Review*, **32**, 223–236.
- Lopez, J., Luis, A., Blanco, S., Lesarri, A., and Alonso, J. (2002) Rotational spectra, nuclear quadrupole coupling constants and structure of dichlorofluoromethane. *Journal of Molecular Structure*, **612**, 287–303.
- Lord, R.C., Marston, A.L., and Miller, F.A. (1957) Infra-red and Raman spectra of the diazines. *Spectrochimica Acta*, **9**(2), 113–125.
- Luckhaus, D. and Quack, M. (1989) The far infrared pure rotational spectrum and the Coriolis coupling between  $\nu_3$  and  $\nu_8$  in  $\text{CH}^{35}\text{ClF}_2$ . *Molecular Physics*, **68**(3), 745–758.
- Luis, A., Lopez, J., Guarnieri, A., and Alonso, J. (1997) Rotational spectra, nuclear quadrupole coupling constants and structure of dichlorofluoromethane. *Journal of Molecular Structure*, **413**, 249–253.
- Lupo, D.W. and Quack, M. (1987) IR-laser photochemistry. *Chemical Reviews*, **87**, 181–216.
- Majewski, W. and Meerts, W.L. (1984) Near-UV spectra with fully resolved rotational structure of naphthalene and perdeuterated naphthalene. *Journal of Molecular Spectroscopy*, **104**(2), 271–281.
- Maki, A.G. and Wells, S. (1991) *Wavenumber Calibration Tables from Heterodyne Frequency Measurements*, NIST Special Publication, USA, p. 821.
- Marcott, C., Faulkner, T.R., Moscowitz, A., and Overend, J. (1977) Vibrational circular dichroism in bromochlorofluoromethane and bromochlorofluoromethane-d. Calculation of the rotational strengths associated with the fundamentals and the binary overtones and combinations. *Journal of the American Chemical Society*, **99**(25), 8169–8175.
- Marquardt, R. and Quack, M. (1998) Global analytical potential hypersurfaces for large amplitude nuclear motion and reaction in methane. I. Formulation of the potentials and adjustment of parameters to ab initio data and experimental constraints. *Journal of Chemical Physics*, **109**, 10628–10643.
- Marquardt, R. and Quack, M. (2001) Energy redistribution in reacting systems, in *Encyclopedia of Chemical Physics and Physical Chemistry*, Chapter A.3.13, Moore, J. and Spencer, N. (eds), IOP Publication, Bristol, pp. 897–936, Vol. 1 (Fundamentals).
- Marquardt, R. and Quack, M. (2004) Global analytical potential hypersurface for large amplitude nuclear motion and reactions in methane. II. Characteristic properties of the potential and comparison to other potentials and experimental information. *The Journal of Physical Chemistry A*, **108**, 3166–3181.
- Marquardt, R. and Quack, M. (2011) Global analytical potential energy surfaces for high-resolution molecular spectroscopy and reaction dynamics, in *Handbook of High-resolution Spectroscopy*, Quack, M. and Merkt, F. (eds), John Wiley & Sons, Ltd., Chichester, UK.
- Marquardt, R., Quack, M., Thanopoulos, I., and Luckhaus, D. (2003) Tunneling dynamics of the NH chromophore in  $\text{NHD}_2$  during and after coherent infrared excitation. *The Journal of Chemical Physics*, **118**, 643–658.
- Mastalerz, R. and Reiher, M. (2011) Relativistic electronic structure theory for molecular spectroscopy, in *Handbook of High-resolution Spectroscopy*, Quack, M. and Merkt, F. (eds), John Wiley & Sons, Ltd., Chichester, UK.
- McKellar, A.R.W., Tokaryk, D.W., Xu, L.-H., Appadoo, D.R.T., and May, T. (2007) High resolution analysis of the  $\nu_{12}$  and  $\nu_{17}$  fundamental bands of acrolein,  $\text{CH}_2\text{CHCHO}$ , in the  $600\text{cm}^{-1}$  region. *Journal of Molecular Spectroscopy*, **242**(1), 31–38. 0022–2852.
- Mc Naughton, D. (2002) Instrumentation and methods for high-resolution gas-phase spectroscopy, in *Handbook of Vibrational Spectroscopy*, Chalmers, J.M. and Griffith, P.R. (eds), John Wiley & Sons Ltd., Chichester, pp. 165–175, Vol. 1.

- McKellar, A.R.W. (2010) High-resolution infrared spectroscopy with synchrotron sources. *Journal of Molecular Spectroscopy*, **262**, 1–10.
- McLay, D.B. (1964) The microwave spectrum of dichlorofluoromethane. *Canadian Journal of Physics*, **42**, 720.
- Medvedev, I.R., Winnewisser, M., Winnewisser, B.P., De Lucia, F.C., and Herbst, E. (2005) The use of CAAARS (Computer Aided Assignment of Asymmetric Rotor Spectra) in the analysis of rotational spectra. *Journal of Molecular Structure*, **742**(1–3), 229–236.
- Merkt, F., Willitsch, S., and Hollenstein, U. (2011) High-resolution photoelectron spectroscopy, in *Handbook of High-resolution Spectroscopy*, Quack, M. and Merkt, F. (eds), John Wiley & Sons, Ltd., Chichester, UK.
- Merkt, F. and Quack, M. (2011) Molecular quantum mechanics and molecular spectra, molecular symmetry, and interaction of matter with radiation, in *Handbook of High-resolution Spectroscopy*, Quack, M. and Merkt, F. (eds), John Wiley & Sons, Ltd., Chichester, UK.
- Mertz, L. (1965) *Transformation in Optics*, Wiley, New York.
- Michelson, A.A. (1881) Interference phenomena in a new form of refractometer. *Philosophical Magazine*, **13**, 236–242.
- Michelson, A.A. (1927) *Studies in Optics*, University of Chicago Press, Chicago.
- Mittapalli, G.K., Osornio, Y.M., Guerrero, M.A., Reddy, K.R., Krishnamurthy, R., and Eschenmoser, A. (2007) Mapping the landscape of potentially primordial informational oligomers: oligodipeptides tagged with 2,4-Disubstituted 5-Aminopyrimidines as recognition elements. *Angewandte Chemie (International ed. in English)*, **46**(14), 2478–2484.
- Mladenovic, M., Elhiyani, M., and Lewerenz, M. (2009) Electric and magnetic properties of the four most stable CHNO isomers from ab initio CCSD(T) studies. *Journal of Chemical Physics*, **131**(3), 34302–34314.
- Murty, M.V.R.K. (1960) Some more aspects of the Michelson interferometer with cube corners. *Journal of the Optical Society of America. A*, **50**(1), 7–9.
- Nassar, R., Bernath, P.F., Boone, C.D., Manney, G.L., McLeod, S.D., Rinsland, C.P., Skelton, R., and Walker, K.A. (2005) ACE-FTS measurements across the edge of the winter 2004 Arctic vortex. *Geophysical Research Letters*, **32**, L15S05.
- Nelander, B. (1993) The beam line for infrared spectroscopy at the Lund University synchrotron radiation source. *Journal of Molecular Structure*, **294**, 205. 0022–2860.
- Nett, H., Frerick, J., Paulsen, T., and Levrini, G. (2001) The atmospheric instruments and their applications: GOMOS, MIPAS and SCIAMACHY. *ESA Bulletin*, **106**, 77–87.
- Niederer, H.-M., Albert, S., Bauerecker, V., Boudon, V., Champion, J.P., and Quack, M. (2008) Global analysis of the infrared spectrum of  $^{13}\text{CH}_4$ : Lines in the region 0 to  $3200\text{ cm}^{-1}$ . *Chimia*, **62**(4), 273–276.
- Norton, R.H. and Beer, R. (1976) New apodizing functions for Fourier spectrometry. *Journal of the Optical Society of America*, **66**, 259–264.
- Norton, R.H. and Beer, R. (1977) Errata-new apodizing functions for Fourier spectrometry. *Journal of the Optical Society of America*, **67**, 419.
- Palmer, M.H., Maier, R.R.J., Hegelund, F., and Newnham, D.A. (1998) Structure and high-resolution IR spectroscopy of 1,2,4-triazine vapor. *Journal of Molecular Spectroscopy*, **192**(2), 331–337.
- Papoušek, D. and Aliev, M.R. (1982) *Molecular Vibrational-Rotational Spectra*, Elsevier, New York, USA.
- Partal Urena, F., Fernandez Gomes, M., Lopez Gonzalez, E., and Martinez Torres, E. (2003) A new insight into the vibrational analysis of pyridine. *Spectrochimica Acta A*, **59**, 2815–2839.
- Petkie, D.T., Goyette, T.M., Bettens, R.P.A., Belov, S.P., Albert, S., Helminger, P., and De Lucia, F.C. (1997) A fast scan submillimeter spectroscopic technique. *The Review of Scientific Instruments*, **68**, 1675–1683.
- Philis, J.G. (2005) The multiphoton ionization spectrum of jet-cooled pyrimidine in the  $3p$  Rydberg and  $^3B_1$  ( $\pi^*$ , n) states. *Journal of Molecular Spectroscopy*, **232**(1), 26–29.
- Pickett, H.M. (1991) The fitting and prediction of vibration-rotation spectra with spin interactions. *Journal of Molecular Spectroscopy*, **148**, 371–377.
- Pirali, O., Vervloet, M., Mulas, G., Mallocci, G., and Joblin, C. (2009) High-resolution infrared absorption spectroscopy of thermally excited naphthalene. Measurements and calculations of anharmonic parameters and vibrational interactions. *Physical Chemistry Chemical Physics*, **11**(18), 3443–3454.
- Pliva, J., Johns, J.W.C., and Lu, Z. (1996) The difference bands  $\nu_{11} - \nu_4$  and  $\nu_{10} - \nu_{18}$  of benzene at high resolution. *Molecular Physics*, **87**, 859–863.
- Prasad, P. and Burow, D.F. (1979) Raman optical activity. Computation of circular intensity differentials for bromochlorofluoromethane. *Journal of the American Chemical Society*, **101**, 806.
- Pratt, D.W. (2011) Electronic spectroscopy in the gas phase, in *Handbook of High-resolution Spectroscopy*, Quack, M. and Merkt, F. (eds), John Wiley & Sons, Ltd., Chichester, UK.
- Puttkamer, K.v., Dübal, H.-R., and Quack, M. (1983) Time-dependent processes in polyatomic molecules during and after intense infrared irradiation. *Faraday Discussions of the Chemical Society*, **75**, 197–210.
- Puttkamer, K.v. and Quack, M. (1987) High resolution interferometric FTIR spectroscopy of  $(\text{HF})_2$ : analysis of a low frequency fundamental near  $400\text{ cm}^{-1}$ . *Molecular Physics*, **62**(5), 1047–1064.
- Puttkamer, K.v. and Quack, M. (1989) Vibrational spectra of  $(\text{HF})_2$ ,  $(\text{HF})_n$  and their D-isotopomers: mode selective rearrangements and nonstatistical unimolecular decay. *Chemical Physics*, **139**, 31–53.
- Puttkamer, K.v., Quack, M., and Suhm, M.A. (1988) Observation and assignment of tunnelling-rotational transitions in the far infrared spectrum of  $(\text{HF})_2$ . *Molecular Physics*, **65**(5), 1025–1045.
- Quack, M. (1977) Detailed symmetry selection rules for reactive collisions. *Molecular Physics*, **34**(2), 477–504.
- Quack, M. (1986) On the measurement of the parity violating energy difference between enantiomers. *Chemical Physics Letters*, **132**(2), 147–153.
- Quack, M. (1989a) Infrared laser chemistry and the dynamics of molecular multiphoton excitation. *Infrared Physics*, **29**, 441–466.

- Quack, M. (1989b) Structure and dynamics of chiral molecules. *Angewandte Chemie (International ed. in English)*, **28**, 571–586.
- Quack, M. (1990) Spectra and dynamics of coupled vibrations in polyatomic molecules. *Annual Review of Physical Chemistry*, **41**, 839–874.
- Quack, M. (1995) IR laser chemistry. *Infrared Physics and Technology*, **36**(1), 365–380.
- Quack, M. (2001) Molecules in motion. *Chimia*, **55**, 753–758.
- Quack, M. (2002) How important is parity violation for molecular and biomolecular chirality? *Angewandte Chemie (International ed. in English)*, **41**, 4618–4630.
- Quack, M. (2003) Molecular spectra, reaction dynamics, symmetries and life. *Chimia*, **57**, 147–160.
- Quack, M. (2004) Time and time reversal symmetry in quantum chemical kinetics, in *Fundamental World of Quantum Chemistry. A Tribute to the Memory Löwdin*, Brandas, E.J. and Kryachko, E.S. (eds), Kluwer Academic Publishers, Dordrecht, pp. 423–474, Vol. 3.
- Quack, M. (2006) Electroweak quantum chemistry and the dynamics of parity violation in chiral molecules, in *Modelling Molecular Structure and Reactivity in Biological Systems, Proceedings of 7th WATOC Congress, Cape Town January 2005*, Naidoo, K.J., Brady, J., Field, M.J., Gao, J., and Hann, M. (eds), Royal Society of Chemistry, Cambridge, pp. 3–38.
- Quack, M. (2011) Fundamental symmetries and symmetry violations from high-resolution spectroscopy, in *Handbook of High-resolution Spectroscopy*, Quack, M. and Merkt, F. (eds), John Wiley & Sons, Ltd., Chichester, UK.
- Quack, M. and Stohner, J. (2000) On the influence of parity violating weak nuclear potentials on vibrational and rotational frequencies in chiral molecules. *Physical Review Letters*, **84**, 3807–3810.
- Quack, M. and Stohner, J. (2003) Combined multidimensional anharmonic and parity violating effects in CDBrClF. *Journal of Chemical Physics*, **119**, 11228–11240.
- Quack, M. and Stohner, J. (2005) Parity violation in chiral molecules. *Chimia*, **59**, 530–538.
- Quack, M. and Suhm, M.A. (1990) Observation and assignment of the hydrogen bond exchange disrotatory in-plane bending vibration  $\nu_5$  in (HF)<sub>2</sub>. *Chemical Physics Letters*, **171**(5, 6), 517–524.
- Quack, M. and Willeke, M. (2006) Stereomutation tunneling switching dynamics and parity violation in chlorineperoxide Cl-O-O-Cl. *Journal of Physical Chemistry A*, **110**(9), 3338–3348.
- Quack, M., Schmitt, M., and Suhm, M. (1997) FTIR spectroscopy of hydrogen fluoride clusters. *Chemical Physics Letters*, **269**, 29–38.
- Quack, M., Stohner, J., and Willeke, M. (2008) High-resolution spectroscopic studies and theory of parity violation in chiral molecules. *Annual Review Physical Chemistry*, **59**, 741–769.
- Quapp, W., Albert, S., Winnewisser, B.P., and Winnewisser, M. (1993) The FT-IR spectrum of HC<sup>15</sup>N<sup>18</sup>O: the  $\nu_1$ ,  $\nu_2$ ,  $2\nu_3$  and  $\nu_2 + \nu_3$  band systems. *Journal of Molecular Spectroscopy*, **160**, 540–553.
- Rauhut, G., Azhary, E.A., Eckert, F., Schuhmann, U., and Werner, H.J. (1999) Impact of local approximations on MP2 vibrational frequencies. *Spectrochimica Acta A*, **55**, 647–658.
- Ridgway, S.T. and Brault, J.W. (1984) Astronomical Fourier transform spectroscopy revisited. *Annual Review of Astronomy and Astrophysics*, **22**(1), 291–317.
- Riedle, E., Beil, A., Luckhaus, D., and Quack, M. (1994) Sub-doppler supersonic jet spectra of the coupled  $6a_0^+$  and  $6b_0^+$  vibronic bands of the  $S_1(^1B_{2u}) \leftarrow S_0(^1A_{1g})$  transition in mono-deuterobenzene and their rovibrational analysis. *Molecular Physics*, **81**(1), 1–15.
- Rinsland, C.P., Johnson, D.W., Goldman, A., and Levine, J.S. (1989) Evidence for a decline in the atmospheric accumulation rate of CHClF<sub>2</sub> (CFC-22). *Nature*, **337**, 535.
- Roy, P., Rouzières, M., Qi, Z., and Chubar, O. (2006) The AILES infrared beamline on the third generation synchrotron radiation facility SOLEIL. *Infrared Physics and Technology*, **49**(1–2), 139–146.
- Rubens, H. and Baeyer, O. (1911) On extremely long waves, emitted by the Quartz Mercury Lamp. *Philosophical Magazine*, **21**, 689–694.
- Rubens, H. and Wood, R.W. (1911) Focal isolation of long heat-waves. *Philosophical Magazine*, **21**, 249–260.
- Schnell, M. (2011) Group theory for high-resolution spectroscopy of nonrigid molecules, in *Handbook of High-resolution Spectroscopy*, Quack, M. and Merkt, F. (eds), John Wiley & Sons, Ltd., Chichester, UK.
- Schmitt, M. and Meerts, W.L. (2011) Rotationally resolved electronic spectroscopy and automatic assignment techniques using evolutionary algorithms, in *Handbook of High-resolution Spectroscopy*, Quack, M. and Merkt, F. (eds), John Wiley & Sons, Ltd., Chichester, UK.
- Schulze, G., Koja, O., Winnewisser, B., and Winnewisser, M. (2000) High resolution FIR spectra of HCNO and DCNO. *Journal of Molecular Structure*, **518**, 307–325.
- Schweiger, A. and Jeschke, G. (2001) *Principles of Pulse Electron Paramagnetic Resonance*, Oxford University Press, Oxford.
- Shipman, S.T. and Pate, B.H. (2011) New techniques in microwave spectroscopy, in *Handbook of High-resolution Spectroscopy*, Quack, M. and Merkt, F. (eds), John Wiley & Sons, Ltd., Chichester, UK.
- Short, L.N. and Thompson, H.W. (1952) Infrared spectra of derivatives of pyrimidines. *Journal of the Chemical Society* 168–187.
- Signorell, R., Marquardt, R., Quack, M., and Suhm, M.A. (1996) The permanent electric dipole moment of CH<sub>2</sub>D<sub>2</sub>: FIR spectroscopy, centrifugal distortion effects and quantum Monte Carlo calculations with 9-dimensional analytical dipole moment and potential functions of methane. *Molecular Physics*, **89**(1), 297–313.
- Sigrist, M.W. (2011) High-resolution infrared laser spectroscopy and gas sensing applications, in *Handbook of High-resolution Spectroscopy*, Quack, M. and Merkt, F. (eds), John Wiley & Sons, Ltd., Chichester, UK.
- Snels, M. and Quack, M. (1991) High resolution Fourier-transform infrared spectroscopy of CHCl<sub>2</sub>F in supersonic jets: analysis of  $\nu_3$ ,  $\nu_7$ , and  $\nu_8$ . *Journal of Chemical Physics*, **95**(9), 6355–6361.
- Snels, M., Beil, A., Hollenstein, H., and Quack, M. (1997) Excited vibrational states of benzene: High resolution FTIR

- spectra and analysis of some out-of-plane vibrational fundamentals of  $C_6H_5D$ . *Chemical Physics*, **225**(0), 107–130.
- Snels, M., Hollenstein, H., Quack, M., Cané, E., Miani, J., and Trombetti, A. (2002) High Resolution FTIR spectra and analysis of the  $\nu_{11}$  fundamental and of the  $\nu_2 + \nu_{11}$ ,  $\nu_5 + \nu_{12}$  and  $\nu_7 + \nu_{16}$  combination bands of  $^{12}C_6H_6$ . *Molecular Physics*, **100**, 981–1001.
- Snels, M., Horká-Zelenková, V., Hollenstein, H., and Quack, M. (2011) High-resolution FTIR and diode laser spectroscopy of supersonic jets, in *Handbook of High-resolution Spectroscopy*, Quack, M. and Merkt, F. (eds), John Wiley & Sons, Ltd., Chichester, UK.
- Soulard, P., Asselin, P., Cuisset, A., Moreno, J.R.A., Huet, T.R., Petitprez, D., Demaison, J., Freedman, T.B., Cao, X., Nafie, L.A. *et al.* (2006) Chlorofluoriodomethane as a potential candidate for parity violation measurements. *PCCP*, **8**, 79–92.
- Stanca-Kaposta, E.C. and Simons, J.P. (2011) High-resolution infrared–ultraviolet (IR–UV) double-resonance spectroscopy of biological molecules, in *Handbook of High-resolution Spectroscopy*, Quack, M. and Merkt, F. (eds), John Wiley & Sons, Ltd., Chichester, UK.
- Stidham, H.D. and DiLella, D.P. (1979) Vibrational perturbations: a chemical aid to assignment. *Journal of Raman Spectroscopy*, **8**(3), 180–184.
- Stidham, H.D. and DiLella, D.P. (1980) Vibrational spectra of  $C_{2v}$  deuterium substituted pyridines 2. *Journal of Raman Spectroscopy*, **8**(2), 90–106.
- Stohner, J., and Quack, M. (2011) Conventions, symbols, quantities, units and constants for high-resolution molecular spectroscopy, in *Handbook of High-resolution Spectroscopy*, Quack, M. and Merkt, F. (eds), John Wiley & Sons, Ltd., Chichester, UK.
- Suhm, M. (1990) *Die Dynamik des Wasserstoffbrückenmoleküls (HF)<sub>2</sub>: Ferninfrarotspektroskopie und Theorie*, Doctoral thesis, Eidgenössische Technische Hochschule Zürich, diss ETH Nr. 9288.
- Tanaka, K., Harada, K., and Yamada, K.M.T. (2011) THz and submillimeter-wave spectroscopy of molecular complexes, in *Handbook of High-resolution Spectroscopy*, Quack, M. and Merkt, F. (eds), John Wiley & Sons, Ltd., Chichester, UK.
- Thiel, Y., Walters, V.A., Wiberg, K.B., and Colson, S.D. (1991) High-resolution infrared analysis of the  $\nu_{17}$  band of pyridine. *International Journal of Quantum Chemistry*, **34**, 423–436.
- Tielens, A.G.G.M. (2008) Interstellar polycyclic aromatic hydrocarbon molecules. *Annual Review of Astronomy and Astrophysics*, **46**(1), 289–337.
- Turkevich, J. and Stevenson, P.C. (1943) Infrared absorption of pyridine vapor. *Journal of Chemical Physics*, **11**(7), 328–329.
- Ulenikov, O., Bekhtereva, E., Albert, S., Bauerecker, S., Hollenstein, H., and Quack, M. (2009) High-resolution near infrared spectroscopy and vibrational dynamics of dideuteromethane ( $CH_2D_2$ ). *Journal of Physical Chemistry A*, **113**(10), 2218–2231.
- Ulenikov, O.N., Onopenko, G.A., Bekhtereva, E.S., Petrova, T.M., Solodov, A.M., and Solodov, A.A. (2010a) High-resolution study of the  $\nu_5 + \nu_{12}$  band of  $C_2H_4$ . *Molecular Physics*, **108**(5), 637–647.
- Ulenikov, N., Bekhtereva, E., Albert, S., Bauerecker, S., Hollenstein, H., and Quack, M. (2010b) High-resolution infrared spectroscopy and global vibrational analysis for the  $CHD_3$  and  $CH_3D$  isotopomer of methane. *Molecular Physics*, **108**, 1209–1240.
- Uskola, A., Basterretxea, F.J., and Castano, F. (2000) Diode-laser spectroscopy of the  $\nu_{19a}$  band of chlorobenzene in a supersonic jet. *Journal of Molecular Spectroscopy*, **202**(2), 262–271.
- Vagin, V.A. (1980) Optimal apodization in Fourier spectrometry. *Optics and Spectroscopy*, **48**, 190–193.
- Wagner, G., Winnewisser, B.P., and Winnewisser, M. (1991) The effects of a strong coriolis resonance on rovibrational line intensities of  $H^{13}CNO$ . *Journal of Molecular Spectroscopy*, **146**, 104–119.
- Walters, V.A., Snavely, D.L., Wiberg, K.B., Colson, S.D., and Wong, K.N. (1986) New vibrational constants for pyridine from low-temperature and high-resolution infrared spectra. *Journal of Physical Chemistry*, **90**, 592–597.
- Watson, J.K.G. (1978) Aspects of quartic and sextic centrifugal effects on rotational energy levels, in *Vibrational Spectra and Structure*, Durig, J. (ed.), Elsevier, Amsterdam, pp. 1–89, Vol. 6.
- Watson, J.K.G. (2011) Indeterminacies of fitting parameters in molecular spectroscopy, in *Handbook of High-resolution Spectroscopy*, Quack, M. and Merkt, F. (eds), John Wiley & Sons, Ltd., Chichester, UK.
- Weber, A. (2011) High-resolution Raman spectroscopy of gases, in *Handbook of High-resolution Spectroscopy*, Quack, M. and Merkt, F., (eds) John Wiley & Sons.
- Wester, R. (2011) Spectroscopy and reaction dynamics of anions, in *Handbook of High-resolution Spectroscopy*, Quack, M. and Merkt, F. (eds), John Wiley & Sons, Ltd., Chichester, UK.
- Western, C.M. (2011) Introduction to modeling high-resolution spectra, in *Handbook of High-resolution Spectroscopy*, Quack, M. and Merkt, F. (eds), John Wiley & Sons, Ltd., Chichester, UK.
- Willitsch, S. (2011) Experimental methods in cation spectroscopy, in *Handbook of High-resolution Spectroscopy*, Quack, M. and Merkt, F. (eds), John Wiley & Sons, Ltd., Chichester, UK.
- Wilson, E.B. (1934) The normal modes and frequencies of vibration of the regular plane hexagon model of the benzene molecule. *Physical Review*, **45**, 706–714.
- Wilson, E.B. and Wells, A.J. (1946) The experimental determination of the intensities of infra-red absorption bands. 1. Theory of the method. *Journal of Chemical Physics*, **14**(10), 578–580.
- Winnewisser, B.P., Reinstädler, J., Yamada, K.M.T., and Behrend, J. (1989) Interactive Loomis-Wood assignment programs. *Journal of Molecular Spectroscopy*, **136**, 12–18.
- Winnewisser, B.P., Winnewisser, M., Medvedev, I.R., Behnke, M., De Lucia, F.C., Ross, S.C., and Koput, J. (2005) Experimental confirmation of quantum monodromy: the millimeter wave spectrum of cyanogen isothiocyanate NCNCS. *Physical Review Letters*, **95**(24), 243002.
- Wong, K.N. and Colson, S.D. (1983) Rotational contour analysis of the  $\nu_{6a}$  band in the infrared spectrum of pyridine- $d_5$ . *Journal of Physical Chemistry*, **87**, 2102–2109.

- Wong, K.N. and Colson, S.D. (1984) The FT-IR spectra of pyridine and pyridine-*d*<sub>5</sub>. *Journal of Molecular Spectroscopy*, **104**, 129–151.
- Yamaguchi, Y. and Schäfer, H.F. (2011) Analytic derivative methods in molecular electronic structure theory: a new dimension to quantum chemistry and its applications to spectroscopy, in *Handbook of High-resolution Spectroscopy*, Quack, M. and Merkt, F. (eds), John Wiley & Sons, Ltd., Chichester, UK.
- Ye, E., Bettens, R.P.A., De Lucia, F.C., Petkie, D.T., and Albert, S. (2005) Millimeter and submillimeter wave rotational spectrum of pyridine in the ground and excited vibrational states. *Journal of Molecular Spectroscopy*, **232**, 39–43.
- Zare, R. (1988) *Angular Momentum Understanding Spatial Aspects in Chemistry and Physics*, Wiley, New York.

## FURTHER READING

### Calibration

The FTIR spectra must be calibrated for an absolute frequency measurement. In general, secondary standards are used which are FTIR measurements calibrated by heterodyne measurements. The books by Maki and Wells 1991 and the two books by Guelachvili and Rao 1986 and 1993 as well as the HITRAN data base are commonly used as sources for secondary standards.

- Guelachvili, G. and Narahari Rao, K. (1986) *Handbook of Infrared Standards*, Academic Press, Inc., Orlando, FL.
- Guelachvili, G. and Narahari Rao, K. (1993) *Handbook of Infrared Standards II*, Academic Press, Inc., San Diego, CA.
- Guelachvili, G., Birk, M., Borde, Ch.J, Brault, J.W., Brown, L.R., Carli, B., Cole, A.R.H., Evenson, K.M., Fayt, A., Hausmann, D. *et al.* (1996) High-resolution wavenumber standards for the infrared (IUPAC Technical Report). *Pure and Applied Chemistry*, **68**(1), 193–208.
- Maki, A.G. and Wells, J.S. (1991) *Wavenumber Calibration Tables from Heterodyne Frequency Measurements*, National Institute of Standards and Technology Publication 821, U.S. Department of Commerce, Washington, DC.
- Rothman, L.S. *et al.* (2009) The HITRAN 2008 molecular spectroscopic database. *Journal of Quantitative Spectroscopy and Radiative Transfer*, **110**, 533–572.

The following heterodyne measurements, primary standards were used for this data bases following Guelachvili and Rao 1993.

### CO up to 150 cm<sup>-1</sup>:

- Varberg, T.D. and Evenson, K.M. (1992) Accurate far-infrared rotational frequencies of carbon monoxide. *Astrophysics Journal*, **385**, 763–765.

### CO at 2000 cm<sup>-1</sup>:

- Schneider, M., Wells, J.S., and Maki, A.G. (1990) Heterodyne frequency measurements of <sup>12</sup>C<sup>16</sup>O laser transitions near 2050 cm<sup>-1</sup>. *Journal of Molecular Spectroscopy*, **139**, 432–438 and **141**, 351 (errata).
- Wu, W., George, T., Schneider, M., Urban, W., and Nelles, B. (1991) Saturation stabilization of the CO fundamental band laser. *Applied Physics B*, **52**, 1–6.

### CO<sub>2</sub>:

- Bradley, L.C., Soohoo, K.L. and Freed, C. (1986) Absolute frequencies of lasing transitions in nine CO<sub>2</sub> isotopic species. *IEEE Journal of Quantum Electronics*, **QE-22**, 234–267.
- Groh, A., Goddon, D., Schneider, M., Zimmermann, W., and Urban, W. (1991) Sub-doppler heterodyne frequency measurements on the CO<sub>2</sub> 10<sup>0</sup>11-00<sup>0</sup>01 vibrational band: new reference lines near 3714 cm<sup>-1</sup>. *Journal of Molecular Spectroscopy*, **146**, 161–168.
- Peterson, F.R., Wells, J.S., Siemsen, K.J., Robinson, A.M., and Maki, A.G. (1984) Heterodyne frequency measurements and analysis of <sup>12</sup>C<sup>16</sup>O<sub>2</sub> laser hot band transitions. *Journal of Molecular Spectroscopy*, **105**, 324–330.

### N<sub>2</sub>O:

- Hinz, A., Wells, J.S., and Maki, A.G. (1987) Heterodyne frequency measurements of hot bands and isotopic transition of N<sub>2</sub>O near 7.8 μm. *Zeitschrift für Physik D Atoms*, **5**, 426–433.
- Vanek, M.D., Schneider, M., Wells, J.S., and Maki, A.G. (1987) Heterodyne measurements on N<sub>2</sub>O near 1635 cm<sup>-1</sup>. *Journal of Molecular Spectroscopy*, **134**, 154–158.

### OCS

- Dax, A., Mürtz, M., Wells, J.S., Schneider, M., Bachem, E., Urban, W., and Maki, A.G. (1992) Extension of heterodyne frequency measurements on OCS to 87 THz (2900 cm<sup>-1</sup>). *Journal of Molecular Spectroscopy*, **156**, 98–103.
- Maki, A.G., Olson, W.B., Wells, J.S., and Vanek, M.D. (1989) Heterodyne and FTS measurement on the OCS hot band near 1890 cm<sup>-1</sup>. *Journal of Molecular Spectroscopy*, **130**, 69–70.
- Wells, J.S., Peterson, F.R., and Maki, A.G. (1979) Heterodyne frequency measurements with a tunable diode laser - CO<sub>2</sub> laser spectrometer: spectroscopic reference frequencies in the 9.5 μm band of carbonyl sulfide. *Applied Optics*, **18**, 3567–3573.
- Wells, J.S., Peterson, F.R., Maki, A.G., and Sukle, D.J. (1981) Heterodyne frequency measurements on the 11.6-μm band of OCS: new frequency/wavelength calibration tables for 11.6- and 5.8-μm OCS bands. *Applied Optics*, **20**, 1676–1684 and **20**, 2874.

### HF

- Godson, D., Groh, A., Hanses, H.J., Schneider, M., and Urban, W. (1991) Heterodyne frequency measurements of the 1-0 band of HF at 2.7 μm. *Journal of Molecular Spectroscopy*, **147**, 392–397.

### NH<sub>3</sub>, HCN, C<sub>2</sub>H<sub>2</sub>

- Sasada, H., Takeuchi, S., Iritani, M., and Nakatani, K. (1991) Semiconductor-laser heterodyne frequency measurements on 1.52-μm molecular transitions. *Journal of the Optical Society of America B*, **8**, 713–718.

## RELATED ARTICLES

- Albert *et al.* 2011: **Fundamentals of Rotation–Vibration Spectra**

- Amano 2011: **High-resolution Microwave and Infrared Spectroscopy of Molecular Cations**
- Bauder 2011: **Fundamentals of Rotational Spectroscopy**
- Breidung and Thiel 2011: **Prediction of Vibrational Spectra from Ab Initio Theory**
- Boudon *et al.* 2011: **Spherical Top Theory and Molecular Spectra**
- Caminati 2011: **Microwave Spectroscopy of Large Molecules and Molecular Complexes**
- Demtröder 2011: **Doppler-free Laser Spectroscopy**
- Eikema and Ubachs 2011: **Precision Laser Spectroscopy in the Extreme Ultraviolet**
- Flaud and Orphal 2011: **Spectroscopy of the Earth's Atmosphere**
- Frey *et al.* 2011: **High-resolution Rotational Raman Coherence Spectroscopy with Femtosecond Pulses**
- Grabow 2011: **Fourier Transform Microwave Spectroscopy Measurement and Instrumentation**
- Guenoun and Maier 2011: **Electronic Spectroscopy of Transient Molecules**
- Häber and Kleinermanns 2011: **Multiphoton Resonance Spectroscopy of Biological Molecules**
- Hamm 2011: **2D-Infrared Spectroscopy**
- Havenith and Birner 2011: **High-resolution IR-laser Jet Spectroscopy of Formic Acid Dimer**
- Herman 2011: **High-resolution Infrared Spectroscopy of Acetylene: Theoretical Background and Research Trends**
- Hippler *et al.* 2011: **Mass and Isotope-selective Infrared Spectroscopy**
- Jäger and Xu 2011: **Fourier Transform Microwave Spectroscopy of Doped Helium Clusters**
- Marquardt and Quack 2011: **Global Analytical Potential Energy Surfaces for High-resolution Molecular Spectroscopy and Reaction Dynamics**
- Mastalerz and Reiher 2011: **Relativistic Electronic Structure Theory for Molecular Spectroscopy**
- Merkt and Quack 2011: **Molecular Quantum Mechanics and Molecular Spectra, Molecular Symmetry, and Interaction of Matter with Radiation**
- Merkt *et al.* 2011: **High-resolution Photoelectron Spectroscopy**
- Quack 2011: **Fundamental Symmetries and Symmetry Violations from High-resolution Spectroscopy**
- Schmitt and Meerts 2011: **Rotationally Resolved Electronic Spectroscopy and Automatic Assignment Techniques using Evolutionary Algorithms**
- Schnell 2011: **Group Theory for High-resolution Spectroscopy of Nonrigid Molecules**
- Shipman and Pate 2011: **New Techniques in Microwave Spectroscopy**
- Sigrist 2011: **High-resolution Infrared Laser Spectroscopy and Gas Sensing Applications**
- Snels *et al.* 2011: **High-resolution FTIR and Diode Laser Spectroscopy of Supersonic Jets**
- Stanca-Kaposta and Simons 2011: **High-resolution Infrared–Ultraviolet (IR–UV) Double-resonance Spectroscopy of Biological Molecules**
- Stohner and Quack 2011: **Conventions, Symbols, Quantities, Units and Constants for High-resolution Molecular Spectroscopy**
- Tanaka *et al.* 2011: **THz and Submillimeter-wave Spectroscopy of Molecular Complexes**
- Watson 2011: **Indeterminacies of Fitting Parameters in Molecular Spectroscopy**
- Weber 2011: **High-resolution Raman Spectroscopy of Gases**
- Western 2011: **Introduction to Modeling High-resolution Spectra**
- Willitsch 2011: **Experimental Methods in Cation Spectroscopy**
- Yamaguchi and Schäfer 2011: **Analytic Derivative Methods in Molecular Electronic Structure Theory: A New Dimension to Quantum Chemistry and its Applications to Spectroscopy**

